FACULDADE DE ENGENHARIA DA UNIVERSIDADE DO PORTO

Integration of Power-to-Hydrogen Systems in Renewable Energy Communities

David Machado Reis

Master's Degree in Electrical and Computer Engineering

Supervisor: Doutor Tiago André Teixeira Soares

October 2, 2025

Recognitions

This work was carried out with the support of INESC-TEC and supervised at this institution by Tiago André Soares.

The following person collaborated with the supervising team in carrying out this work: Luís Manuel Rodrigues.

Resumo

As alterações climáticas e a instabilidade geopolítica têm acelerado a transição global para sistemas energéticos sustentáveis e descentralizados. A adoção generalizada de tecnologias de energia renovável, nomeadamente solar e eólica, tem sido impulsionada pela redução dos custos e pela melhoria da eficiência, permitindo que os consumidores assumam um papel ativo na geração de energia. Com o apoio de enquadramentos regulatórios e financeiros favoráveis, os prosumidores começaram a formar comunidades de energia renovável, que podem ser concebidas para maximizar o lucro ou o autoconsumo local. No entanto, a intermitência inerente às fontes renováveis continua a ser um grande desafio para garantir a fiabilidade do fornecimento de energia e a estabilidade da rede.

Neste contexto, o hidrogénio tem-se afirmado como um vetor promissor de armazenamento e flexibilidade energética. As comunidades de energia renovável podem utilizar excedentes de eletricidade renovável para produzir hidrogénio através de eletrólise, armazená-lo sob forma química e, mais tarde, reconvertê-lo em eletricidade através de células de combustível. Esta abordagem oferece vantagens em termos de segurança energética e viabilidade económica, especialmente em períodos de baixa produção renovável ou quando a exportação para a rede é pouco rentável.

Esta dissertação propõe uma metodologia para a gestão de comunidades de energia renovável que integra sistemas descentralizados de potência para hidrogénio. O enquadramento proposto está dividido em duas etapas: um modelo de dimensionamento que otimiza o investimento em recursos energéticos distribuídos, e um modelo operacional que avalia o desempenho da comunidade sob diferentes configurações. Foram desenvolvidos quatro cenários para avaliar o impacto económico e operacional da integração de sistemas fotovoltaicos, armazenamento em baterias e tecnologias potência para hidrogénio numa comunidade de energia renovável.

Os resultados das simulações mostram que a combinação de sistemas fotovoltaicos, baterias e sistemas potência para hidrogénio gera o valor atual líquido mais elevado ao longo dos 20 anos de vida útil do projeto. O cenário com apenas fotovoltaicos e potência para hidrogénio apresenta o menor período de retorno, com 12,93 anos. Nos cenários com sistemas potência para hidrogénio, a viabilidade mostrou-se mais sensível aos custos de investimento e às condições de mercado. A análise de sensibilidade revelou que a redução do custo dos sistemas fotovoltaicos melhora significativamente a autossuficiência energética e a partilha de energia na comunidade. A análise dos custos dos eletrólisadores indicou que, a um preço de venda de hidrogénio de 2 €/kg, a comunidade adota sistemas potência para hidrogénio se o custo do eletrólisador for inferior a 700 €/kW. Este resultado é relevante por estar alinhado com as projeções da UE para tornar o hidrogénio verde competitivo com alternativas baseadas em combustíveis fósseis. Preços de venda mais elevados aumentam ainda mais a atratividade e a rentabilidade destes sistemas.

De forma geral, a metodologia proposta apoia o planeamento e avaliação de comunidades de energia, oferecendo contributos práticos sobre como diferentes combinações tecnológicas afetam o desempenho energético e a viabilidade do investimento à escala comunitária.

Abstract

Climate change and geopolitical instability have accelerated the global shift toward sustainable, decentralized energy systems. The widespread adoption of renewable energy technologies, namely solar and wind, has been driven by falling costs and improved efficiency, enabling consumers to take an active role in energy generation. Supported by favorable regulatory and financial frameworks, prosumers have begun forming renewable energy communities, which can be designed to maximize either profit or local self-consumption. However, the inherent intermittency of renewable sources remains a major challenge for ensuring reliable energy supply and grid stability.

In this context, hydrogen has emerged as a promising vector for energy storage and flexibility. Renewable energy communities can use excess renewable electricity to produce hydrogen via electrolysis, store it in chemical form, and later convert it back into electricity using fuel cells. This approach offers advantages in terms of energy security and economic viability, especially during periods of low renewable production or when exporting to the grid is not financially beneficial.

This dissertation proposes a methodology for managing renewable energy communities that incorporates decentralized power-to-hydrogen systems. The framework is divided into two stages: a sizing model that optimizes investment in distributed energy resources, and an operational model that evaluates community performance under different configurations. Four scenarios were developed to assess the economic and operational impact of integrating photovoltaic systems, battery storage, and power-to-hydrogen technologies into a renewable energy community.

Simulation results show that combining photovoltaic systems, batteries, and power-to-hydrogen yields the highest net present value over the project's 20-year lifespan. The scenario with only photovoltaic and power-to-hydrogen systems provides the shortest payback period of 12.93 years. In the power-to-hydrogen scenarios, feasibility proved more sensitive to investment costs and market conditions. Sensitivity analysis revealed that lower photovoltaic system costs significantly improve energy self-sufficiency and energy sharing within the community. Electrolyzer cost analysis indicated that, at a hydrogen sale price of 2 €/kg, the community adopts power-to-hydrogen systems if electrolyzer costs fall below 700 €/kW. This result is significant as it aligns with the EU's projections for green hydrogen to become competitive with fossil-based alternatives. Higher hydrogen sale prices further increase the attractiveness and profitability of these systems.

Overall, the proposed methodology supports the planning and evaluation of energy communities, offering practical insights into how different technology combinations affect energy performance and investment viability at the community scale.

Keywords: Renewable energy communities, power-to-hydrogen, distributed energy resources, techno-economic analysis, optimization

Sustainable Development Goals

This chapter analyses the contribution of the proposed integration of power-to-hydrogen systems in renewable energy communities to the United Nations Sustainable Development Goals (SDGs). The SDGs provide a global framework for addressing pressing environmental, social, and economic challenges. Identifying and aligning with specific SDG targets helps contextualize the impact of the project beyond technical performance, highlighting its potential contribution to climate action, energy access, innovation, and collaborative governance.

This dissertation tackles the following SDGs by investigating the viability of integrating hydrogen in renewable energy communities, which will become indispensable for achieving the UN's goals.

- **SDG 7 – Affordable and Clean Energy:** Ensure access to affordable, reliable, sustainable, and modern energy for all.
- **SDG 12 – Responsible Consumption and Production:** Improve resource efficiency and reduce environmental footprint.

The table summarizes the most relevant SDG targets addressed by the project, describing how the proposed solution contributes to each target and listing metrics that can be used to evaluate impact.

SDG	Goal	Contribution	Metrics
7	7.1	Improves access to clean, affordable energy	% population with access
	7.2	Enables renewable generation and hydrogen storage in communities	Average bill reduction (€)
12	12.2	Increases efficiency, reduces resource use	System efficiency

Acknowledgments

I would like to thank all those who accompanied and supported me throughout my academic journey, especially in the final stretch of this dissertation.

First and foremost, to my supervisor, Tiago Soares, for the constant motivation to always go a little further. His enthusiasm and vision were essential to the quality of this work.

To my co-supervisor, Luís Rodrigues, I express my deepest gratitude for his tireless support and close guidance throughout all phases of this dissertation. The many meetings and error-hunting sessions made all the difference.

To my friends, thank you for the good moments, and the bad ones, we shared over the years. For the sleepless nights, the laughter, and the unconditional friendship.

To my girlfriend, Beatriz, thank you for always being by my side, with patience, love, and understanding, even during the toughest times.

To my brother, Fábio, thank you for always being there for me and for the advice that came when it mattered most. To my sister, Alice, your presence reminded me to pause, smile, and not take everything so seriously and for that, I'm deeply grateful.

Finally, to my parents: words cannot express how grateful I am for your sacrifice, unconditional support, and love. Every opportunity I've had is thanks to the effort you made for me. This work is as much yours as it is mine.

Thank you,

David Reis

"Coming together is a beginning,
staying together is progress,
and working together is success. "

Henry Ford

Contents

List of Figures

List of Tables

Abbreviations

AC	Allocation Coefficient
ALK	Alkaline Water Electrolyzer
BESS	Battery Energy Storage System
CAPEX	Capital Expenditure
CCS	Carbon Capture and Storage
CSC	Collective Self-Consumption
DER	Distributed Energy Resource
DSO	Distribution System Operator
ESS	Energy Storage System
EU	European Union
EV	Electric Vehicle
FC	Fuel Cell
GHG	Greenhouse Gases
HHV	Higher Heating Value
IEA	International Energy Agency
LCOE	Levelized Cost of Electricity
LCOS	Levelized Cost of Storage
LEM	Local Energy Market
LHV	Lower Heating Value
MILP	Mixed-Integer Linear Programming
NG	Natural Gas
NPV	Net Present Value
OPEX	Operational Expenditure
OSTEC	Optimal Scheduling Tool for Energy Communities
P2H	Power-to-Hydrogen
P2P	Peer-to-Peer
PEM	Proton Exchange Membrane
PV	Photovoltaic
REC	Renewable Energy Community
RED	Renewable Energy Directive
RES	Renewable Energy Source
SDG	Sustainable Development Goals
SITEC	Sizing Individual and Shared Assets for Energy Communities
SOE	Solid Oxide Electrolyzer
STP	Standard Temperature and Pressure
TOTEX	Total Expenditure
TRL	Technology Readiness Level

Chapter 1

Introduction

This chapter presents the motivation and objectives of the work carried out in this dissertation. First, it outlines the context in which the research was conducted and the reasons for pursuing it. The project's key objectives are discussed, followed by a brief overview of related projects and relevant publications. Finally, the structure and organization of the document are described.

1.1 Context and Motivation

The 2015 Paris Agreement established the goal of limiting global average temperature to well below 2°C above pre-industrial levels, aiming to keep the temperature increase below 1.5°C above pre-industrial levels [1]. This target is closely aligned with the United Nations' Sustainable Development Goals (SDG), which aims, among other priorities, to ensure access to affordable, reliable, sustainable, and modern energy for all. In line with this objective, the SDG reported that 28.2% of the total electric consumption came from Renewable Energy Sources (RES) [2].

The growing share of RES in the energy mix can be attributed to several key factors: (*i*) increased public and political awareness of the need for sustainable energy practices, (*ii*) significant cost reductions in Photovoltaic (PV) technology (*iii*) supportive financial incentives and policy frameworks [3].

Together, these factors have contributed to the shift toward decentralized energy generation. At the same time, recent global conflicts highlighted the volatility of energy markets, the vulnerability of the supply chain, and our heavy reliance on fossil fuels [4]. The Russo-Ukranian war is a clear example of how geopolitical events can dramatically disrupt the energy market, as shown in Figure 1.1 with the increase in energy prices. The plot displays a gradual rise in energy prices linked to the escalating tensions between Russia and Ukraine, followed by a significant spike across multiple energy vectors after the invasion of Ukraine in February 2022. In response to this crisis, the European Union (EU) launched the REPowerEU plan in 2022, aiming to reduce energy dependence and enhance resilience. This initiative has already led to an 18% reduction in overall gas consumption [5] and a significant decline in EU imports of Russian pipeline, from over 40% in 2021 to 8% in 2023 [6].

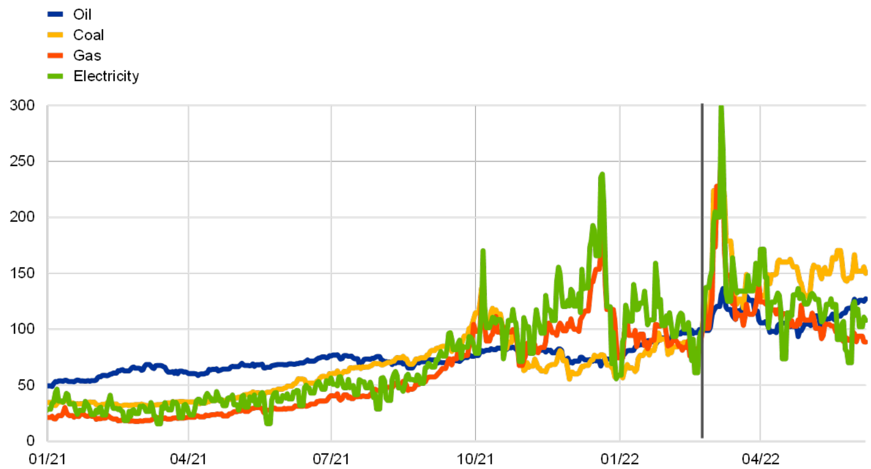

Figure 1.1: Energy prices before and after the invasion of Ukraine [7].

Energy communities offer a practical and decentralized solution to the challenges of centralized energy grids, addressing issues such as instability and high costs, while helping meet global sustainability goals [8]. Building on this concept, a Renewable Energy Community (REC) emphasizes sustainable energy sources like solar, wind, and biomass. RECs pool resources in clean energy projects, acting as unified entities that can compete equally in energy markets [9]. Under EU law, they can adopt various legal forms, including cooperatives, non-profits, associations, partnerships, or limited liability companies [10].

The EU adopted the Renewable Energy Directive (RED) (2018/2001/EU), which came into force in December 2018, marking a significant step toward empowering both consumers and RECs. The mandate focused on simplifying administrative processes, which have often delayed renewable energy projects because authorization bodies lacked transparency and coordination [11].

Among the EU member states, Portugal has several initiatives with RECs. One notable example is Cleanwatts' *100 Villages* project, which aims to establish at least 100 RECs in rural areas [12]. A successful case is the energy community in Miranda do Douro, which operates with a PV production capacity of 73.3 kWp and reported estimated savings of 31,500 € in its first year of operation [13].

RES's inherent volatility of solar and wind generation due to weather conditions and time of day presents a challenge for communities and other bodies. A common approach to overcome the problem of production variability is energy storage to satisfy both demand and cost reductions [14]. Among these, H_2 storage stands out as a more sustainable option than traditional Battery Energy Storage System (BESS) due to its potential for large-scale, long-duration storage and its ability to be produced from renewable sources [15]. Recent advancements in electrolyzer technology and increased availability of renewable energy are driving down costs. Investments in research, government incentives, and the growing global focus on energy transition are further accelerating its affordability. These developments pave the way for H_2 to become a competitive and scalable solution for widespread adoption [16].

According to the 2021 International Energy Agency (IEA) roadmap, by 2050, nearly half of the necessary reductions will depend on innovations currently in the prototype or demonstration phase. H_2 electrolyzers are among the most promising areas for innovation as this technology is vital for producing clean H_2 at scale, which can serve as a key energy carrier for decarbonizing different sectors [17].

In this view, this dissertation focuses on studying the viability of integrating H_2 in RECs while understanding its effects based on market architectures. The goal is to assess the impact that H_2 may have in RECs, accounting for different scenarios to explore how its operation behaves with different Distributed Energy Resources (DER)s.

1.2 Objectives

The decarbonization of several sectors (e.g., industry, energy, etc.) will rely significantly on the ability to produce and integrate H_2 into these systems. To speed up such integration, energy communities may play a crucial role by democratizing energy access and distribution among their members. Hence, this dissertation aims to develop a methodology for managing RECs that integrate local H_2 production.

In this context, this dissertation will explore the integration of a REC made up of several members, each equipped with DERs like PV systems, BESS, and Electric Vehicles (EV) with a Power-to-Hydrogen (P2H) system. The simulations will be performed using Python and will involve modifying a sizing and optimization algorithm to model how the energy community and P2H operate.

In this way, the specific objectives for this dissertation are the following:

- Analyze the integration of P2H systems in RECs, focusing on technical feasibility, economic performance, and their impact on energy self-sufficiency and sharing;
- Design and implement a methodology for optimal sizing and operational management of P2H systems in a REC context;
- Integrate P2H system model into the REC sizing tool for optimal DER selection and the REC operation tool for simulating community performance and internal energy flows;

The goal is to deliver a methodology for integrating P2H systems into RECs to enhance their economic and operational performance. This involves evaluating the impact H_2 can make in decentralized setups under a Peer-to-Peer (P2P) market.

1.3 Related projects and publications

The work developed in the scope of this dissertation partially concerns the objectives and results of two research projects, namely:

- BEFLEXIBLE - Boosting Engagement to Increase Flexibility - European Union's Horizon 2020, No. 101075438;
- ENPOWER - Energy Activated Citizens and Data-Driven Energy-Secure Communities for a Consumer-Centric Energy System - European Union's Horizon 2020, No. 101096354;
- DECMERGE - Decentralized decision-making for multi-energy distribution grid management
(2021.01353.CEECIND).

The developed work has resulted in the writing of one scientific paper for journal publication. The following should be referred to:

- David Machado Reis, Luís Rodrigues, Tiago Soares, José Villar, "Integration and operation of power-to-hydrogen systems in renewable energy communities", Electric Power Systems Research (EPSR), ongoing;

1.4 Structure of the Dissertation

This section outlines the structure of the dissertation and briefly summarizes each chapter:

- Chapter 1 introduces the topic, motivation, and main objectives, and provides an overview of the dissertation's structure.
- Chapter 2 reviews the fundamentals of H_2 technologies and RECs, including production methods, P2P market models, and key literature and projects.
- Chapter 3 details the integration of P2H systems into the REC modeling framework. It describes the community structure, the sizing methodology using Sizing Individual and Shared Assets for Energy Communities (SITEC), and the operational modeling with Optimal Scheduling Tool for Energy Communities (OSTEC), including tool modifications to support H_2 integration.
- Chapter 4 presents simulations of the REC under different scenarios. It includes community characterization, DER sizing results, sensitivity analysis, and comparing baseline and alternative scenarios to assess performance and internal energy dynamics.
- Chapter 5 summarizes the main findings, highlights key contributions, and suggests future research directions in hydrogen integration for energy communities.

Chapter 2

State of the Art

2.1 Hydrogen

Hydrogen is the most abundant element in the Universe, accounting for approximately 75% of its mass. As the simplest and lightest element, it consists of a single proton, making it fundamental to the structure of matter. Hydrogen is colorless, odorless, and highly flammable. Under Standard Temperature and Pressure (STP) conditions (25ºC and 1 bar pressure), H_2 can be encountered in a gaseous state. Despite its prevalence, H_2 is relatively rare in the Earth's atmosphere, as it readily escapes into space. However, H_2 plays a crucial role in forming water, which dominates Earth's oceans and sustains life [18].

Hydrogen was first observed in the 1500s by Paracelsus and later by Robert Boyle, but it was not until 1766 that Henry Cavendish identified it as a distinct gas. He demonstrated that burning hydrogen produces water, challenging the earlier belief that water was an element. Antoine Lavoisier later named the gas "hydrogen", meaning "water-former" [19].

H_2 forms weak bonds with nearby oxygen, nitrogen, or fluorine atoms, known as H_2 bonds. These bonds are what give water many of its unique properties. Without them, water's boiling point would drop below -70ºC, making liquid water impossible on Earth, a change that would profoundly affect the planet's ability to support life as we know it [19].

Table 2.1 contains some general data about H_2 at STP.

Table 2.1: H_2 physical properties [19].

Property	**Value**	**Unit**
Boiling point	-253	ºC
Melting point	-259	ºC
Density	0.0899	kg/m^3
HHV	39.4	kWh/kg
LHV	33.3	kWh/kg

Energy density measures how much energy a fuel can release per unit of volume or mass. H_2 stands out among energy sources for its exceptionally high energy density by weight (gravimetric, as seen in Figure 2.1) but relatively low energy density by volume [20]. The amount of heat released when a fuel is completely burned can be classified as Lower Heating Value (LHV) or Higher Heating Value (HHV). The difference between LHV and HHV lies in the recovery of latent heat in the vaporized water through condensation, in addition to the heat released from the fuel [21].

Unlike traditional fossil fuels such as oil or Natural Gas (NG), H_2 combustion produces only water vapor as a byproduct when burned in pure oxygen, emitting no carbon dioxide CO_2 or other Greenhouse Gases (GHG). This makes H_2 a cleaner and more environmentally friendly energy carrier.

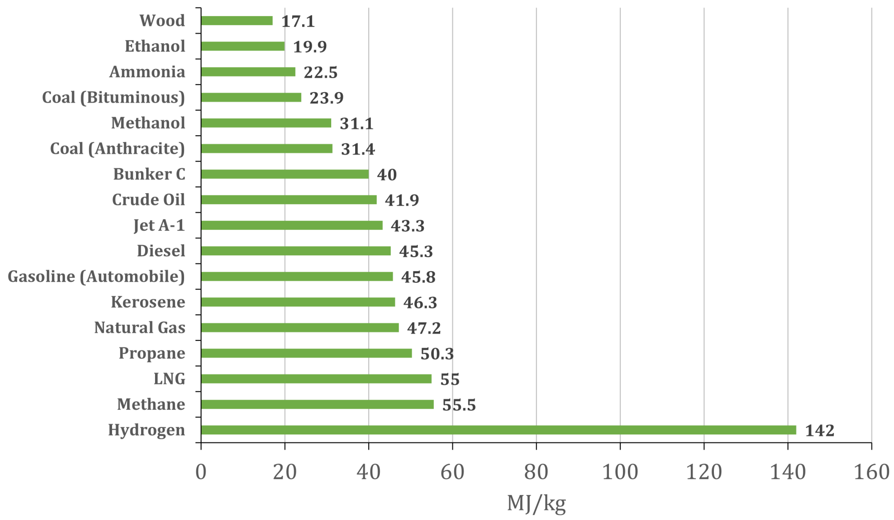

Figure 2.1: Gravimetric energy density of multiple fuel sources [20].

2.1.1 Hydrogen color spectrum

Hydrogen is a versatile energy carrier, often considered vital for a sustainable energy future. However, its production methods significantly impact its environmental footprint, which is why the "H_2 color spectrum" categorizes these methods, offering clarity on their ecological and energy implications [22]. The various methods can be seen in Figure 2.2.

Green hydrogen is the most sustainable form, produced by electrolyzing water using RESs such as wind, solar, or hydropower. This method emits no GHG, making it crucial for decarbonizing industries and achieving net-zero targets. Compared to other production methods, it represents a small share of the total H_2 production due to its high production cost [23].

Grey H_2 is achieved through an endothermic process known as Steam Methane Reforming (SMR). The reaction necessary to produce grey H_2 is shown in Equation 2.1, releasing 5.5g of carbon dioxide (CO_2) per gram of H_2 produced [24].

$$CH_4 + 2H_2O \rightarrow 4H_2 + CO_2, \qquad \Delta H_0 = 41.25 \text{kJ/mol } H_2 \tag{2.1}$$

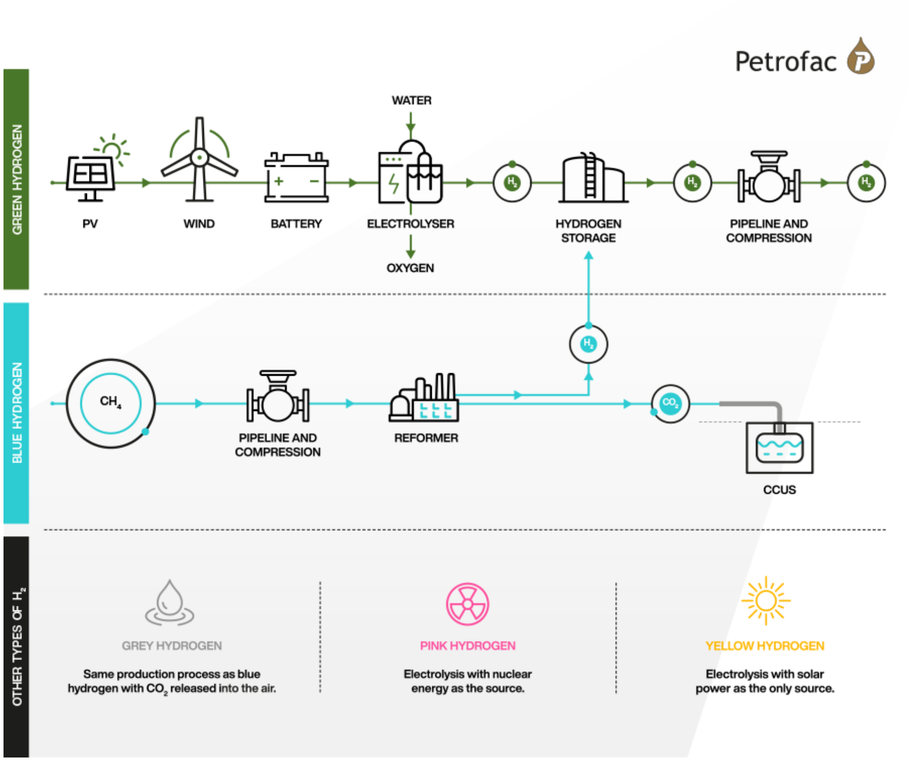

Figure 2.2: Hydrogen color spectrum [22].

Blue H_2 is similar to grey H_2 because both are produced from NG. The key distinction lies in handling CO_2 emissions. During blue H_2 production, the CO_2 generated is captured and stored, often in depleted oil or gas fields, through a process known as Carbon Capture and Storage (CCS) [25].

Pink H_2 is produced through water electrolysis powered by electricity from nuclear energy. Similarly, purple H_2 involves nuclear power but combines electricity and heat for electrolysis and thermochemical water splitting [26]. Red H_2, on the other hand, uses nuclear thermal power to split water at high temperatures through a catalytic process. While these terms have subtle differences, some argue they can be grouped due to their reliance on nuclear energy. This production method is promising as it does not depend on weather patterns, and its generation can be controlled [27].

The global H_2 demand continued to grow in 2023, reaching a peak of 97 megatonnes, representing a 2.5% year-over-year increase relative to 2022. Figure 2.3 presents the global distribution of hydrogen demand by region. China is the largest hydrogen consumer, accounting for approximately 29% of global demand, followed by the rest of the world (24%) and North America (16%). Regional H_2 demand grew across most major markets, except for the Middle East, which experienced a substantial increase, exceeding 6% year-over-year. This surge is attributed to increased demand within the refining and methanol production sectors [29].

In Europe, hydrogen demand in 2023 was 7.93 megatonnes, representing a 3.2% decline compared to the previous year. Sectoral analysis reveals that petroleum refineries constituted the pri-

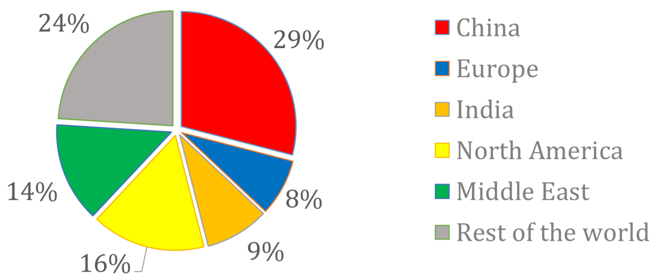

Figure 2.3: Total hydrogen demand by region in 2023 [28].

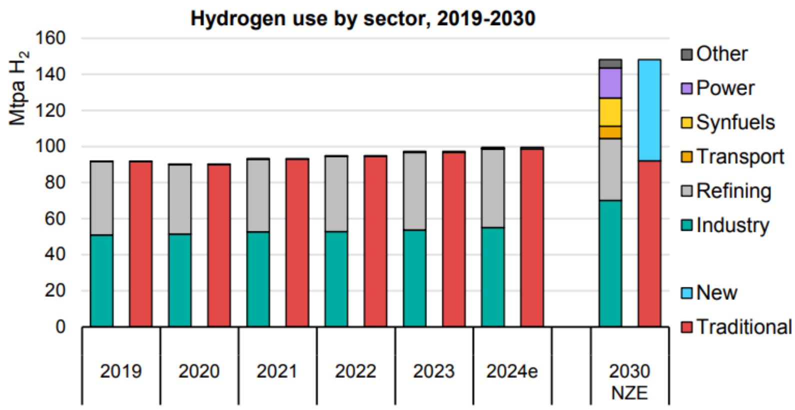

Figure 2.4: Hydrogen demand by sector [29].

mary consumer of H_2, representing 57% of the total European H_2 consumption, shown in Figure 2.4. The ammonia synthesis industry represented the second-largest consumer, with 25% of the total. Collectively, these two industrial sectors accounted for 82% of the total European hydrogen consumption. The demand for low-carbon hydrogen, comprising less than 0.4% of the total European demand, is primarily driven by applications in industrial thermal processes and mobility solutions [30].

2.2 Water electrolysis

Water electrolysis is the process of splitting water into hydrogen and oxygen gases using electricity. Electrolysis involves two reactions at the electrodes, requiring a minimum potential difference of 1.23 V to overcome thermodynamic barriers [31].

$$\text{Anode} : 2H_2O \rightarrow O_2 + 4H^+ + 4e^- \tag{2.2}$$

$$\text{Cathode} : 4H^+ + 4e^- \rightarrow 2H_2 \tag{2.3}$$

Figure 2.5 shows how water molecules split into oxygen gas, protons, and electrons during water electrolysis at the anode. The protons move through the electrolyte to the cathode, while the electrons travel through an external circuit. At the cathode, the protons and electrons form hydrogen gas [31, 32]. The rate of hydrogen production is directly linked to the current applied,

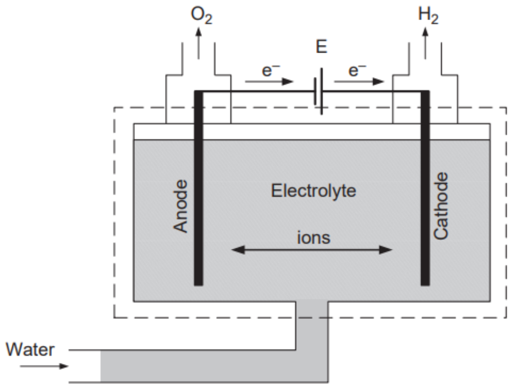

Figure 2.5: Diagram of water electrolysis [33].

as it dictates the number of electrons available to drive the reactions [34].

2.2.1 Electrolyzer technologies

Electrolyzers are the core components in water electrolysis systems, responsible for splitting water into hydrogen and oxygen using electricity. These devices are generally classified based on the type of electrolyte they use, liquid or solid, and their operating temperature. Figures 2.6 and 2.7 provide a visual overview of the main electrolyzer types currently in development or commercial use [35].

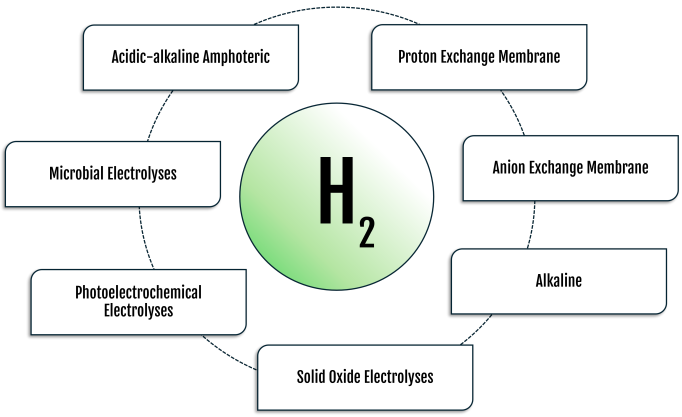

Figure 2.6: Electrolyzer technologies, adapted from [32].

Among the various types, Alkaline Water Electrolyzer (ALK) is the most established and widely used technology. It operates using a liquid electrolyte, typically a potassium hydroxide (KOH) solution, and separates the hydrogen and oxygen gases with a porous diaphragm. One of ALK's strongest advantages is its relatively low capital cost, making it an attractive choice for large-scale applications. Additionally, it has a long operational lifespan and can rely on more affordable, non-noble metal catalysts, which helps keep ongoing costs down [36].

ALK has its limitations, as it tends to operate at lower current densities, which means it can't produce hydrogen as quickly as some other technologies. Furthermore, its slower response time to changes in power input can make it less suitable for integration with highly variable renewable energy sources like solar or wind [32].

Proton Exchange Membrane Electrolyzer (PEME) represents a newer generation of technology and is gaining traction, especially in applications where rapid response and system compactness are crucial. Instead of a liquid electrolyte, PEME uses a solid polymer membrane to conduct protons from the anode to the cathode. This design allows the system to react quickly to changes in power input, making it ideal for pairing with intermittent renewables.

PEME systems are also capable of operating at higher current densities than ALK, which enables greater hydrogen production rates in smaller footprints. However, these benefits come at a cost. The acidic environment in which PEME operates requires the use of expensive noble metal catalysts, such as platinum or iridium, and corrosion-resistant materials throughout the system. These requirements drive up both the capital and operational expenses [32].

Solid Oxide Electrolyzer (SOE) takes a different approach by operating at high temperatures, typically between 600 and 850°C. This elevated temperature environment enables the use of ceramic electrolytes that transport oxygen ions rather than protons. One of the main advantages of SOE is its high efficiency, as part of the energy required for water splitting comes from thermal sources rather than electricity alone. This makes SOE particularly attractive for integration with high-temperature industrial processes or systems that can supply waste heat, such as ammonia, chemical, and steel plants [37]. High operating temperatures cause thermal expansion and contraction that can degrade materials over time. The repeated heating and cooling cycles also place stress on system components, limiting durability and complicating commercialization efforts. As a result, SOE remains in the demonstration or pilot stage for most applications [32]. The diagram

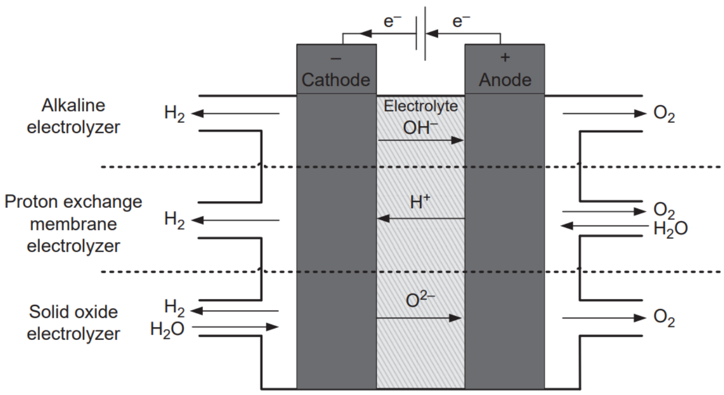

Figure 2.7: Water electrolysis types [33].

in Figure 2.7 shows that the fundamental difference lies in the ionic agent transported through the electrolyte. In an ALK, negatively charged hydroxide ions OH^- are formed at the cathode from the reduction of water and migrate to the anode to produce oxygen. For the PEME, the process is reversed in polarity; positively charged protons H^+ are generated at the anode and travel across a solid membrane to the cathode to form hydrogen. The SOE uses a solid ceramic electrolyte to transport doubly-negative oxide ions O^{2-} from the cathode, where steam is reduced, to the anode, where oxygen gas is formed. As Figure 2.8 illustrates, alongside mature technologies like ALK,

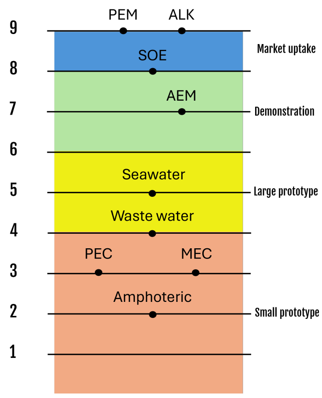

Figure 2.8: TRL of various electrolyzer technologies, adapted from [38].

PEME, and SOE, several emerging electrolyzer concepts are being developed at lower Technology Readiness Level (TRL) levels. Anion Exchange Membrane (AEM) electrolysis, for example, combines benefits of ALK and PEME but still faces challenges in stability. Seawater and wastewater electrolysis aim to reduce freshwater use, though technical hurdles persist [39]. Additionally, Photoelectrochemical (PEC) and Microbial (MEC) systems explore integrating solar or biological processes, while amphoteric electrolyzers are designed for broader pH operation. Despite their potential, these technologies remain largely experimental [40, 41].

Several types of electrolyzers are available today, each with its strengths and trade-offs. Table 2.2 gives a simple comparison between the main technologies.

Table 2.2: Comparative overview of electrolyzer technologies.

Attribute	**ALK**	**PEME**	**SOE**
Electrolyte	KOH (liquid)	Solid polymer	Ceramic (solid)
Operating Temp.	60–80°C	50–80°C	600–850°C
Efficiency	Moderate	High	Very high
Response Time	Slow	Fast	Slow (due to heat-up)
Capital Cost	Low	High	Moderate to High
Materials	Abundant metals	Noble metals	Ceramic materials
System Lifetime	Long	Moderate	Under development
Technology Maturity	Commercial	Commercial	Pre-commercial
Main Advantages	Low cost, durable	Compact, responsive	High efficiency, reversible
Main Challenges	Slow dynamics	High cost	Thermal stress, startup time

2.3 Fuel cells

While electrolyzers use electricity to produce hydrogen, fuel cells do the reverse: they convert hydrogen into electricity through an electrochemical process, emitting only water and heat as by-products. This makes them a key enabling technology for clean energy systems, particularly in applications requiring efficient, low-emission power generation [42]. The reaction that produces electricity comes from Equation 2.4.

$$2H_2 + O_2 \rightarrow 2H_2O - \Delta G \tag{2.4}$$

The Gibs free energy change (ΔG) describes the maximum amount of useful electrical work that can be extracted from the system under constant pressure and temperature. The total energy released by this reaction is given by the enthalpy change (ΔH), which includes both electrical work and heat. However, only ΔG is convertible into electrical energy, as the rest is converted into heat. At STP conditions, $\Delta G = -237.13\text{kJ}/\text{mol}$ and the total enthalpy change is $-285.83\text{kJ}/\text{mol}$, which indicates that the ideal efficiency for electricity production is 83% [43].

$$\frac{\Delta G}{\Delta H} = \frac{-237.13}{-285.83} \approx 83\% \tag{2.5}$$

In Figure 2.9, a general structure for the Fuel Cell (FC) can be seen.

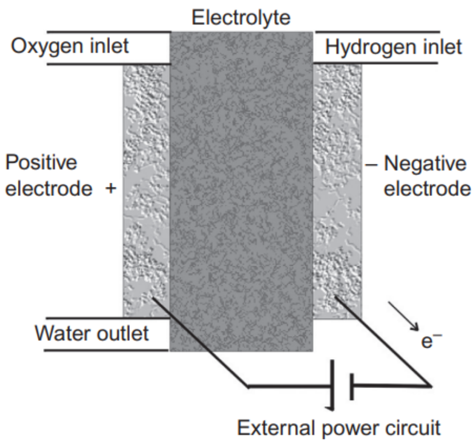

Figure 2.9: Fuel cell operation diagram [42].

Fuel cells are categorized based on the type of electrolyte used and their operating temperature, similar to electrolyzers. Each fuel cell type offers a different balance between efficiency, cost, durability, and application suitability.

Fuel cells vary widely in terms of operating conditions, fuel compatibility, and material requirements. Table 2.3 provides a summary of the key characteristics of five major types, highlighting differences in temperature range, efficiency, fuel flexibility, and catalyst use. These distinctions help determine their suitability for specific applications, from portable power to industrial-scale electricity and heat generation.

Table 2.3: Summary of key characteristics of major fuel cell types.

Parameter	AFC	PEMFC	PAFC	MCFC	SOFC
Temp. (°C)	<100	60–80	150–210	~650	600–1000
Efficiency	Up to 70%	40–60%	40–60%	50–60%	50–60%
CHP Option	–	–	Yes	Yes	Yes
Fuel Type	H_2/O_2	H_2	H_2, CO	NG, Biogas	HC, H_2
Power Density	Med	High	Low	Med	Low–Med
Catalyst	Ni, Ag	Pt	Pt	Ni[44]	Ceramic
Source	[45]	[44]	[45]	[44]	[46]

2.4 Variable efficiency of electrolyzer and fuel cells

Traditional models for electrolyzers and FCs often assume a fixed efficiency. To achieve a more realistic simulation, one can consider a variable efficiency that depends on the power input. The efficiency of this equipment is inherently nonlinear, which makes it unsuitable for a Mixed-Integer Linear Programming (MILP). To address this challenge, a piecewise linearization approach is employed. This approach segments the nonlinear efficiency curve into multiple linear intervals, each represented by a slope and an intercept. This allows for a linear representation of variable efficiency within the PuLP optimization framework [47].

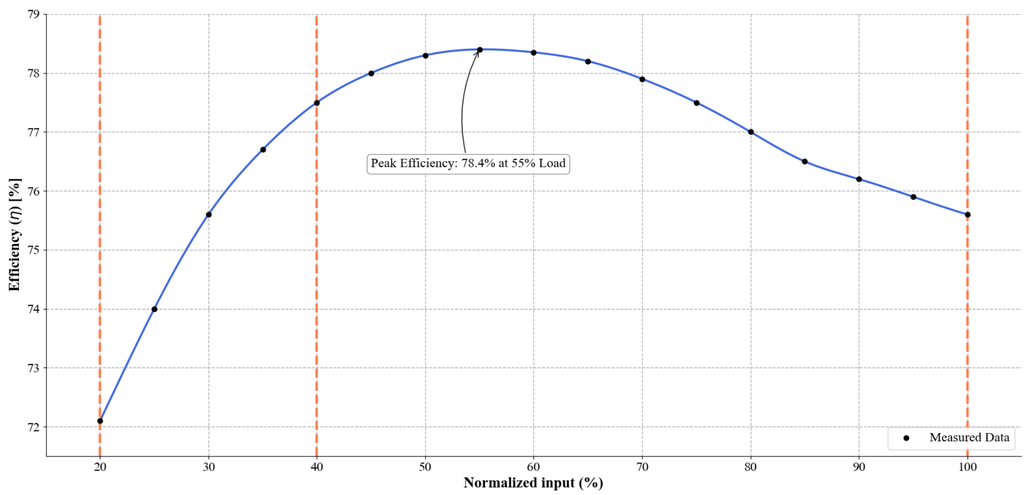

Figure 2.10: Efficiency curve of an electrolyzer.

The normalized power input determines the efficiency of the electrolyzer, as seen in Figure 2.10, which can be used to calculate the output of the mass of H_2 by applying the following formula:

$$m(P) = \frac{\eta(P)}{100} \cdot \frac{P}{100} \cdot \frac{\hat{P}_n}{\hat{\mathrm{HHV}}} \tag{2.6}$$

where $m(P)$ represents the mass of hydrogen produced for a given normalized input, $\eta(P)$ is the resulting efficiency, $\hat{P}_n$ is a parameter that defines the power rating of the electrolyzer, and $\hat{\mathrm{HHV}}$ the higher heating value for H_2. It has a constant value of 39.4 kWh/kg. By sampling points from the efficiency curve and applying Equation 2.6, we can obtain the mass of H_2 produced for a given normalized power input.

To incorporate this into a linear optimization model, the curve is approximated by a set of linear segments. For a partition of the curve into s segments, the mass output is given by:

$$m(P) = \begin{cases} \hat{A}_1 \cdot P + \hat{B}_1, & P_1 \leq P \leq P_2 \\ \vdots \\ \hat{A}_s \cdot P + \hat{B}_s, & P_s \leq P \leq P_{s+1} \end{cases} \tag{2.7}$$

Each segment is characterized by a slope $\hat{A}_s$ and a y-intercept $\hat{B}_s$, which are calculated as follows:

$$\hat{A}_s = \frac{m_{s+1} - m_s}{P_{s+1} - P_s} \tag{2.8}$$

$$\hat{B}_s = m_s - \hat{A}_s \cdot P_s \tag{2.9}$$

For $s = 2$ segments and by picking points 20, 40 and 100 % we can reach the linear approximation presented in Figure 2.11a: Figure 2.11b compares the original nonlinear efficiency curve of the

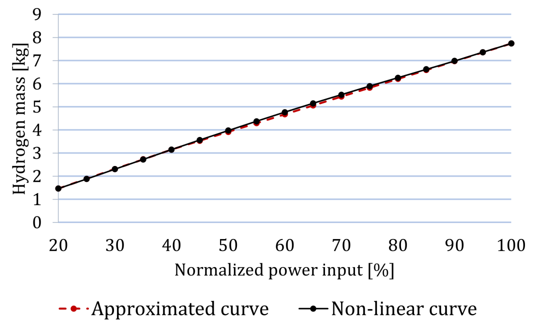

(a) Approximated and non-linear hydrogen mass output ($s = 2$).

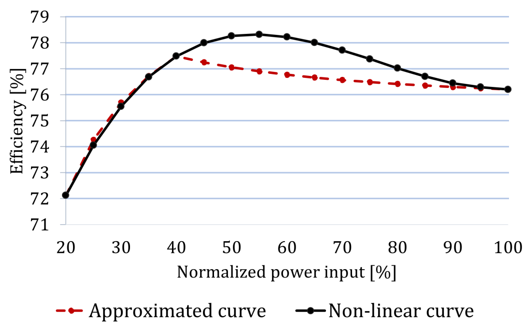

(b) Variable efficiency curve.

Figure 2.11: Comparison of hydrogen mass output and efficiency curves.

electrolyzer with its piecewise linear approximation. This simplified model captures the overall trend well while keeping the formulation computationally manageable. Such a trade-off is essential for compatibility with MILP formulations, which require linear constraints. In Figure 2.12, we observe that increasing the number of segments reduces the approximation error, with both the Mean Absolute Error (MAE) and Root Mean Squared Error (RMSE) decreasing as more breakpoints are introduced. However, this improvement plateaus beyond a certain point, indicating that

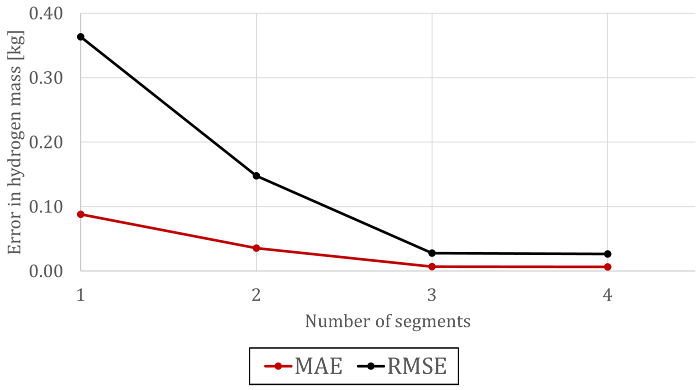

Figure 2.12: MAE and RMSE values for increasing segment counts in the piecewise linearization.

a trade-off between model complexity and accuracy must be considered.

2.5 Renewable energy communities

Recent revisions to the RED III have positioned RECs as a core mechanism for achieving the EU's accelerated renewable energy targets, now set at 45% by 2030 [48]. While policy frameworks emphasize inclusion and citizen empowerment, particularly for low-income households, implementation still faces practical, technical, and regulatory challenges.

In the academic and technical literature, RECs are increasingly examined as decentralized systems capable of integrating diverse DERs, such as PV, wind, and BESS. Studies explore their potential to enhance grid flexibility, reduce energy poverty, and support prosumer participation [49]. However, gaps remain around the scalability of REC models, especially when incorporating emerging technologies like H_2 storage, P2P trading, or dynamic pricing mechanisms [50].

Furthermore, although the RED encourages equitable participation, it leaves open questions about how to operationalize accessibility in diverse socioeconomic contexts. Research efforts are beginning to address these issues, but a consistent framework for REC planning, governance, and financing is still lacking across Member States.

2.5.1 Definitions

The EU defines two main types of energy communities: RECs and Citizen Energy Community (CEC)s. Both aim to empower local actors in the energy system, though they differ slightly in their scope, regulatory frameworks, and the types of energy they handle [51].

CECs are legal entities that produce, consume, store, and sell renewable and non-renewable energy. They operate under democratic governance and focus on delivering environmental, social, and economic benefits to the community rather than maximizing financial profit. CECs welcome a broad range of participants, including households, small businesses, and local authorities, without limiting involvement based on proximity to the energy projects [52].

RECs focus exclusively on RES. They share many characteristics previously mentioned for CECs regarding the production and allocation of energy. A key characteristic of RECs is local ownership and control, i.e., members and shareholders must reside near the community's renewable installations and have decision-making authority. These communities operate independently and prioritize providing environmental, social, and economic benefits to their members and the surrounding area over financial profit [53].

In both RECs and CECs, the community consists of citizens who can join as members or shareholders, alongside small businesses and local authorities [53]. These participants actively produce, manage, and utilize energy within their communities. Participation is voluntary, open, and inclusive, ensuring that the community's interests and priorities are reflected [54].

Within the scope of a REC, surplus energy may arise for certain members, which can be shared with others in the community to minimize overall energy costs. This leads to two distinct forms of self-consumption: Individual Self-Consumption (ISC), where a single member uses the energy they generate for their own needs, thereby reducing reliance on the public grid, and Collective Self-Consumption (CSC), which enables multiple members to share locally generated energy collaboratively, distributing it according to individual consumption profiles [55].

The core concept of energy communities is to actively involve citizens in the local production and management of energy [56], and the organizational structure may differ, as shown in Figure 2.13.

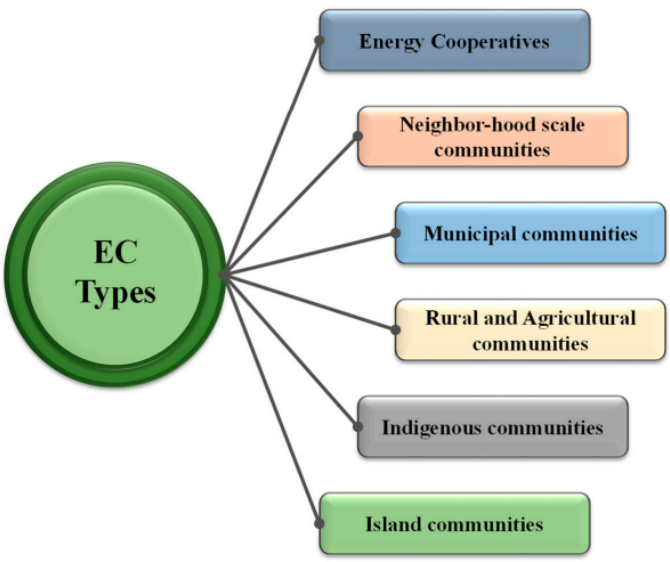

Figure 2.13: Scope of energy communities per application [57].

These entities prioritize community benefits and promote local economic development over profit maximization [57]. Sharing energy for maximum social welfare implies that members share their surplus electricity at a lower price with vulnerable members, thus mitigating energy poverty. RECs can respond to three significant global challenges: energy poverty, supply and security, and climate change [58, 59].

A practical example of these principles in action is OurPower. Founded in Vienna in 2018, which is a cooperative-based REC that facilitates P2P electricity trading between over 300 local producers and 1,100 consumers. In Figure 2.14, the multiple energy suppliers situated across Austria forming an extensive REC. It combines PV installations (10 kW to 4 MW) with other

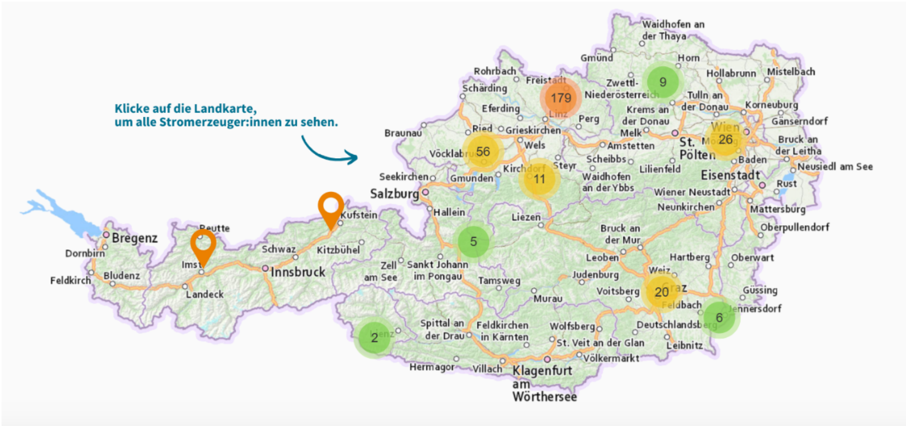

Figure 2.14: OurPower's extent over Austria [60].

RES like wind and hydro. Its business model hinges on community crowdfunding and cost-sharing, with producers setting prices (e.g., 0.13 €/kWh) and consumers paying slightly more (e.g., 0.185 €/kWh) to cover grid and operational costs [61].

In 2019, Minoan Energy established a REC that has grown to more than 400 members, individuals, municipalities, and small businesses. The REC operates PV systems to cover the consumption needs of the members. Becoming a member requires an initial investment in shares, which is reimbursed upon leaving the REC, and additional shares can be bought to support new projects that include wind turbines, PV or biomass [62].

Figure 2.15: PV installation to supply REC in Minoa, Greece [63].

The PV installation shown in Figure 2.15 is 405 kWp, and it is designed to supply energy to households and businesses over the following 25 years. It spans a total area of 5500 m^2 at Sarafali

Mantra in the Municipality of Minoa Pediada and is implemented with virtual net metering, which allows consumers to benefit from energy generated at a remote location by receiving proportional credits on their electricity bills [63].

2.5.2 Tariff structures

The REC members use the public grid infrastructure to conduct energy transactions. Since the generation and consumption units are connected through the public grid, the self-consumption regulations for public grid use are applicable. This means grid access tariffs must be paid on the value of the shared energy. That payment is REC's managing entity's responsibility and the billing amount is paid to the Distribution System Operator (DSO) [64].

The grid access tariff covers the shared costs of infrastructure and services used collectively by consumers. This includes the technical system operation tariff, transmission network tariff, and distribution network tariffs, added together to form the total [65].

2.5.3 Allocation coefficients

In Portugal, the allocation of energy in a CSC scheme is regulated by *Regulamento n.º 815/2023*, issued by the Entidade Reguladora de Serviços Energéticos (ERSE). This regulation outlines how much energy each participating community member receives from locally generated sources, based on pre-established Allocation Coefficients (AC) or energy sharing coefficients [66]. The Entidade Gestora de Autoconsumo Coletivo (EGAC) is tasked with selecting the allocation method and communicating the corresponding coefficients to the DSO. The four types of AC models described in the regulation are illustrated in Figure 2.16 and summarized as follows:

- **Fixed AC** – Constant shares for each member set by EGAC during licensing. These can vary by day type and season. If a member doesn't consume their share, the ACs of other members are adjusted proportionally to keep the total at 100%.

- **Proportional Coefficients** – Allocation is based on each member's consumption, with the DSO distributing the local surplus proportionally among active members.

- **Hierarchical Sharing** – Energy is allocated within and between predefined groups based on rules from the CSC manager to the DSO. Any surplus left after group allocation can be shared with other groups.

- **Dynamic Sharing** – The CSC manager submits the ACs post-metering to the DSO, which checks that the coefficients are positive and total 100%, using them to allocate energy among members.

For the fixed and proportional sharing models, coefficients must be communicated in advance and remain valid for the billing cycle unless updated. In contrast, dynamic sharing enables coefficients to be submitted retrospectively, allowing communities to adjust distributions according to

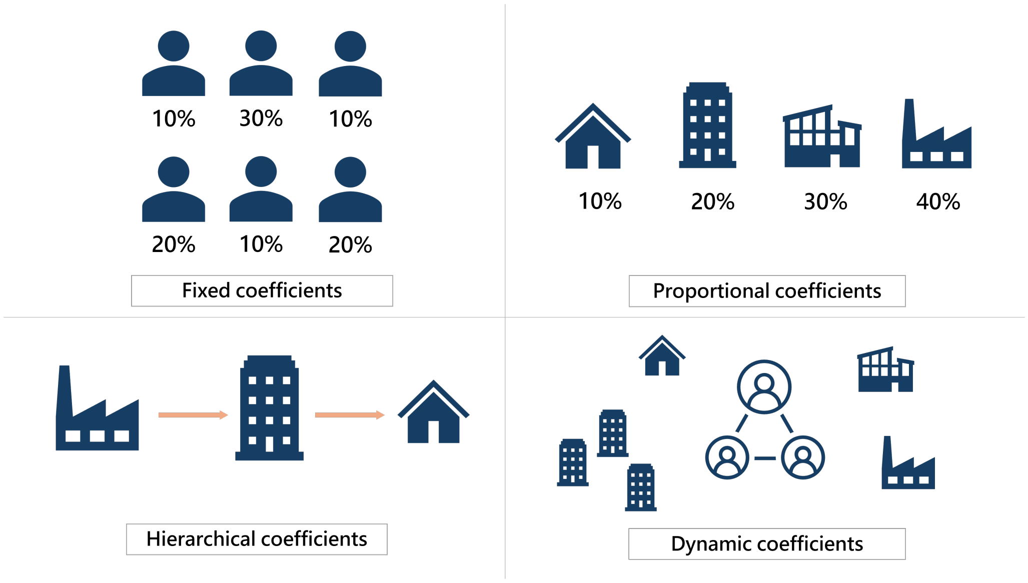

Figure 2.16: AC types.

real-time consumption patterns [67]. It is important to note that these rules are specific to Portugal and derive from the national regulatory framework. While some of these models (particularly fixed and proportional) are found in other EU countries, their definitions, implementation, and legal requirements can vary significantly.

In Spain, the *Royal Decree 244/2019* was a major development for the sector, as it established the technical, administrative, and economic conditions for self-consumption, including the legal framework for collective self-consumption and energy sharing among multiple users connected to the same low-voltage transformer [68]. ACs are referred to as β coefficients [69]. The regulation grants full flexibility to the participants to agree on the criteria for distribution, which can be based on: energy consumption, contracted power, ownership share in the property and contribution to installation costs.

Spain has an additional variation of the fixed coefficients, hourly fixed coefficients, where each hour of the year may have a different distribution profile. This second option enables the adaptation of energy sharing to match user-specific demand profiles. This flexibility not only supports fairness but also enhances the efficiency and responsiveness of energy communities to actual consumption patterns [70].

2.5.4 Market architectures

2.5.4.1 Full peer-to-peer

In full P2P architectures, participants directly interact with energy trading without the involvement of a centralized entity. Each peer can engage in bilateral negotiations and energy transactions, allowing for complete autonomy and flexibility [71], as seen in Figure 2.17. Buyers' decisions are shaped by their distance from sellers, the prices offered, and the current market price [72]. Negotiations become more complex, and profits diminish over longer distances, which may limit P2P markets to operate within local distribution networks and smaller regions [73]. The system's bottom-up design enables localized energy trading, reducing dependence on traditional energy retailers [74].

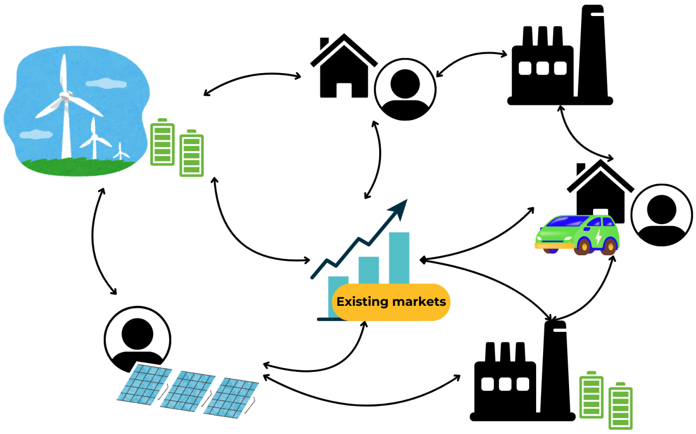

Figure 2.17: Full P2P design, adapted from [71].

The distinction between a community market, or CSC, and a P2P market lies in their objectives. Whereas a P2P market emphasizes individual autonomy and competition through the engagement of users with the energy market, the CSC is often non-profit-oriented and focuses on collective outcomes [73].

2.5.4.2 Community-based

In centralized frameworks, the energy community is treated as an entity that manages transactions and resources collectively. Typically, a community manager oversees energy management, which includes operating community assets and determining how energy and costs are allocated among members. In most cases, energy bills are calculated using standard retailer prices. However, when the community functions as a single entity with multiple members, determining individual bills becomes more complex [75]. This complexity arises due to variations in asset ownership and energy consumption patterns among community members.

Several methods for distributing costs or benefits, commonly referred to as bill repartition, have been developed to address this. These include approaches based on game theory, optimization techniques, and rule-based control strategies, each tailored to meet specific objectives. In parallel, community-led energy initiatives have increasingly been defined as "grassroots innovations," emphasizing technological advances and the social innovation required to create new decision-making frameworks and shared value systems [76].

The interaction between community managers, members, shared assets, and existing markets is illustrated in Figure 2.18, which highlights the diversity of internal structures and energy exchange mechanisms that characterize community-based models.

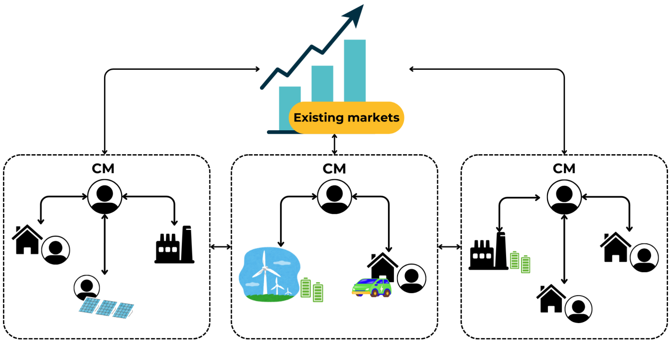

Figure 2.18: Community based design, adapted from [71].

2.6 Related projects and publications

In this section, the current state of P2H systems within RECs is shown in order to contextualize the developed dissertation work. This analysis contains three projects around the world that have been completed, or are still ongoing, with a focus on the electrolyzers, H_2 tanks, and fuel cells. Additionally, various relevant publications and their contributions are presented to determine H_2 impact on RECs. This review will present and analyze existing research on H_2 integration in REC and their main findings.

2.6.1 Projects review

This subsection provides an overview of 3 relevant projects, namely: *(i)* HydroGlen [77], *(ii)* SEAFUEL project in Tenerife [78],*(iii)* HyP SA [79].

2.6.1.1 HydroGlen

The HydroGlen project involves a research farm and residential community at Glensaugh (northeast Scotland). It is an ongoing project with unspecified completion time [80]. The HydroGlen project aims to show that rural and farming communities can become self-sufficient, low-carbon energy producers and even exporters. By combining RES with on-site H_2 production, compression, and storage, the project aims to demonstrate a practical path toward clean energy independence [80].

This initiative serves as a model for rural areas and the agricultural sector, which contributed 18.9% of Scotland's carbon emissions in 2022, as illustrated in Figure 2.19. By setting this example, HydroGlen will help Scotland move closer to its goal of achieving net-zero greenhouse gas emissions by 2045 [81].

Across all cases, an 800 kW wind turbine is the primary energy generator, with a PV system acting as a secondary energy source to compensate for periods of reduced wind generation. A 100 kWh BESS is installed for short-term energy storage and to reduce grid dependence. The Proton Exchange Membrane (PEM) electrolyzer produces H_2 at 30 bar and comprises several

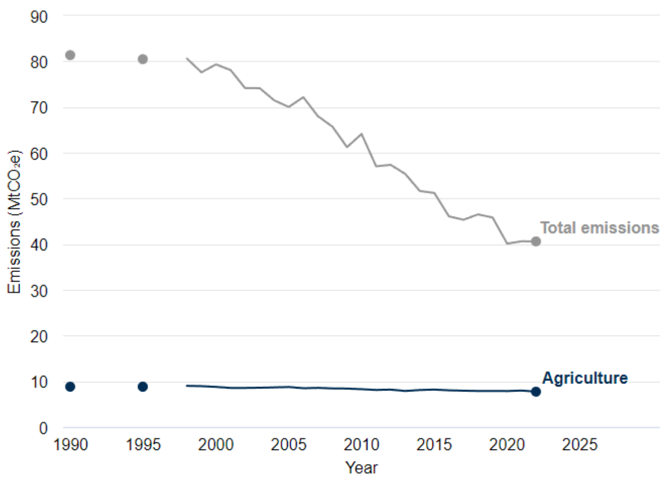

Figure 2.19: Scotland GHG emissions timeline [82].

stacks to facilitate scaling. The FC is a last resort to minimize grid imports when no renewable generation or stored energy in the BESS is available.

The first case represents the off-grid case, where the P2H system only operates with RES and can use both BESS and the FC to meet demand. It only considers two H_2 vehicles, and the remaining 10 are EV.

For the second case, a 100 kVA connection with the grid is established, and the amount of H_2 vehicles increases to 6, which implies the addition of PEM electrolyzer stacks to meet H_2 demand. The H_2 tank is reduced as the reliance on H_2 as energy storage is unnecessary due to the grid connection.

This increased demand necessitates a further scale-up of the electrolyzer power and an expansion of the H_2 tank. The PV is also increased to 150 kW to better support the higher renewable energy requirement. No EV or EV charging infrastructure is included in this configuration.

The base case demonstrated that an off-grid system requires significantly more H_2 storage to handle energy demand peaks compared to grid-connected scenarios (case 2 and case 3). Designed to maximize H_2 availability for the backup power FC, the base case incorporates just two H_2 vehicles, with the remainder of the fleet being battery-electric. The base case also results in the highest Levelized Cost of Electricity (LCOE) of the three scenarios, primarily due to the need for extensive backup storage [80].

In case 2, the study explores a balanced system where H_2 and EV are evenly distributed. Supported by a grid connection, this configuration meets all energy demands using direct power, H_2, and batteries. The grid connection provides balancing support and export opportunities, leading to the smallest H_2 storage requirement and the lowest LCOE of the three cases [80].

In case 3, the entire vehicle fleet runs on H_2, while the grid connection continues to provide balancing and export functions, as in case 2. H_2 production increases by 40% compared to case 2, however, overall storage needs are reduced because H_2 vehicles effectively act as additional H_2 storage units. This scenario also includes an additional 100 kW of solar PV, enhancing primary electricity generation. Although case 3 incurs a slight increase in LCOE due to additional electrolyzers and solar capacity, it significantly boosts available H_2 supply [80].

A case-study farm similar to a Glensaugh property analysis found that the current renewable system meets only 11% of the farm's commercial and residential demands and none of its transport needs. To address this, a hybrid PV and H_2 system was proposed, including additional PV capacity to increase renewable energy supply and a H_2 storage system to store surplus energy as green H_2 for transport fuel [83].

For HydroGlen, maintaining a grid connection with import/export capacity was found to be the most suitable configuration. This approach simplifies system design, reduces the need for redundancy during periods of low or zero renewable energy production, and provides opportunities to contribute clean energy to the national grid. Additionally, grid export facilitates revenue generation, enhancing the system's economic and operational viability [80].

2.6.1.2 SEAFUEL project in Tenerife

The SEAFUEL project highlights H_2's potential to decarbonize energy systems, stabilize grids, and foster energy self-sufficiency in island communities. The SEAFUEL project assesses Tenerife's energy resources and its readiness for H_2 adoption, producing targeted recommendations for policymakers. These measures outline how Tenerife and the broader Canary Islands can harness their unique societal and geographical strengths to develop a thriving H_2 economy [84].

Tenerife's renewable energy landscape is characterized by significant solar and wind potential. However, it is constrained by land availability, grid isolation, and high variability in energy demand. This makes H_2 a promising vector for energy storage and distribution [85]. In Figure 2.20,

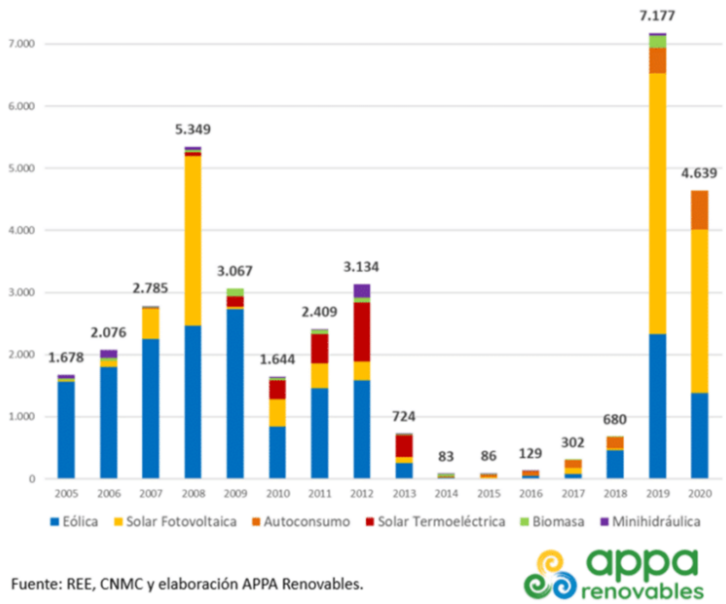

Figure 2.20: Installed renewable capacity per year in Spain [86].

one can observe significant investment in renewable energy capacity, although progress stalled between 2013 and 2018 due to unfavorable government policies. However, with the EU 's ambitious net-zero emissions targets and commitments under the Paris Agreement, interest in PV technology has surged, leading to a notable increase in capacity starting in 2019.

The SEAFUEL project highlights Tenerife's heavy dependence on fossil fuels, particularly oil, which dominates its energy landscape. Unlike mainland Europe, the island lacks access to natural gas and relies on a poor power grid that hinders the efficient development of modern energy systems. As shown in Figure 2.21, Spain historically relied heavily on fossil fuels, with renewables playing a minor role in its energy mix. However, recent (the last two decades) initiatives and incentives have driven a shift toward solar and wind energy, resulting in renewables accounting for 46.7% of the energy mix in 2021, which increased to 50.8% by 2023 [87].

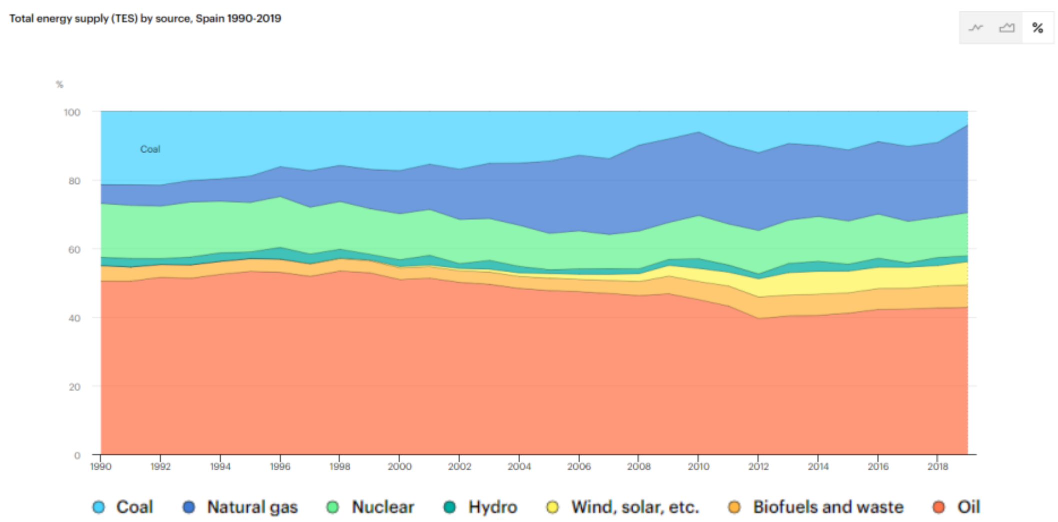

Figure 2.21: Total energy supply by source in Spain [86].

Hydrogen stands as a promising solution for carbon neutrality in Tenerife as it can repurpose its preinstalled PV panel capacity to produce green H_2. This approach offers two key advantages: *(i)* it reduces the need for costly and large-scale upgrades to the current grid infrastructure; and *(ii)* it addresses the island's seasonal energy supply and demand by allowing surplus energy to be stored as H_2 and used during periods of higher demand [77].

The SEAFUEL project explores using seawater for electrolysis, supported by an on-site seawater treatment plant that desalinates and prepares water for a PEM electrolyzer, as illustrated in Figure 2.22. Powered by surplus energy from wind turbines and PV panels, the electrolyzer splits water into H_2 and oxygen, with H_2 collected for compression and storage while oxygen is vented. The H_2 is compressed to 450 bar and stored in tanks capable of holding up to 30 kg. A 350-bar dispenser, similar to a standard fuel pump, refuels vehicles in 3–5 minutes, showcasing a practical and efficient green H_2 production and refueling system [77].

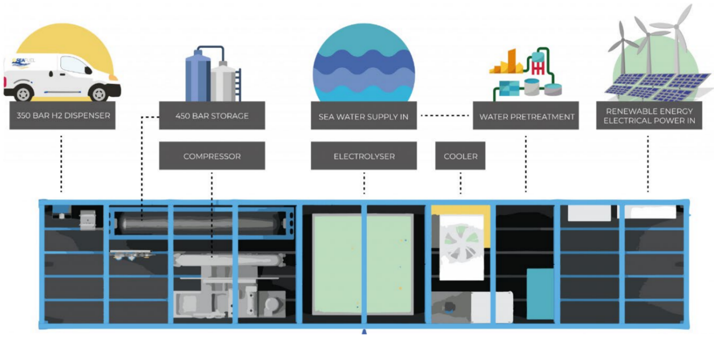

Figure 2.22: SEAFUEL project in Tenerife [77].

2.6.1.3 HyP SA

Hydrogen Park South Australia (HyP SA), located in the Tonsley Innovation District, is Australia's first green H_2 production project. Supported by a $4.9 million grant from the South Australian Government, the $14.5 million initiative aligns with the state's vision to leverage RES and infrastructure to become a global leader in H_2 technology and achieve net-zero emissions by 2050 [88].

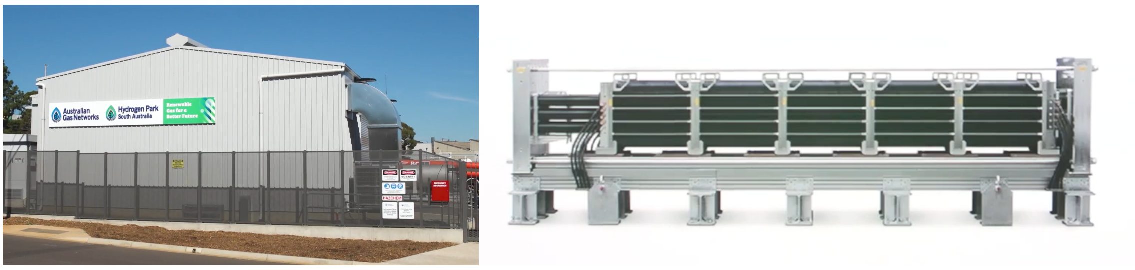

(a) (b)

Figure 2.23: (a) Hydrogen Park at Tonsley (b) HyP SA Siemens electrolyzer [89].

Table 2.4 contains data regarding the custom-made Siemens electrolyzer, illustrated in Figure 2.23b. HyP SA began operations in May 2021, supplying 700 customers with a renewable gas

Table 2.4: HyP SA P2H characteristics [90].

Parameter	**Value**
Rated power (MW)	1.25
H_2 production (kg/h)	20
Onsite storage (kg)	40
Water consumption (L/kg)	15

blend of up to 5% by volume. This expanded to 3,000 customers across southern Adelaide suburbs in 2023, and by 2024, the blend increased to 10%, further cutting emissions. The project, as seen in Figure 2.24, also serves industrial and transport sectors via tube trailers and continues to expand with H_2 blending initiatives in Gladstone, Albury, and Wodonga, supported by investments like the Australian Hydrogen Centre [90].

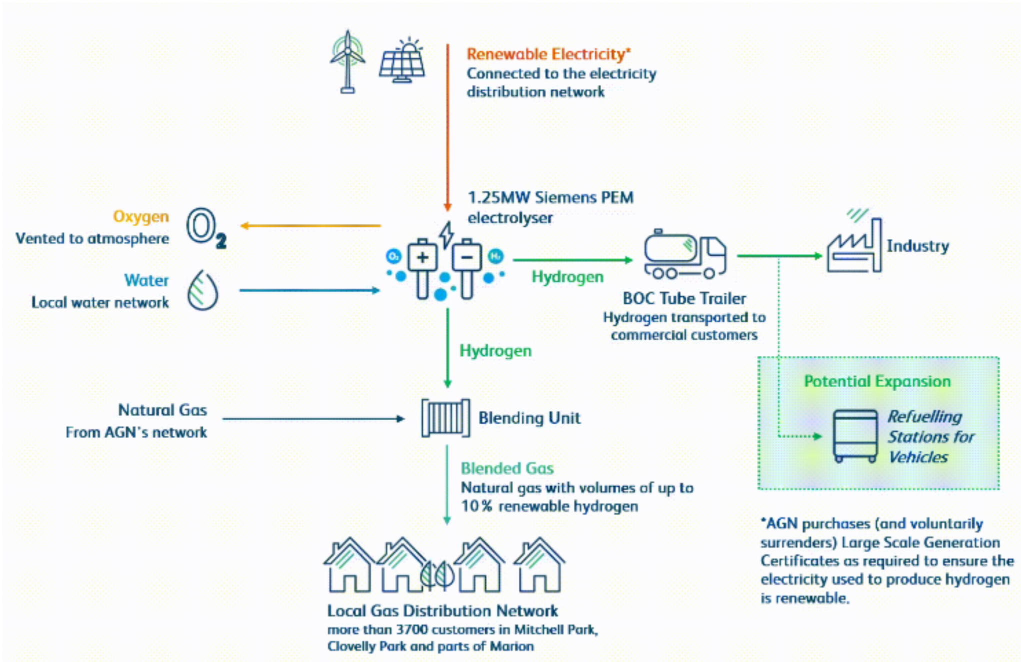

Figure 2.24: HyP SA project overview [90].

HyP SA has been operating since 2021, showing major strides in reducing carbon emissions with the replacement of methane with H_2, roughly 21,347 kg [90].

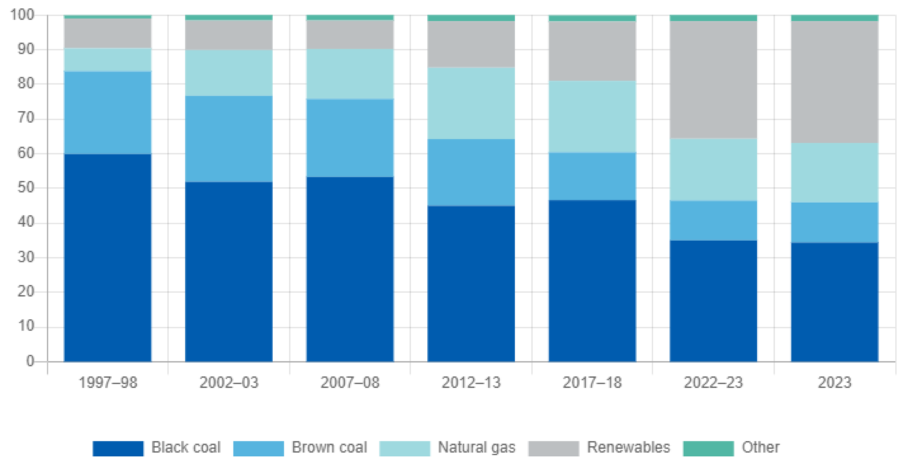

Figure 2.25: Australian energy mix from 1997 until 2023 [91].

Figure 2.25 illustrates the significant transformation in Australia's energy mix between 1997 and 2023. Over this period, there has been a noticeable shift towards renewable energy sources, such as wind, solar, and hydro, which have steadily increased in contribution. This growth in renewables is contrasted by a marked decline in the use of brown and black coal, as well as natural gas, which have traditionally dominated Australia's energy generation.

2.6.2 Scientific papers review

Numerous studies have been conducted and continue to emerge aimed at evaluating the economics of H_2 production across various countries. A selection of key scientific contributions is summarized below.

First, [92] explores the performance of a residential REC connected to a PV system and wind turbine under two different scenarios. For the first scenario, the medium-voltage DSO grid connects the RESs to the REC through one point of delivery. The second scenario divides the original REC into two groups: REC 1 has access to the RESs and a P2H system, and REC 2 relies on a FC that operates with H_2 bought from REC 1. Both REC 1 and REC 2 can import energy from the grid to meet consumption. The P2H system increased electric autonomy from 68.6% to 83.7% and helped the REC to decrease energy injections to the grid from the RESs as it went from 69.5% to 9.1%.

A different approach is taken in [93], which assesses the economic impact of H_2 as a long-term energy storage in microgrids under multiple scenarios to ascertain the minimum energy cost needed to sustain the system. The authors consider a total of 6 cases, where cases 1, 2, and 3 are connected to the grid and the rest are off-grid. Using the HOMER software, the authors use different metrics to evaluate each case, such as Net Present Cost (NPC), Cost of Energy (COE) and pollutant emissions. The H_2 produced from the electrolyzer is stored in a H_2 tank and is consumed by a FC to aid the microgrid in meetings its consumption. The case that proves to be most beneficial is the grid-connected microgrid, showing lower NPC, lower COE, and significantly lower operational costs. Overall, the total cost dropped by 7.51%, while the LCOE decreased from 0.085 $/kWh to 0.051 $/kWh, representing a 40% reduction.

In [94], the authors examine the integration of Energy Storage System (ESS) with a 220 kW run-of-the-river hydropower plant for supporting a 48 kW off-grid energy consumer. The study compares a BESS with a H_2 storage system across three phases: analyzing a baseline scenario and exploring off-grid operations with each ESS. The H_2 system, which includes an electrolyzer, FC, and large-capacity tank, is found to be more cost-effective for long-term storage, as the BESS faces high self-discharge and economic limitations for high energy-to-power ratios. The results showed that for over 30 hours and energy volumes above 1 MWh, H_2 storage becomes more cost-effective than BESS. The Levelized Cost of Storage (LCOS) for both systems intersects at around 400 €/MWh. Beyond 1 MWh, expanding BESS capacity becomes more expensive than investing in H_2 systems. For periods greater than 1,000 hours, H_2 storage is far more beneficial with an LCOS of 1 €/MWh and BESS stands at an LCOS of 10 €/MWh.

In [95], the authors present a business model involving a set of RECs that can allocate their surplus energy to a H_2 company that owns P2H systems. The production of H_2 obtains incentives for energy sharing that would be exported out of the DSO grid. The H_2 company has a reserved electrolyzer for each REC, but all H_2 produced is stored in the same H_2 storage that can be sold to an electricity provider with a 1 MW FC. The conclusion states that the business model is expected to become economically viable by 2035 in RECs with more than 3000 members with high PV generation of 1.8 kWp/capita.

In [96], a particle swarm optimization (PSO) algorithm is used to find the optimal sizing of multiple RES, combined with k-means clustering to accurately reflect weather patterns and their long-term impact on energy generation. The sizing results then feed into a MILP model that simulates the operation of an energy community. Compared to the unoptimized case, this approach cuts operational costs by 65.45% and reduces carbon emissions by 96.82%.

In [97], an optimal sizing MILP model of PV and BESS within RECs is explored. The sizing is specifically performed for a REC that allows for P2P energy exchanges and can be comprised of households and businesses alike. The model employs a two-stage stochastic optimization to handle load and PV generation uncertainties. As for the objective function, it minimizes electricity, operational, and scaled investment costs for both DERs, while setting economic fairness constraints among participants. Assuming a fixed electricity tariff model, the study found that households showed savings of 20% while businesses managed to achieve 67% of savings through the optimal DER configuration and P2P trading.

In [98], a MILP-based optimization framework for designing and dispatching a stand-alone renewable P2P system, including a P2H system, was developed. It was applied to the Italian off-grid island of Ginostra and showed a significant decrease in the LCOE from 0.86 €/kWh to 0.455 €/kWh. Hydrogen stood out as a viable solution for long-term energy balancing. Additionally, the model incorporated variable REC and FC efficiency using a piecewise linearization to improve the accuracy of the system's performance.

2.6.3 Overview of the related projects and papers

Table 2.5 summarizes key aspects regarding the use, modeling and integration of hydrogen in practical projects and scientific studies.

As discussed in Section 1, the shift toward decentralized generation and the growing role of prosumers are key to evaluating H_2 techno-economic viability within a REC. Notably, these studies do not assess the economics of using H_2 directly to maximize self-sufficiency or reduce operating costs. This work addresses that gap by incorporating variable efficiencies for electrolyzers and fuel cells, and by optimizing DER sizing for P2H systems.

Table 2.5: Overview of the reviewed studies.

Reference	Electrolyzer	FC	Feedstock	Prosumers	DER sizing
HydroGlen	✓		✓		
SEAFUEL Tenerife	✓	✓	✓		
HyP SA	✓		✓		
[92]	✓	✓			
[93]	✓	✓			
[94]	✓	✓			
[99]	✓				
[95]	✓	✓		✓	
[96]	✓	✓			
[97]				✓	✓
[98]	✓	✓		✓	✓

Chapter 3

Integration of Power-to-Hydrogen Systems into REC Modeling

This chapter outlines the structure of the REC, the participating members, the DERs, and how each is modeled.

First, the structure of the REC and its community members is introduced. Then, the system sizing model SITEC model's structure is presented, including data clustering methods for selecting representative days, and the related mathematical formulation. Finally, the operational phase is modeled with the OSTEC framework, focusing on intra-community dynamics and their mathematical representation.

These elements provide a comprehensive formulation of P2H systems within the REC context.

3.1 Renewable energy community structure

The REC is composed of multiple members capable of managing their energy production and consumption with energy meters, enabling them to interact with the retailer or each other. Members may also own EVs equipped with bidirectional charging capabilities, whose energy requirements must be met to ensure their availability for mobility.

A DER sizing model named SITEC is applied to select the optimal DER capacity for each member of the REC. The DERs that can be installed are PV systems, BESS, the electrolyzer, H_2 and the FC. The P2H system converts electricity into H_2, the stored H_2 may either be sold in its chemical form or used in a FC, contributing with additional revenue and enhancing system flexibility. Energy flow among REC members and retailers is optimized to ensure effective use of locally generated energy, storage, and trading opportunities.

Figure 3.1 illustrates the configuration of the REC, where each member may have access to a PV system and/or BESS, depending on their economic viability within the REC framework.

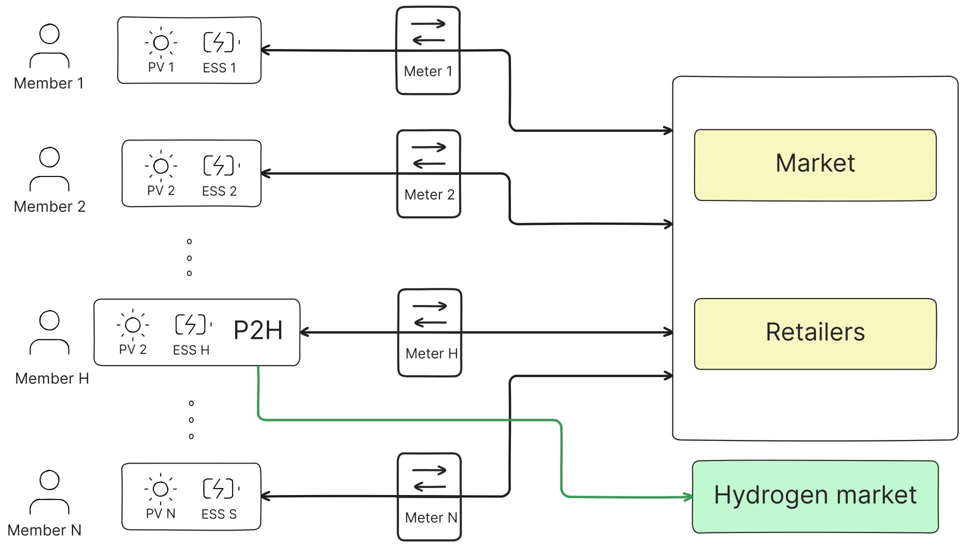

Figure 3.1: REC structure.

3.2 Renewable energy community model

The modeling framework for the REC is organized into two sequential stages, incorporating both the SITEC and OSTEC tools. SITEC is responsible for determining the optimal sizing for the REC based on input data such as consumption profiles, generation potential, and economic factors. It outputs the recommended capacities, power ratings, and other key specifications for DERs such as PV panels, BESS, and P2H systems.

At its core, both SITEC and OSTEC are defined as MILP problems using the PuLP modeling framework. Figure 3.2 summarizes the simulation workflow, illustrating the data and constraints that flow through SITEC and OSTEC tools to achieve optimal sizing, strategies, and REC performance metrics.

The results from SITEC are used as inputs for OSTEC, which focuses on optimizing the day-to-day operation of the REC. OSTEC models how members manage local PV generation, BESS and a P2H system to minimize operational costs. This stage ensures that the system is appropriately dimensioned.

The OSTEC tool specifically emphasizes P2P energy sharing, which reduces dependence on external retailers and benefits members economically. The chosen business model shapes the allocation of shared resources and cost distributions, fostering collaborative energy management within the REC.

The OSTEC model consists in two stages. The first stage optimizes each member individually to calculate their operational costs when they are not part of the REC. The second stage performs a collective optimization, allowing members to exchange energy within the community.

For the first stage, each prosumer (as illustrated in Figure 3.1) is treated individually to assess the lowest possible operational cost based on their unique consumption patterns and technology availability. A retailer covers any shortfall in energy, while surplus energy is sold back to the

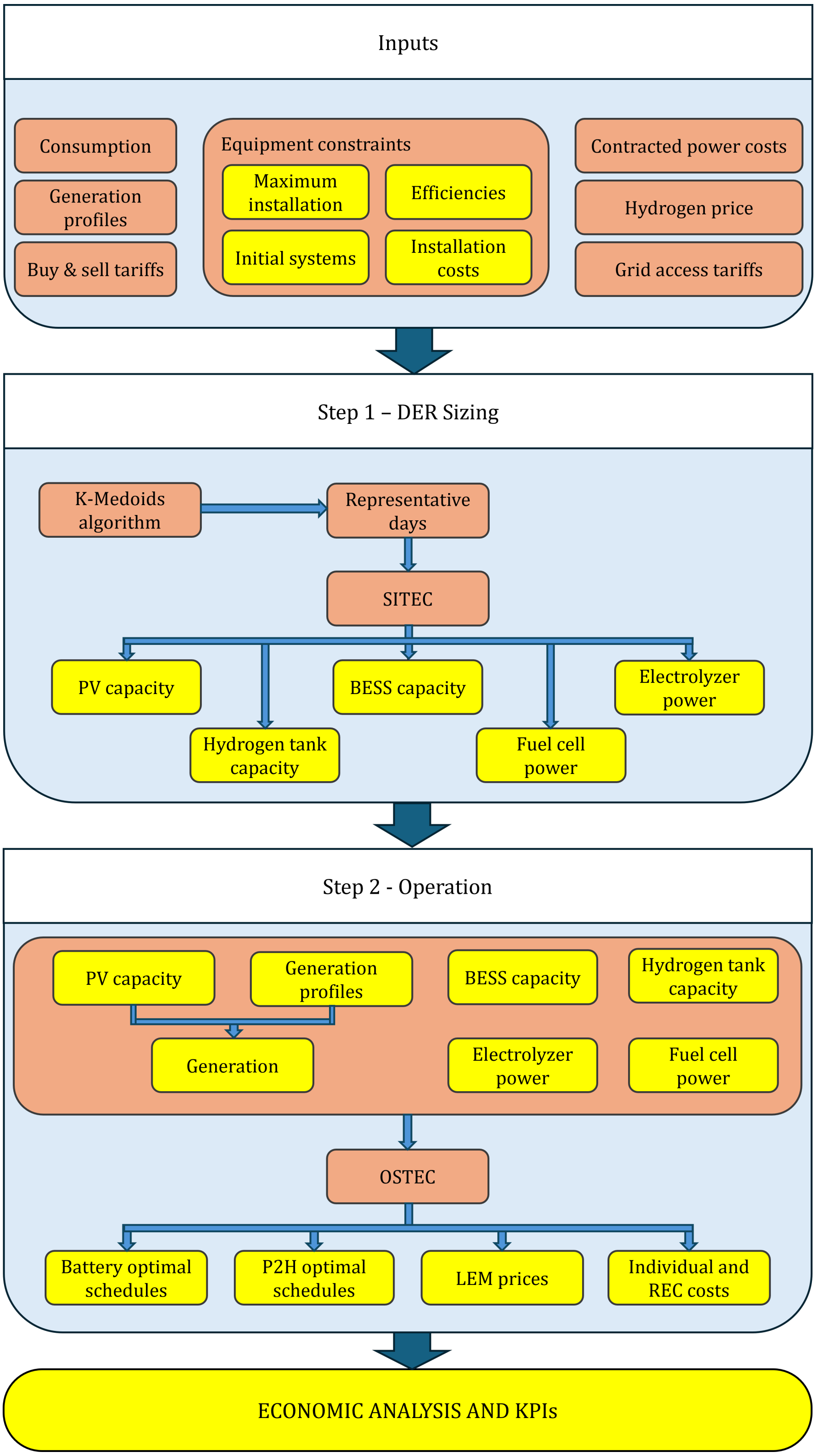

Figure 3.2: Diagram of the sizing and operation models.

retailer, as shown in Figure 3.3. The P2H system is not considered for OSTEC's first stage, as such systems are not yet considered viable for small-scale residential use due to technical and economic constraints [100].

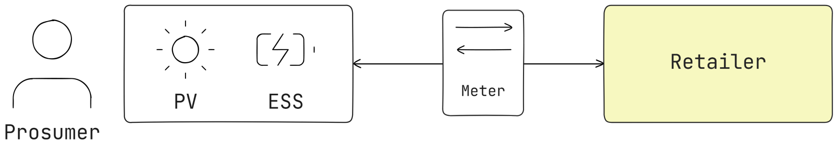

Figure 3.3: Stage 1 overview of prosumer and supplier interactions.

The outcomes from this individual modeling phase are then carried over to OSTEC's second stage, where the prosumers are integrated into a REC. This work focuses exclusively on the second stage, applying the previously computed results without additional modification.

3.2.1 System sizing with SITEC

A fundamental stage involves sizing the DER assets for the REC using SITEC. This stage aims to reach the optimal investment strategy, including PV systems, BESS and the P2H system to optimize intra-community exchanges on top of the total cost incurred on the REC.

The model employs a pool-based Local Energy Market (LEM), where pricing is determined through the uniform market mechanism. To account for uncertainty and seasonality, full-year data was used to achieve more precise results. However, since this can lead to computational issues, data clustering was used to reduce computational effort and memory requirements.

3.2.1.1 SITEC model overview

This subsection presents the structural components and input requirements of the SITEC model. These inputs collectively define the feasible solution space and ensure that sizing results reflect both technical constraints and community-level dynamics.

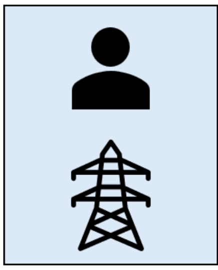

Consumption	$-\hat{E}^{C}_{n,t}$
Generation factor profile	$-\hat{f}^{G}_{n,t}$
Tariffs buy/sell retailer	$-\hat{\lambda}^{buy}; \hat{\lambda}^{sell}$
Grid access tariff	$-\hat{\lambda}^{grid}$
CHP demand profile	$-\hat{m}^{CHP}_{t}; \hat{\lambda}^{CHP}$
Contracted power	$-\hat{\lambda}^{CONT}_{n}; \hat{P}^{CPE,\max}_{n}$

Figure 3.4: SITEC input member data.

Member data includes time series of energy consumption, generation profiles and retailer prices for buying and selling energy. Complementary economic parameters include the Combined Heat and Power (CHP) purchase price, grid access fees, and contracted power costs, as seen in Figure 3.4.

H_2	Costs per day	$-\hat{\lambda}_n^{ELEC}; \hat{\lambda}_n^{Tank}; \hat{\lambda}_n^{FC}$
	Bounds	$-\hat{P}_n^{ELEC,min}; \hat{P}_n^{ELEC,max}$
		$-\hat{C}_n^{H_2,min}; \hat{C}_n^{H_2,max}$
		$-\hat{P}_n^{FC,min}; \hat{P}_n^{FC,max}$
	Initial system	$-\hat{P}_n^{ELEC,Initial}$
		$-\hat{C}_n^{Initial}$
		$-\hat{P}_n^{FC,Initial}$
	Efficiency	$-\hat{\eta}^{ELEC}; \hat{\eta}^{FC}$

Figure 3.5: P2H equipment inputs for SITEC.

	Costs per day	$-\hat{\lambda}_n^{G,ic}$
	Bounds	$-\hat{P}_n^{GN,min}; \hat{P}_n^{GN,max}$
	Initial system	$-\hat{P}_n^{GN,Initial}$

	Costs per day	$-\hat{\lambda}_n^{B,ic}$
	Bounds	$-\hat{E}_n^{BN,min}; \hat{E}_n^{BN,max}$
	Initial system	$-\hat{E}_n^{BN,Initial}$
	Efficiency	$-\hat{\eta}^{BC}; \hat{\eta}^{BD}$

Figure 3.6: PV and BESS equipment inputs for SITEC.

The DER sizing details investment and related parameters for constraining the PV systems, BESS, and P2H can be seen in Figures 3.5 and 3.6. These specifications encompass daily investment costs (e.g. €/(kVA · day) and equipment investment (e.g. €/kW), operational boundaries, starting capacity, and efficiency values. The variable efficiency mode for both the electrolyzer and FC will only be incorporated for OSTEC as this mode of operation for the P2H causes a significant increase in model complexity for SITEC. The parameters that describe the EVs are the minimum amount of energy and the capacity of the battery and the respective efficiencies for charging/discharging the EV, which is similar to the inputs defined for the BESS. The energy used up for trips on the EV must also be defined, in addition to a binary parameter that simply defines if the EV is connected to the REC for charging/discharging. The covered parameters for the EV can be seen in Figure 3.7.

	Capacity	$-\hat{E}_{n,ev}^{EV,min,Charge}; \hat{E}_{n,ev}^{EV,Battery\ Capacity}$
	Efficiency	$-\hat{\eta}_{n,ev}^{Charge}; \hat{\eta}_{n,ev}^{Discharge}$
	Trip and connection to REC	$-\hat{E}_{n,ev,t}^{Trip}; \hat{\delta}_{n,ev,t}$

Figure 3.7: EV equipment inputs for SITEC.

The k-medoids algorithm is employed on both consumption and generation time series to identify the most representative days throughout the year. These representative days are then used as input scenarios in the optimization model. The resulting DER configuration is optimized at the community level rather than for individual members.

3.2.1.2 Clustering for community structuring

The number of potential members or locations within the REC can be large in practical applications. This leads to significant computational complexity when formulating and solving an optimization model, such as a MILP model. To address this, clustering techniques like k-medoids can effectively reduce the problem size.

The k-medoids algorithm, illustrated in Figure 3.8, typically proceeds as follows: Initially, k data points are selected as possible medoids. Each remaining data point is assigned to the cluster whose medoid it is closest to, based on a chosen distance metric (e.g., Euclidean, Manhattan). The algorithm then attempts to improve the clustering quality by swapping one of the current

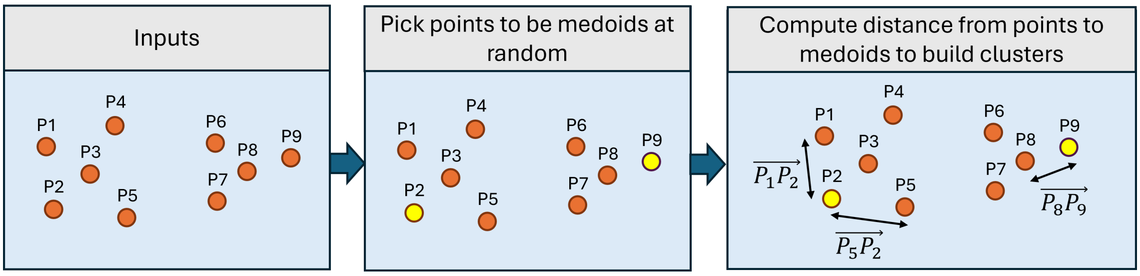

Figure 3.8: Initialization and cluster assignment in k-medoids clustering algorithm.

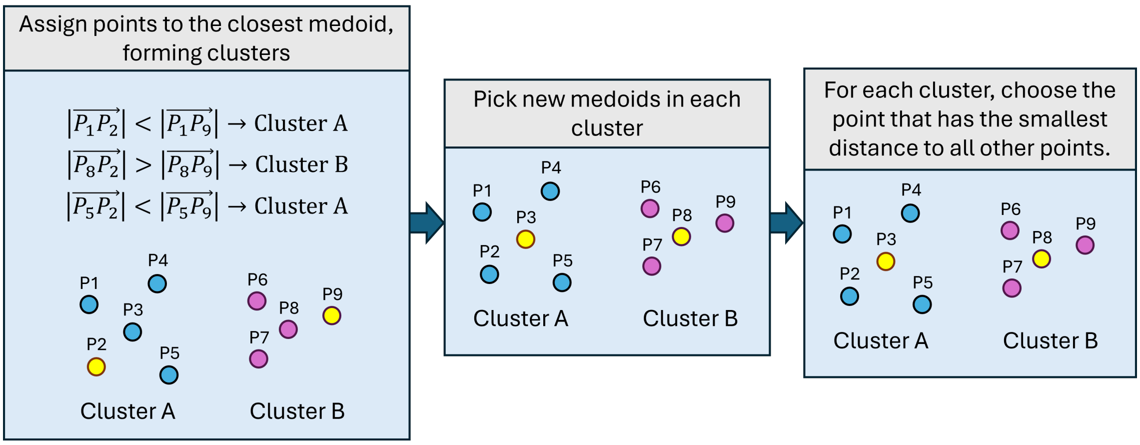

Figure 3.9: Medoid update and cluster refinement in k-medoids clustering algorithm.

medoids with a non-medoid point. If a swap reduces the total sum of distances, the change is accepted, and the new point becomes the medoid. This process is repeated until the objective function shows no further improvement over a predefined number of iterations or swaps [101] and the final configuration is reached, as shown in Figure 3.9.

By selecting only these k medoids as representative nodes for the MILP modeling, the optimization problem's dimension can be significantly reduced. However, this simplification comes with an inherent trade-off, as some granular information about individual entities within a cluster is aggregated.

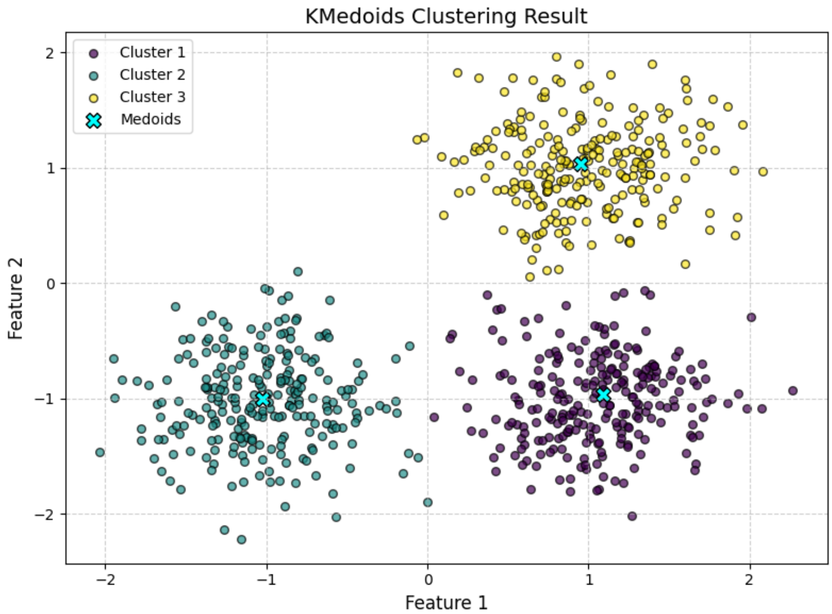

Figure 3.10: k-medoids clustering [102].

The application of the k-medoids clustering algorithm to a broader dataset is illustrated in Figure 3.10. In this example, $k = 3$, indicating that three medoids were initially selected. The algorithm computes the distance (or another dissimilarity metric) between each data point and the chosen medoids. Each point is then assigned to the cluster associated with the nearest medoid based on the one for which the distance is minimal. This process groups points based on proximity to each cluster's most centrally located representative. Subsequent iterations refine the medoid selection by identifying the point within each cluster that minimizes the total distance to all other points in that cluster, ultimately leading to a stable clustering configuration.

3.2.1.3 Mathematical formulation

The objective function in Equation 3.1 minimizes the total cost of the REC, combining investment costs for energy technologies with representative operational costs. It includes the expenditures on DERs, as well as energy transaction costs with the grid and the external CHP client.

$$
\begin{aligned}
\min \sum_{t \in T} \sum_{n \in N} & (E_{n,t}^{SUP} \cdot \hat{\lambda}^{buy} - E_{n,t}^{SUR} \cdot \hat{\lambda}^{sell} + E_{n,t}^{SLC} \cdot \hat{\lambda}^{grid} - m_{n,t}^{CHP} \cdot \hat{\lambda}^{CHP}) \cdot \hat{w}_t^{cluster} \cdot \hat{Y} \\
+ \sum_{n \in N} & (P_n^{CONT} \cdot \hat{\lambda}_n^{cont} + P_n^{GN} \cdot \hat{\lambda}_n^{G,ic} + E_n^{BN} \cdot \hat{\lambda}_n^{B,ic} + P_n^{ELEC} \cdot \hat{\lambda}_n^{ELEC} + C_n^{H_2} \cdot \hat{\lambda}_n^{Tank} + P_n^{FC} \cdot \hat{\lambda}_n^{FC}) \cdot \hat{D}
\end{aligned}
\tag{3.1}
$$

where, for each member $n \in N$, $E_{n,t}^{SUP}$ is the energy supplied by its retailer at price $\hat{\lambda}^{buy}$, $E_{n,t}^{SUR}$ is the surplus sold to its aggregator at feed-in price $\hat{\lambda}_{n,t}^{sell}$ and $E_{n,t}^{SLC}$ is the self-consumed energy which pays a grid access tariff $\hat{\lambda}_t^{grid}$. As discussed in Section 3.2.1.2, clustering reduces input data, with $\hat{w}_t^{cluster}$ representing the number of days each cluster stands for and $\hat{Y}$ scales the energy transaction cost over the system lifetime in years. The second parcel of Equation 3.1 represents the installation cost of each piece of DERs for each member. P_n^{CONT} is the contracted power with a daily tariff $\hat{\lambda}_n^{cont}$. $\hat{D}$ is the number of days in the optimization horizon. P_n^{GN} is the newly installed PV capacity with unit investment cost $\hat{\lambda}_n^{G,ic}$, E_n^{BN} is the newly installed BESS capacity with investment cost $\hat{\lambda}_n^{B,ic}$. The electrolyzer, H_2 tank and FC are the P2H system's components where P_n^{ELEC} is the newly installed power for the electrolyzer with a unit investment cost of $\hat{\lambda}_n^{ELEC}$, $C_n^{H_2}$ is the newly installed H_2 tank's capacity with a unit investment cost of $\hat{\lambda}_n^{Tank}$ and the P_n^{FC} is the newly installed power for the FC with a unit investment cost of $\hat{\lambda}_n^{FC}$.

Meter energy balance constraints – the energy at each meter is constrained by Equations 3.2 and 3.3, ensuring a balance between inflows and outflows of energy for each member at any time. Equations 3.4 and 3.5 enforce that the power exchanged respects the contracted limits and does not exceed the technical capacity of the connection point.

$$E_{n,t}^{CMET} = \hat{E}_{n,t}^{C} - E_{n,t}^{G} + (E_{n,t}^{B,C} - E_{n,t}^{B,D}) + \sum_{ev \in EV} (E_{n,ev,t}^{Charge} - E_{n,ev,t}^{Discharge}) + E_{n,t}^{ELEC} - E_{n,t}^{FC} \qquad \forall t \in T, n \in N \tag{3.2}$$

$$E_{n,t}^{CMET} = E_{n,t}^{SUP} - E_{n,t}^{SUR} + E_{n,t}^{PUR} - E_{n,t}^{SALE} \qquad \forall t \in T, n \in N \tag{3.3}$$

$$-P_n^{CONT} \leq \frac{E_{n,t}^{CMET}}{\Delta t} \leq P_n^{CONT} \qquad \forall t \in T, n \in N \tag{3.4}$$

$$P_n^{CONT} \leq \hat{P}_n^{CPE,\max} \qquad \forall n \in N \tag{3.5}$$

where $E_{n,t}^{CMET}$ denotes the net metered consumption of member n at time t. The term $\hat{E}_{n,t}^{C}$ captures consumption, while $E_{n,t}^{G}$ represents photovoltaic generation. Battery interactions are reflected via $E_{n,t}^{B,C}$ (charging) and $E_{n,t}^{B,D}$ (discharging). Alternatively, the net metered energy can also be expressed based on market transactions and grid exchanges using $E_{n,t}^{SUP}$ and $E_{n,t}^{SUR}$ (grid supply and surplus), and $E_{n,t}^{PUR}$ and $E_{n,t}^{SALE}$ (LEM buy/sell activities). The following constraint bounds the average power drawn from or injected into the grid, computed as energy over time step Δt, within the member's contracted power P_n^{CONT}. Finally, the contractual limit P_n^{CONT} must not surpass $\hat{P}_n^{CPE,\max}$, which sets the technical limit for the connection point.

PV sizing constraints – the PV system design is governed by Equations 3.6 to 3.8, which define the additional installable capacity, calculate expected generation, and enforce design limits.

$$P_n^{GN} = P_n^{GN,Total} - \hat{P}_n^{GN,Initial} \qquad \forall n \in N \tag{3.6}$$

$$E^{G}_{n,t} = \hat{f}^{G}_{n,t} \cdot P^{GN,Total}_{n} \cdot \Delta t \qquad \forall t \in T, n \in N \tag{3.7}$$

$$\hat{P}^{GN,\min}_{n} \leq P^{GN}_{n} \leq \hat{P}^{GN,\max}_{n} \qquad \forall n \in N \tag{3.8}$$

where $P^{GN,Total}_{n}$ is the total PV capacity after installation, while $\hat{P}^{GN,Initial}_{n}$ denotes the existing installed capacity. Equation (3.6) defines the optimization variable P^{GN}_{n} as the additional PV capacity to be installed. The PV energy output at each time step is calculated in Equation (3.7), where $\hat{f}^{G}_{n,t}$ is the generation profile (a fractional value) and Δt is the time step. Finally, Equation (3.8) ensures that the newly installed PV capacity remains within predefined design limits, bounded by $\hat{P}^{GN,\min}_{n}$ and $\hat{P}^{GN,\max}_{n}$.

BESS constraints – the BESS is governed by Equations 3.9 to 3.16, which define installable capacity, operational charge/discharge limits, initial conditions, and enforce State of Charge (SOC) boundaries over time.

$$E^{BN}_{n} = E^{BN,Total}_{n} - \hat{E}^{BN,Initial}_{n} \tag{3.9}$$

$$\hat{E}^{BN,\min}_{n} \leq E^{BN}_{n} \leq \hat{E}^{BN,\max}_{n} \tag{3.10}$$

$$\frac{E^{B,C}_{n,t}}{\Delta t} \leq E^{BN,Total}_{n} \cdot \frac{\hat{P}^{B,ref}}{\hat{E}^{B,ref}} \tag{3.11}$$

$$\frac{E^{B,D}_{n,t}}{\Delta t} \leq E^{BN,Total}_{n} \cdot \frac{\hat{P}^{B,ref}}{\hat{E}^{B,ref}} \tag{3.12}$$

$$E^{B,Initial}_{n} = \frac{S\hat{O}C^{B,\min}_{n}}{100} \cdot E^{BN,Total}_{n} \tag{3.13}$$

$$E^{B}_{n,t} = E^{B,0}_{n} + (E^{B,C}_{n,t} \cdot \hat{\eta}^{B,C}_{n} - \frac{E^{B,D}_{n,t}}{\hat{\eta}^{B,D}_{n}}) \quad t = 0, \forall n \in N \tag{3.14}$$

$$E^{B}_{n,t} = E^{B}_{n,t-1} + (E^{B,C}_{n,t} \cdot \hat{\eta}^{B,C}_{n} - \frac{E^{B,D}_{n,t}}{\hat{\eta}^{B,D}_{n}}) \quad \forall t > 0 \in T, n \in N \tag{3.15}$$

$$\frac{S\hat{O}C^{B,\min}_{n}}{100} \cdot E^{BN,Total}_{n} \leq E^{B}_{n,t} \leq \frac{S\hat{O}C^{B,\max}_{n}}{100} \cdot E^{BN,Total}_{n} \qquad \forall n; \forall t \tag{3.16}$$

where $E^{BN,Total}_{n}$ is the total BESS capacity composed of the existing installed capacity $\hat{E}^{BN,Initial}_{n}$ and an optimization variable representing the additional BESS capacity to be installed. This variable must fall within defined installation bounds, where $\hat{E}^{BN,\min}_{n}$ and $\hat{E}^{BN,\max}_{n}$ represent the minimum and maximum permissible limits, ensuring technical and design feasibility. The charging power is further constrained by the ratio $\hat{P}^{B,ref}/\hat{E}^{B,ref}$, which reflects the hardware's allowable charge/discharge rate. The energy stored in the system, $E_n^{B,0}$, is initialized to a minimum allowable state of charge $\hat{SOC}_n^{B,\min}$ as a fraction of the installed capacity. For time $t > 0$, the battery energy content $E_{n,t}^{B}$ is updated based on the charge/discharge efficiencies $\hat{\eta}_n^{B,C}$ and $\hat{\eta}_n^{B,D}$, ensuring an accurate representation of initial system conditions. Throughout the time horizon, $E_{n,t}^{B}$ must remain within the SOC limits $\hat{SOC}_n^{B,\min}$ and $\hat{SOC}_n^{B,\max}$, both expressed as percentages of $E_n^{BN,Total}$, to maintain operational reliability.

Electrolyzer constraints - The constraints outlined in Equations 3.17 to 3.28 govern several aspects of the electrolyzer. These include the installed power rating, operating limits, the amount of hydrogen produced for a specific energy input, and the maximum energy that can be supplied to the electrolyzer without exceeding its total power rating.

$$P_n^{ELEC} = P_n^{ELEC,\text{Total}} - \hat{P}_n^{ELEC,Initial} \qquad \forall n \tag{3.17}$$

$$\hat{P}_n^{ELEC,\min} \leq P_n^{ELEC} \leq \hat{P}_n^{ELEC,\max} \qquad \forall n \tag{3.18}$$

$$m_{\text{H}_2,n,t} = \frac{E_{n,t}^{ELEC} \cdot \hat{\eta}_n^{ELEC}}{\hat{\text{HHV}}} \qquad \forall n; \forall t \tag{3.19}$$

$$E_{n,t}^{ELEC} \leq P_n^{ELEC,\text{Total}} \cdot \Delta t \tag{3.20}$$

where $P_n^{ELEC,\text{Total}}$ refers to the total installed electrolyzer capacity for member n, calculated as the sum of newly added capacity P_n^{ELEC} and the initial capacity $\hat{P}_n^{ELEC,\text{Initial}}$. $\hat{P}_n^{ELEC,\min}$ and $\hat{P}_n^{ELEC,\max}$ represent the lower and upper installation bounds for the electrolyzers. The electricity input to the electrolyzer, $E_{n,t}^{ELEC}$, is limited by its total installed capacity and the time step Δt. Hydrogen production, $m_{\text{H}_2,n,t}$, is a function of the electrolyzer input $E_{n,t}^{ELEC}$, its efficiency $\hat{\eta}_n^{ELEC}$, and the higher heating value $\hat{\text{HHV}}$.

Hydrogen tank constraints - The constraints encompass the installed capacity of each member's H_2 tank, imposing limits on the minimum and maximum amount of storage, ensuring the amount of stored H_2 is not greater than the total installed capacity and the inflow and outflows of H_2 from the tank.

$$C_n^{\text{H}_2} = C_n^{\text{Total}} - \hat{C}_n^{\text{Initial}} \qquad \forall n \in N \tag{3.21}$$

$$\hat{C}_n^{\text{H}_2,\min} \leq C_n^{\text{H}_2} \leq \hat{C}_n^{\text{H}_2,\max} \tag{3.22}$$

$$m_{\text{H}_2,n,t}^{\text{Stored}} = m_{\text{H}_2,n,t-1}^{\text{Stored}} + m_{\text{H}_2,n,t} - (m_{n,t}^{\text{FC}} + m_{n,t}^{\text{CHP}}) \qquad \forall n; \forall t \tag{3.23}$$

$$m_{\text{H}_2,n,t}^{\text{Stored}} \leq C_n^{\text{Total}} \qquad \forall n; \forall t \tag{3.24}$$

where C_n^{Total} is the sum of the initial installed capacity, $\hat{C}_n^{\text{Initial}}$ and $C_n^{\text{H}_2}$ the newly added capacity to the tank. The bounds set on the amount of storage are defined by $\hat{C}_n^{\text{H}_2,\min}$ and $\hat{C}_n^{\text{H}_2,\max}$. The amount of H_2 stored in the tank is given by the stored amount from the previous time step $m_{\text{H}_2,n,t-1}^{\text{Stored}}$ followed by the inflow of H_2 from the electrolyzer and outflows to the FC and to the CHP client.

Fuel cell constraints - The constraints presented in Equations 3.25-3.28 model the installed power rating for the FC, limits of installed power, the amount of energy extracted from H_2 and the energy that can be supplied to the FC without exceeding its total power rating. The hydrogen tank's contents, $m_{\text{H}_2,n,t}^{\text{Stored}}$, changes based on hydrogen produced, fuel cell consumption $m_{n,t}^{\text{FC}}$, and CHP unit consumption m_t^{CHP}, and must remain within the limit defined by $C_{\text{H}_2}^{\text{Total}}$.

$$P_n^{\text{FC},N} = P_n^{\text{FC,Total}} - \hat{P}_n^{\text{FC,Initial}} \qquad \forall n \tag{3.25}$$

$$\hat{P}_n^{\text{FC,min}} \leq P_n^{\text{FC},N} \leq \hat{P}_n^{\text{FC,max}} \qquad \forall n \tag{3.26}$$

$$E_{n,t}^{\text{FC}} = m_{n,t}^{\text{FC}} \cdot \hat{\eta}_n^{\text{FC}} \cdot \text{H}\hat{\text{H}}\text{V} \qquad \forall n; \forall t \tag{3.27}$$

$$E_{n,t}^{\text{FC}} \leq P_n^{\text{FC,Total}} \cdot \Delta t \qquad \forall n; \forall t \tag{3.28}$$

where $P_n^{\text{FC,Total}}$ denotes the overall installed FC capacity given by the sum of the initial installed power $\hat{P}_n^{FC,\text{Initial}}$ and the newly installed power $P_n^{FC,\text{N}}$. $\hat{P}_n^{\text{FC,min}}$ and $\hat{P}_n^{\text{FC,max}}$ represent the limits of power installation for the FC. $E_{n,t}^{\text{FC}}$ represents the electricity generated by the FC at time t and $m_{n,t}^{FC}$ is the mass of H_2 used by the FC. Lastly, the output from the fuel cell is determined by its efficiency $\hat{\eta}_n^{\text{FC}}$ and constrained by the installed capacity $P_n^{\text{FC,Total}}$.

EV constraints – The constraints in Equations 3.29 to 3.31 model the energy dynamics of EV. These include the battery energy balance, limited discharge power based on availability and rated capacity, and storage bounds.

$$E_{n,ev,t}^{Stored} = E_{n,ev,t-1}^{Stored} + \hat{\eta}_{n,ev}^{Charge} \cdot E_{n,ev,t}^{Charge} - \frac{1}{\hat{\eta}_{n,ev}^{Discharge}} \cdot E_{n,ev,t}^{Discharge} - \hat{E}_{n,ev,t}^{Trip} \qquad \forall n; \forall ev; \forall t \tag{3.29}$$

$$\frac{E_{n,ev,t}^{Discharge}}{\hat{\eta}_{n,ev}^{Discharge}} \leq \hat{P}_{n,ev}^{Discharge,Limit} \cdot \hat{\delta}_{n,ev,t} \cdot \Delta t \qquad \forall n; \forall ev; \forall t \tag{3.30}$$

$$\hat{E}_{n,ev}^{EV,Min\_Charge} \leq E_{n,ev,t}^{EV,stored} \leq \hat{E}_{n,ev}^{EV,Battery\_Capacity} \qquad \forall n; \forall ev; \forall t \tag{3.31}$$

where $E_{n,ev,t}^{Stored}$ represents the energy stored in the EV battery of vehicle ev at time t, with $E_{n,ev,t}^{Charge}$ and $E_{n,ev,t}^{Discharge}$ denoting the charged and discharged energy, respectively. $\hat{E}_{n,ev,t}^{Trip}$ captures the energy consumed for mobility, while $\hat{\eta}_{n,ev}^{Charge}$ and $\hat{\eta}_{n,ev}^{Discharge}$ represent the charging and discharging efficiencies. This constraint models the energy balance of each EV over time, accounting for efficiency losses and driving demands. The discharged energy $E^{Discharge}_{n,ev,t}$ is constrained by the rated discharge power $\hat{P}^{Discharge,Limit}_{n,ev}$, and controlled by the binary variable $\hat{\delta}_{n,ev,t}$, which indicates whether the EV is plugged in, thereby ensuring that discharging occurs only under feasible conditions. Additionally, the stored energy $E^{EV,stored}_{n,ev,t}$ must remain within the defined bounds, between the minimum required charge $\hat{E}^{EV,Min\_Charge}_{n,ev}$ and the battery's total capacity $\hat{E}^{EV,Battery\_Capacity}_{n,ev}$, ensuring safe and reliable operation throughout the optimization horizon.

CHP microturbine client – the CHP client refers to an external entity to which the REC can export H_2 in its chemical form for profit. This demand is optional, meaning it does not need to be fully met, but it must not be exceeded, as there is an upper limit on the quantity of H_2 that can be exported.

$$\sum_{n \in N} m^{CHP}_{n,t} \leq \hat{m}^{CHP}_{t} \tag{3.32}$$

LEM and self-consumption constraints – these constraints, given in Equations 3.33 to 3.41, handle energy trading within the LEM, enforce mutual exclusivity in retailer interactions, and ensure self-consumption and allocation.

$$\sum_{n \in N} E^{PUR}_{n,t} - \sum_{n \in N} E^{SALE}_{n,t} = 0 \qquad \forall n; \forall t \tag{3.33}$$

$$E^{SUP}_{n,t} \leq \hat{M} \cdot \delta^{SUP}_{n,t} + \hat{m} \qquad \forall n; \forall t \tag{3.34}$$

$$E^{SUR}_{n,t} \leq \hat{M} \cdot (1 - \delta^{SUP}_{n,t}) + \hat{m} \qquad \forall n; \forall t \tag{3.35}$$

$$E^{CMET+}_{n,t} \geq E^{CMET}_{n,t} \qquad \forall n; \forall t \tag{3.36}$$

$$E^{ALC+}_{n,t} \geq E^{PUR}_{n,t} - E^{SALE}_{n,t} \qquad \forall n; \forall t \tag{3.37}$$

$$E^{SLC}_{n,t} \geq E^{CMET+}_{n,t} - \hat{M} \cdot (1 - \delta^{SLC}_{n,t}) \qquad \forall n; \forall t \tag{3.38}$$

$$E^{SLC}_{n,t} \leq E^{ALC+}_{n,t} - \hat{M} \cdot \delta^{SLC}_{n,t} \qquad \forall n; \forall t \tag{3.39}$$

$$E^{SALE}_{n,t} - E^{PUR}_{n,t} \leq -E^{CMET}_{n,t} + \hat{M} \cdot \delta^{coeff}_{n,t} \qquad \forall n; \forall t \tag{3.40}$$

$$E^{SALE}_{n,t} - E^{PUR}_{n,t} \leq \hat{M} \cdot (1 - \delta^{coeff}_{n,t}) \qquad \forall n; \forall t \tag{3.41}$$

where $E^{PUR}_{n,t}$ and $E^{SALE}_{n,t}$ denote the energy purchased and sold by member n in the LEM at time t, respectively. A balancing constraint ensures that, at each time step, the total energy exported to the

REC pool equals the total energy imported from it across all members. The energy $E_{n,t}^{SUP}$ supplied by the retailer to member n is governed by a binary variable $\delta_{n,t}^{SUP}$, which activates the constraint only when member n buys from the retailer, with constants $\hat{M}$ and $\hat{m}$ used to relax it otherwise. The surplus energy sold to the retailer, $E_{n,t}^{SUR}$, is constrained by $(1-\delta_{n,t}^{SUP})$ to prevent simultaneous buying and selling to the retailer. The auxiliary variable $E_{n,t}^{CMET+}$ captures the positive portion of net meter consumption $E_{n,t}^{CMET}$, ensuring correct self-consumption calculations under positive tariff conditions. For energy allocation, $E_{n,t}^{ALC+}$ represents the positive allocated energy and must be at least $E_{n,t}^{PUR} - E_{n,t}^{SALE}$ to reflect net positive contributions. The self-consumed energy $E_{n,t}^{SLC}$ is tied to the binary variable $\delta_{n,t}^{SLC}$ and must exceed the positive net consumption when active, while remaining below $E_{n,t}^{ALC+}$ when inactive, making it the minimum of $E_{n,t}^{CMET+}$ and $E_{n,t}^{ALC+}$ across constraints (3.38) and (3.39). The binary variable $\delta_{n,t}^{coeff}$ ensures non-negative allocation coefficients for traded energy and is further constrained to prevent invalid positive allocations.

3.2.2 System operation with OSTEC

OSTEC is designed to assess the system's performance, capturing the dynamics of storage operation, energy sharing, and interactions with the external grid. It ensures compliance with physical limits, supports community-level coordination, and enables an evaluation of operational costs.

3.2.2.1 Mathematical formulation

The proposed work and model modifications will currently focus on OSTEC's second stage, as one of the key objectives of this dissertation is to determine the impact of a P2H system on the REC rather than the individual prosumer.

The objective function shown in Equation 3.42 aims to minimize the cost of operation of the REC.

$$\min \sum_{t\in T}\left(\sum_{n\in N}\left(E_{n,t}^{SUP,retail}\cdot\hat{\lambda}^{buy} - E_{n,t}^{SUR,retail}\cdot\hat{\lambda}^{sell} + E_{n,t}^{SLC}\cdot\hat{\lambda}_t^{grid} - m_{n,t}^{CHP}\cdot\hat{\lambda}_t^{CHP}\right)\right) \qquad \forall n;\forall t \tag{3.42}$$

where $E_{n,t}^{SUP,retail}$ denotes the energy supplied to member n at time t, with a corresponding supply energy tariff $\hat{\lambda}^{buy}$. Any surplus energy generated by the member, $E_{n,t}^{SUR,retail}$, can be sold at a surplus energy tariff $\hat{\lambda}^{sell}$. Self-consumed energy by member n, denoted by $E_{n,t}^{SLC}$, incurs a cost determined by the global access tariff $\hat{\lambda}_t^{grid}$. The revenue from the sale of H_2 is determined by the mass of hydrogen sold for CHP operation, m_t^{CHP}, and its price per unit, $\hat{\lambda}_t^{CHP}$. The objective function minimizes the total energy-related costs over all time steps $t \in T$ and for each member $n \in N$ of the REC.

P2H constraints: the operation of the electrolyzer, tank and fuel cell are expressed in Equations 3.43 - 3.51. Since the efficiency curves are nonlinear, we resort to a piecewise-linear approximation, which involves sampling points along the nonlinear curve and approximating it using linear segments [98].

$$m_{H_2,n,t} = \sum_{s \in S} (\hat{A}_s \cdot P^{ELEC}_{s,t} + \hat{B}_s \cdot B^{ELEC}_{s,t}) \qquad \forall n; \forall s; \forall t \tag{3.43}$$

$$\hat{P}^{ELEC}_{s} \cdot B^{ELEC}_{s,t} \leq P^{ELEC}_{s,t} \leq \hat{P}^{ELEC}_{s} \cdot B^{ELEC}_{s,t} \qquad \forall s; \forall t \tag{3.44}$$

$$\delta^{ELEC}_{t} = \sum_{s=1}^{S} B^{ELEC}_{s,t} \qquad \forall s; \forall t \tag{3.45}$$

$$P^{ELEC}_{t} = \sum_{s=1}^{S} P^{ELEC}_{s,t} \qquad \forall s; \forall t \tag{3.46}$$

$$0 \leq P^{ELEC}_{n,t} \leq \hat{P}^{ELEC,Total}_{n} \qquad \forall n; \forall t \tag{3.47}$$

$$m^{\text{Stored}}_{H_2,n,t} = m^{\text{Stored}}_{H_2,n,t-1} + m_{H_2,n,t} - (m^{\text{CHP}}_{n,t} + m^{FC}_{n,t}) \qquad \forall n; \forall t \tag{3.48}$$

$$0 \leq m^{\text{Stored}}_{H_2,n,t} \leq \hat{C}^{Total}_{n} \qquad \forall n; \forall t \tag{3.49}$$

$$m^{FC}_{n,t} = \sum_{s \in S} (\hat{A}_s \cdot P^{FC}_{s,t} + \hat{B}_s \cdot B^{FC}_{s,t}) \qquad \forall n; \forall s; \forall t \tag{3.50}$$

$$0 \leq P^{FC}_{n,t} \leq \hat{P}^{FC,Total}_{n} \qquad \forall n; \forall t \tag{3.51}$$

where $m_{H_2,n,t}$ represents the mass of H_2 produced by member n at time step t, given an energy input of $E^{ELEC}_{n,t}$. The parameters $\hat{A}_s$ and $\hat{B}_s$ define the piecewise-linear efficiency approximation representing the slopes and y intercept of segment s, respectively. The binary variable $B^{ELEC}_{s,t}$ determines the active efficiency segment at time t, ensuring that the electrolyzer operates within the appropriate region of the efficiency curve. δ^{ELEC}_{t} indicates if the electrolyzer is in operation.

CHP constraints: the export of H_2 to the CHP microturbine client constraint is identical to the one mentioned in Equation 3.32 from SITEC.

BESS constraints: the BESS for each user is constrained by the following expressions.

$$E^{B}_{n,t} = E^{B}_{n,t-1} + \left(E^{B,C}_{n,t} \cdot \hat{\eta}^{B,C}_{n} - \frac{E^{B,D}_{n,t}}{\hat{\eta}^{B,D}_{n}} \right) \qquad \forall n; \forall s; \forall t \tag{3.52}$$

$$\hat{SOC}^{B,min}_{n} \leq SOC^{B}_{n,t} = \frac{E^{B}_{n,t}}{\hat{E}^{B,BN}_{n}} \cdot 100\% \leq \hat{SOC}^{B,max}_{n} \qquad \forall n; \forall s; \forall t \tag{3.53}$$

$$\frac{E_{n,t}^{B,C}}{\Delta t} \leq \hat{P}_n^{B,\max} \cdot \delta_{n,t}^{B,C} \quad \forall n; \forall t \tag{3.54}$$

$$\frac{E_{n,t}^{B,D}}{\Delta t} \leq \hat{P}_n^{B,\max} \cdot \left(1 - \delta_{n,t}^{B,C}\right) \qquad \forall n; \forall t \tag{3.55}$$

where $E_{n,t}^{B}$ is the current energy stored in the BESS, $E_{n,t}^{B,C}$ is the charged energy into the BESS, $E_{n,s,t}^{B,D}$ is the discharged energy from the BESS affected by the discharge efficiency. While charging or discharging, the energy is affected by their respective efficiencies ($\hat{\eta}_{n,s}^{B,C}$ and $\hat{\eta}_{n,s}^{B,D}$). In Equation 3.53, it is defined the acceptable range of operation of the BESS by establishing a lower and upper bound relative to the BESS's nominal capacity, namely $S\hat{O}C_n^{B,\min}$ and $S\hat{O}C_n^{B,\max}$. In Equations 3.54 and 3.55, it is defined the power limit constraint for charging and discharging, where $\delta_{n,s,t}^{B,C}$ indicates if the BESS is charging or discharging.

Electrical vehicle constraints: The constraints that govern the energy dynamics of EV, limited discharge power based on availability and rated capacity are the same as the ones presented for the SITEC model from Equations 3.29 to 3.31.

Energy balancing constraints: these constraints, given in Equations 3.33 to 3.41, define energy trading within the LEM, enforce mutual exclusivity in retailer interactions, and ensure self-consumption and allocation logic aligns with positive grid tariff structures.

$$\sum_{n \in N} E_{n,t}^{PUR} - \sum_{n \in N} E_{n,t}^{SALE} = 0 \qquad \forall t \tag{3.56}$$

$$E_{n,t}^{CMET} = E_{n,t}^{SUP,retail} - E_{n,t}^{SUR,retail} + E_{n,t}^{PUR} - E_{n,t}^{SALE} \qquad \forall n; \forall t \tag{3.57}$$

$$E_{n,t}^{CMET} = \hat{E}_{n,t}^{C} - \hat{E}_{n,t}^{G} + E_{n,t}^{B,C} - E_{n,t}^{B,D} + E_{n,t}^{ELEC} - E_{n,t}^{FC} \qquad \forall n; \forall t \tag{3.58}$$

The variables $E_{n,t}^{PUR}$ and $E_{n,t}^{SALE}$ represent the energy purchased and sold locally by member n at time t, respectively. Equation 3.57 defines the net energy consumption at the meter of member n, accounting for all relevant energy quantities, including supplies, surpluses, purchases, and sales. Meanwhile, Equation 3.58 incorporates all energy injections for each member, considering battery activities, electric vehicle operations, and the energy required for electrolyzer and FC operation, denoted as $E_{n,t}^{elec}$ and $E_{n,t}^{FC}$, respectively. Both equations comprehensively represent the energy dynamics for each member n across all time intervals t.

$$-\hat{P}_n^{CPE,max} \leq \frac{E_{n,t}^{CMET}}{\Delta t} \leq \hat{P}_n^{CPE,max} \qquad \forall n; \forall t \tag{3.59}$$

Economical constraint: As discussed in the previous section, OSTEC performs a cost minimization step for each prosumer. This individual cost is then used as a reference to guarantee that the integration of that prosumer in the REC is beneficial or the same as the original, as shown in

Equation 3.60.

$$\sum_{t \in T} \left(E^{SUP,retail}_{n,t} \cdot \hat{\lambda}^{buy}_{n,t} - E^{SUR,retail}_{n,t} \cdot \hat{\lambda}^{sell}_{n,t} + E^{SLC}_{n,t} \cdot \hat{\lambda}^{grid}_{t} + \left(E^{PUR}_{n,t} - E^{SALE}_{n,t} \right) \cdot \hat{\lambda}^{p2p}_{t} \right) \leq c^{ind}_{n} \qquad \forall n; \forall t \tag{3.60}$$

where all the variables and parameters from Equation 3.42 are present, except for $\hat{\lambda}^{p2p}_{t}$, which represents the LEM mid-market rate energy price at a time t.

Grid constraints: when energy transactions with the grid result in an added cost ($\hat{\lambda}^{grid}_{t} \geq 0$), the REC changes its strategy by setting boundaries for the self-consumed energy. The Equations shown in 3.36 - 3.41 are the same as the ones shown in the SITEC formulation.

3.2.3 REC Indicators

This section defines the metrics used to evaluate how effectively members of the REC manage their energy resources. The Energy Sharing Ratio (ESR) measures the share of energy exchanged among members relative to their total generation:

$$\text{ESR} = \frac{\sum_{t=1}^{T} \sum_{n=1}^{N} E^{SALE}_{n,t}}{\sum_{t=1}^{T} \sum_{n=1}^{N} E^{G}_{n,t}} \qquad \forall n; \forall t \tag{3.61}$$

The Self-Sufficiency Ratio (SSR) reflects the proportion of internal generation relative to total demand, including EV charging. It is influenced by the installed PV capacity and each member's generation profile:

$$\text{SSR} = \frac{\sum_{t=1}^{T} \sum_{n=1}^{N} E^{G}_{n,t}}{\sum_{t=1}^{T} \sum_{n=1}^{N} (\hat{E}^{C}_{n,t} + \hat{E}^{EV,Charge}_{n,t})} \qquad \forall n; \forall t \tag{3.62}$$

3.2.4 Economic Indicators

The Net Present Value (NPV) assesses project profitability by discounting future savings or revenues C_t back to their present value, using a rate r, and subtracting the upfront investment cost C_0:

$$\text{NPV} = \sum_{t=1}^{T} \frac{C_t}{(1+r)^t} - C_0 \tag{3.63}$$

A positive NPV indicates a financially viable investment. The current SITECimplementation does not incorporate time-discounting and thus does not evaluate investments using NPV. The Capital Expenditure (CAPEX) represent initial costs for infrastructure and equipment:

$$\text{CAPEX} = \sum_{n \in N} (P^{CONT}_{n} \cdot \hat{\lambda}^{cont}_{n} + P^{GN}_{n} \cdot \hat{\lambda}^{G,ic}_{n} + E^{BN}_{n} \cdot \hat{\lambda}^{B,ic}_{n} + P^{ELEC}_{n} \cdot \hat{\lambda}^{ELEC}_{n} + C^{H_2}_{n} \cdot \hat{\lambda}^{Tank}_{n} + P^{FC}_{n} \cdot \hat{\lambda}^{FC}_{n}) \cdot \hat{D} \tag{3.64}$$

The Operational Expenditure (OPEX) captures all recurring costs associated with energy transactions and maintenance over the project lifetime:

$$\text{OPEX} = \sum_{t \in T} \sum_{n \in N} (E^{SUP}_{n,t} \cdot \hat{\lambda}^{buy} - E^{SUR}_{n,t} \cdot \hat{\lambda}^{sell} + E^{SLC}_{n,t} \cdot \hat{\lambda}^{grid} - m^{CHP}_{n,t} \cdot \hat{\lambda}^{CHP}) \cdot \hat{w}^{cluster}_{t} \cdot \hat{Y} \tag{3.65}$$

The Total Expenditure (TOTEX) is the sum of CAPEX and OPEX and serves as the objective function minimized by SITEC.

$$\text{TOTEX} = \text{CAPEX} + \text{OPEX} \tag{3.66}$$

The payback period indicates how quickly the investment is recovered through savings, measured against a reference scenario. For this work, the savings achieved by a given scenario are obtained by the difference between the OPEX of a reference scenario, OPEX_{ref} and the OPEX of a proposed scenario S, OPEX_{S}.

$$\text{Payback} = \frac{\text{CAPEX}_{S}}{\text{OPEX}_{ref} - \text{OPEX}_{S}} \tag{3.67}$$

Chapter 4

Simulation of a Renewable Energy Community Incorporating Hydrogen

This chapter presents a set of simulations based on a case study involving a P2H system integrated in a REC. These simulations assess the REC's performance under different operational scenarios. To maintain energy balance, the members of the REC can interact with the electricity retailer, buying energy during shortages, selling surplus energy, and enabling internal exchanges among members in a pool-based LEM.

The chapter first characterizes the REC, encompassing the energy profile of each member, the applicable tariffs, an external CHP client that consumes H_2 in its chemical form, DER specifications and limits of installation. The sizing stage of the REC with SITEC is performed to determine the optimal investment strategy and OSTEC is employed to determine metrics indicative of the performance of the REC. A sensitivity analysis is conducted to determine how relevant parameters affect both the sizing and operation of the REC. With the results from SITEC, a comparative base case is presented along with four scenarios to explore the changes in P2P interactions and cost of operation.

4.1 Characterization of the REC

Each REC member contributes to a shared infrastructure while maintaining individual energy profiles, including consumption and PV generation data. These profiles are crucial for determining energy balance, self-consumption levels, and opportunities for energy exchange with other REC members. The gathered measurements of consumption and generation (for members who had PV) for each member were collected at hourly intervals over a year, resulting in 8,760 time steps per member.

In Table 4.1, monthly observations can be made relative to each member's consumption. Members 2, 5, and 8, exhibit significantly higher average and peak consumption levels, suggesting these members have an energy demand comparable to an industrial user. Members 1, 4, and 7 fall into the moderate consumption, characterized by moderate levels of both consumption. Finally, the low consumption group, Members 3, 6, and 9, shows low energy usage that could represent a residential complex.

Table 4.1: Monthly energy consumption (MWh) for each member.

Month	M1	M2	M3	M4	M5	M6	M7	M8	M9
Jan	101.34	258.81	6.82	101.34	258.81	6.81	101.35	258.81	6.84
Feb	108.32	274.55	6.15	108.30	274.57	6.15	108.32	274.54	6.14
Mar	105.62	294.34	5.98	105.63	294.35	6.00	105.60	294.33	5.99
Apr	100.87	288.22	6.04	100.86	288.21	6.03	100.87	288.20	6.05
May	113.17	295.71	6.20	113.17	295.68	6.23	113.15	295.73	6.22
Jun	106.78	289.20	8.15	106.79	289.22	8.18	106.76	289.19	8.18
Jul	122.36	280.06	8.00	122.35	280.06	7.99	122.37	280.05	7.97
Aug	100.09	272.58	8.48	100.09	272.56	8.48	100.08	272.57	8.50
Sep	120.01	246.57	9.79	120.02	246.58	9.77	119.99	246.58	9.79
Oct	114.44	243.51	9.92	114.43	243.52	9.93	114.43	243.51	9.93
Nov	103.30	260.67	10.79	103.31	260.67	10.80	103.29	260.66	10.78
Dec	89.77	242.45	9.22	89.77	242.47	9.22	89.80	242.45	9.20

As discussed in Chapter 3, the generation profiles are normalized between 0 and 1. Therefore, the observed data for members that can have a PV system, shown in Table 4.2 were scaled by 100 kW.

Table 4.2: Monthly PV generation (MWh) of members.

Month	M2	M4	M5	M7	M8
Jan	50.68	13.40	20.27	10.14	40.55
Feb	45.33	12.22	18.13	9.07	36.28
Mar	30.55	15.67	12.22	6.11	24.45
Apr	75.60	12.82	30.24	15.12	60.50
May	44.45	10.24	17.78	8.89	35.58
Jun	35.26	6.92	14.10	7.05	28.21
Jul	17.09	4.19	6.84	3.42	13.67
Aug	11.26	2.08	4.50	2.25	9.01
Sep	10.03	2.17	4.01	2.01	8.03
Oct	16.76	3.52	6.70	3.35	13.41
Nov	29.86	5.64	11.94	5.97	23.90
Dec	53.67	11.11	21.47	10.74	42.95

Based on the data presented in Table 4.2, members 2 and 8 stand out for their higher PV generation potential. This suggests that they are particularly well-suited for PV system installations and can play a key role in reducing the overall operational costs of the REC. Meanwhile, the remaining members may seek to improve their self-sufficiency and cooperate by sharing surplus energy, thereby contributing to a lower global cost of operation for the REC.

4.1.1 Tariffs

SITEC requires the specification of economic parameters, including buying and selling from the retailer, grid access tariffs, as well as equipment details such as efficiencies. The tariff costs are presented in Table 4.3.

Table 4.3: Input cost parameters for SITEC.

Parameter	Value	Units	Source
$\hat{\lambda}^{\text{CONT}}$	0.0642	€/(kVA·day)	[103]
$\hat{\lambda}^{\text{buy}}$	0.1332	€/kWh	[104]
$\hat{\lambda}^{\text{sell}}$	0.08	€/kWh	[105]
$\hat{\lambda}^{\text{grid}}$	0.06	€/kWh	[106]

The contracted power input parameter was calculated by linearly interpolating data provided by EDP, giving a cost of 0.06426 €/(kVA·day) [103]. The CHP client's price per kg of H_2, $\hat{\lambda}^{\text{CHP}}$, is sourced from MIBGAS Green Energy, which provides weekly updates, typically fluctuates within a narrow range of 0.02€/kg around an annual average of 5.87€/kg [107], and may vary between 5.5 and 7 €/kg depending on government subsidies, incentives, and market conditions. For this set of simulations, H_2 assumes a price of 6 €/kg.

For energy exchanged within the REC, the internal price at any given time ($\hat{\lambda}_t^{p2p}$) is established using the mid-market rate. This approach calculates the average between the highest price any member is willing to sell at and the lowest price any member is willing to buy at, based on fixed tariffs [108]. This results in the following cost expression for P2P energy exchanges, as shown in Equation 4.1:

$$\hat{\lambda}^{p2p} = \frac{\hat{\lambda}^{sell} + \hat{\lambda}^{buy}}{2} \tag{4.1}$$

4.1.2 CHP microturbine

The CHP customer uses a 200 kW microturbine for combined heat and power generation. The detailed technical specifications can be found in Table 4.4. The microturbine runs on NG, but it also has the flexibility to operate with a H_2/NG mix, accommodating up to 30% H_2 by volume. [109].

Table 4.4: CHP microturbine technical specifications [109].

Characteristic	Value
Electrical power output	200 kW
Voltage	400/480 VAC
Electrical efficiency (LHV)	33.30%

H_2's contribution to the fuel mix was evaluated in terms of its energy content and mass within the imposed volumetric blending limit. In addition, the hourly fuel intake of each gas was calculated to better understand the relative shares of H_2 and natural gas in the overall consumption. This analysis, illustrated in Table 4.5, provides a clearer picture of H_2's role in the system's primary energy input, particularly concerning the electrical output of the microturbine.

Table 4.5: H_2/NG mix properties.

Parameter	H_2	**NG**
Volume	30%	70%
Mass	5.59%	94.41%
Energy	12.44%	87.56%

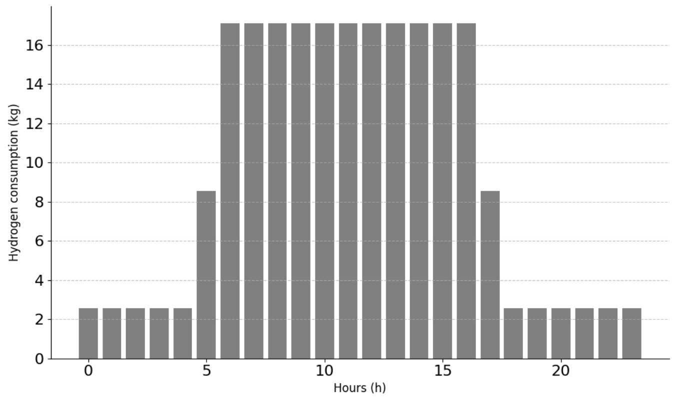

Figure 4.1: CHP microturbine demand over 24 hours.

The customer is a small industrial facility aiming to reduce the environmental impact of its operations and, where possible, to lower its energy costs. The CHP client maintains a consistent and recurring H_2 demand throughout 24 hours, which can be verified in Figure 4.1.

4.1.3 Equipment specifications and installation costs

The case study of the REC includes EVs, whose main characteristics need to be defined for the model, specifically their battery capacity, charging and discharging power, and typical daily energy usage. These EVs models were assigned to members 1, 6, and 9 of the community, as illustrated in Table 4.6. The specifications for each EV were extracted from an EV database [110].

The characteristics of the BESS are calculated by taking the average of the results found in [111], which equates to a charging/discharging efficiency of 88.9%, along with the assumption of a minimum and maximum SOC of 5% and 95%. The BESS technology used for this study is Lithium-ion.

The PEM electrolyzer is considered for this set of simulations with an average efficiency of 80% and producing H_2 at a pressure of 30 bar [32]. The produced H_2 can be directly stored in the

Table 4.6: Technical specifications for the EVs.

	Member 2	*Member 6*	*Member 9*
Capacity (kWh)	50	24	48
Efficiency (%)	90	85	92
Operating range (%)	10–95	10–95	10–95
Charging/discharging (%)	92	92	92
Charging/discharging power (kW)	5.92	6.33	6.33

H_2 tank without the need for the additional step of compression or decompression of H_2. Among the FC technologies discussed in Section 2.3, the PEM FC generally offers higher efficiency than other types, reaching up to 50% [44].

As described in Section 3.2.1.3, the model imposes upper bounds on contracted power, PV generation capacity, BESS storage capacity, and the P2H system, reflecting both physical and economic limitations. These limits are shown in Table 4.7

Table 4.7: DER sizing maximum technical limits.

	$\hat{P}^{CPE}$ (kVA)	$\hat{P}^{GN}$ (kW)	$\hat{E}^{BN}$ (kWh)	$\hat{P}^{\mathrm{ELEC}}$ (kW)	$\hat{\mathrm{C}}$ (kg)	$\hat{P}^{\mathrm{FC}}$ (kW)
Member 1	350	0	0	0	0	0
Member 2	700	1500	1500	0	0	0
Member 3	100	0	0	0	0	0
Member 4	450	1000	700	0	0	0
Member 5	700	1500	1200	0	0	0
Member 6	100	0	0	0	0	0
Member 7	400	800	500	0	0	0
Member 8	1000	2500	1200	1000	600	400
Member 9	50	0	0	0	0	0
Total	3850	7300	5100	1000	600	400

The installation cost of each DER can be found in Table 4.8.

Table 4.8: Prices per unit of DER.

Parameter	**Value**	**Units**	**Source**
PV price	900	€/kW	[112]
BESS price	400	€/kWh	[113]
Electrolyzer price	900	€/kW	[38]
Tank price	400	€/kg	[114]
Fuel cell price	1600	€/kW	[115]

For the techno-economic analysis of the simulation results, a system lifetime of 20 years is assumed for all DERs. The discount rates used in the analysis are based on values provided by Banco de Portugal [116]. However, as discussed in Subsection 3.2.4, the SITEC sizing model does not incorporate discount rates during optimization, meaning it does not account for the time value of money or compute investment decisions based NPV. To evaluate the economic viability of the resulting configurations more realistically, a post-processing NPV analysis is conducted using multiple discount rates.

4.2 Scenario characterization

Four scenarios are considered to understand the impact of each DER on the REC. These are presented in Table 4.9. Each scenario involves a sizing stage using SITEC, followed by an operation stage using OSTEC. To include specific DERs in each scenario, we modify the parameters in Table 4.7, setting the maximum capacity of unwanted DERs to zero. A base scenario is first

Table 4.9: Technology configurations across different scenarios.

Scenarios	$\hat{EV}$	**Contracted power**	**PV**	**BESS**	**P2H**
Base	✓	✓			
S1	✓	✓	✓		
S2	✓	✓	✓	✓	
S3	✓	✓	✓		✓
S4	✓	✓	✓	✓	✓

simulated as a reference, in which all members act solely as passive consumers and energy sharing is not economically viable. S1 then introduces the use of installed PV systems, turning members into prosumers and increasing their level of self-sufficiency. Additionally, any surplus energy can be shared with other members, further optimizing community-wide energy use.

In S2, both PV systems and BESS are enabled. The benefits observed in S1 are expected to persist, with the added advantage of short-term energy storage, allowing members to store excess energy for use during periods of low or no generation. However, since buying and selling tariffs remain constant over time, members cannot benefit from buying energy at a lower price and selling it during high-demand periods.

Finally, in S3 and S4 a new use case for surplus energy presents itself, allowing the REC to profit off of H_2.

4.3 Results

This section presents the analysis of the proposed scenarios in Table 4.9. The economic viability of each scenario is evaluated based on the NPV and payback period. It also evaluates the operational performance of the REC and examines the impact of each DER.

4.3.1 Base scenario

The first simulation serves as a base case, used for comparison with other scenarios. The base case has no addition of DERs, assuming all members are passive consumers. All members rely exclusively on the energy retailer, thereby showing no self-sufficiency, and are unable to engage in P2P energy exchanges.

Using SITEC, we can assess the contracted power necessary for the operation of each member within the REC. With this data, we can make future observations about how each DER affects the amount of energy a member needs to conduct their energy transactions. The sizing results for the base scenario are presented in Table 4.10.

Table 4.10: Base scenario sizing results.

	P^{CPE} (kVA)
Member 1	300.44
Member 2	529.81
Member 3	50.88
Member 4	299.95
Member 5	530.39
Member 6	42.74
Member 7	300.71
Member 8	529.79
Member 9	37.14
Total	2621.85

Table 4.11 summarizes the economic performance of the base scenario. The table shows a total OPEX of 36.811 M€ , with an annual operating cost of 1.841 M€ , reflecting the recurring expense of purchasing energy from the retailer. The CAPEX is minimal in this case 1.229 M€ since no investments in DERs are made. Consequently, the overall TOTEX amounts to 38.039 M€ . As anticipated, there are no savings or payback periods calculated, given the absence of surplus energy that could be exploited through self-consumption or energy sharing.

Table 4.11: Summary of economic metrics (M€) for the base scenario.

Indicator	**Value**
OPEX (total)	36.811
OPEX (annual)	1.841
CAPEX	1.229
TOTEX	38.039
Savings (annual)	–
Payback Period [years]	–

4.3.2 S1 - PV

The PV scenario explores the operation of the REC when its members are equipped exclusively with PV systems. This configuration enables renewable generation but lacks storage, making energy use highly dependent on real-time production and consumption alignment.

Table 4.12: S1 sizing results.

	P^{CPE} (kVA)	P^{GN} (kW)
Member 1	300.44	0.00
Member 2	511.81	292.84
Member 3	50.88	0.00
Member 4	298.94	282.64
Member 5	514.25	259.15
Member 6	42.74	0.00
Member 7	299.23	82.23
Member 8	515.06	243.35
Member 9	37.14	0.00
Total	2570.47	1160.21

Table 4.12 shows the contracted power and installed PV power for each member.

The contracted power for the REC was reduced by 1.96%, which arises from the reduction of peak demand. The average SSR of the REC also supports this fact, as it increases to 8.84%, meaning that members can also reduce their energy bill.

The economic indicators discussed are summarized in Table 4.13. The CAPEX for the installed PV and contracted power over 20 years came to 2.249 M€ , where PV shared 46.43% and the contracted power represented 53.57% of the CAPEX. The yearly OPEX decreased to a cost of 1.686 M€ , which constitutes a reduction of 8.42% compared to the base scenario, with this the savings come to a value of 155 k€ . Combining the CAPEX and the achieved savings, the payback period comes to 14.52 years, which is less than the proposed system lifetime of 20 years.

Table 4.13: Summary of economic indicators (M€) and payback period for S1.

Indicator	**Value**
OPEX (total)	33.713
OPEX (annual)	1.686
CAPEX	2.249
TOTEX	35.962
Savings (annual)	0.155
Payback [years]	14.52

The data shown in Table 4.13 reveals that REC considers that the benefits that come with PV systems outweigh the investment. Compared to the base scenario, S1 nearly doubled the CAPEX, however the reduction in OPEX is able to compensate the higher initial investment and led to an overall reduction in TOTEX.

Regarding the amount of energy sharing that was obtained through PV system of the REC, or ESR, this value reaches 5.79%, with consumers in the REC benefitting the most from these exchanges. As for the NPV, seen in Table 4.14, the increase of the discount rate causes the project's economic viability to decrease. Applying the discount rate of 3.84% for the analysis, the conclusion is that this configuration does not add value to the REC over the 20 year period, as it leads to a negative NPV.

Table 4.14: NPV for different discount rates for S1 (M€).

Discount Rate [%]	0	0.875	1.75	2.625	3.5	3.84
NPV [M€]	0.849	0.582	0.346	0.138	-0.047	-0.114

According to the discount rate from Banco de Portugal of 3.84%, the NPV is -113.66 k€, which implies the sole investment in PV is not economically viable for the REC. With this in mind, the SITEC tool assumes a discount rate to 0%, allowing the sizing model to consider the investment financially justifiable.

4.3.3 S2 - PV + BESS

In this scenario, only the PV and BESS equipments can be utilized by the REC. Using the specified parameters in Tables 4.7 and 4.8, SITEC reached the optimal solution for the REC displayed in Table 4.15:

Table 4.15: S2 sizing results.

	P^{CPE} (kVA)	P^{GN} (kW)	E^{BN}
Member 1	300.44	0	0.00
Member 2	471.56	393.95	1432.24
Member 3	50.88	0	0.00
Member 4	399.72	342.53	821.86
Member 5	472.33	379.31	1409.13
Member 6	42.74	0	0.00
Member 7	250.02	149.50	551.65
Member 8	471.60	381.91	1412.11
Member 9	37.14	0	0.00
Total	2496.43	1647.21	5627.00

The SITEC results show a slight decrease in contracted power (74.04 kVA decrease compared to S1), however there's a very significant increase in the amount of installed PV, reaching 5.627 MW. This is primarily due to the availability of BESS, which enables storage of excess solar generation and encourages larger PV installations. The result is a notable improvement in energy autonomy, as shown by the rise in the SSR to 41.87%, indicating that nearly half of all energy consumed by the REC is self-generated.

In Table 4.16, the monetary results are presented. The CAPEX reached 8.029 M€, with contracted power accounting for 14.57% of the total, PV systems 63.07%, and BESS 22.36%. The annual OPEX was 1.253 M€, which is a significant reduction compared to both the base and S1 scenarios, resulting in yearly savings of 587 k€. Although the initial investment is relatively high, it is recovered through operational savings in 13.67 years, which is faster than the 14.52 years required in S1.

Table 4.16: Summary of economic indicators (M€) and payback period for S2.

Indicator	**Value**
OPEX (total)	25.067
OPEX (annual)	1.253
CAPEX	8.029
TOTEX	33.096
Savings (annual)	0.587
Payback [years]	13.67

This improved performance can also be linked to a significant rise in the ESR, which reached 19.92%. In this case, the deployment of BESS increased the REC's ability to store surplus generation and share it when needed, thus improving the energy trading. The high amount of PV also played a key role in reducing grid dependency.

Table 4.17: NPV for different discount rates for S2 (M€).

Discount Rate [%]	0	0.875	1.75	2.625	3.5	3.84
NPV [M€]	3.714	2.701	1.808	1.017	0.316	0.065

Based on Table 4.17 including the NPV for multiple, the project adds value to the REC over the system lifetime. For the proposed interest rate of 3.84%, the investment profits the REC with the 64.81 k€ .

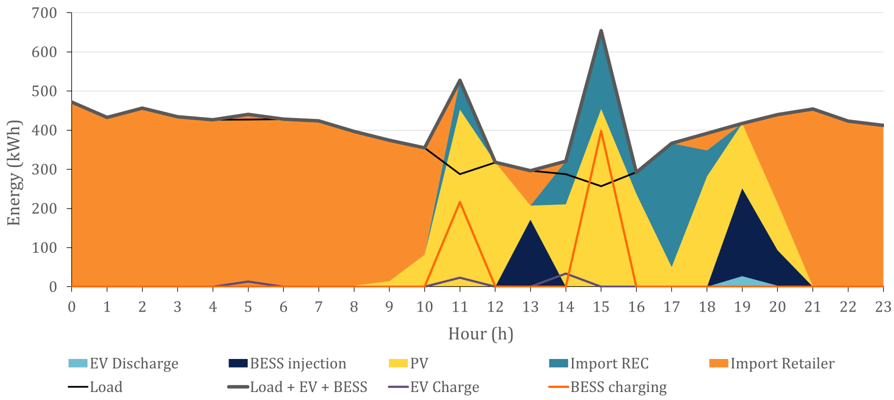

Figure 4.2: S2 operation over 24 hours.

In Figure 4.2, 24 hours of operation of member 2 can be seen. From 0 to 8 AM, the member 2 relies solely on the retailer to meet its energy needs, with a slight energy import for its EV at 5 AM. Between 8 AM and 12 AM, the member 2 begins to use various energy sources to meet its demand and charge both the BESS and EV. It reduces the amount of energy imported from the retailer and starts to use generation from the PV system, in addition to importing from other members in the REC. Interestingly, at 1 PM, there's a decline in generation (from a potential obstruction) that causes the injection of energy stored in the BESS and import from the retailer. Once the PV system returns to its nominal operation, the member maintains the behavior observed from hours 8 AM to 12 AM with significant contributions from the REC to meet demand. Energy is also stored in the BESS for later use (as seen from hours 6 PM to 9 PM) and, notably, the EV is discharged to meet demand, functioning as a storage system.

4.3.4 S3 - PV + P2H

This scenario allows for the installation of PV and P2H components, namely an electrolyzer, H_2 tank and a FC. This study is designed to evaluate if the P2H system can operate as an energy storage, and, if so, how it compares to traditional BESS. In this context, the P2H system can be used to both satisfy the demand of the CHP client and/or can leverage its stored H_2 to meet its own consumption with the FC. The sizing results for S3 can be seen in Table 4.18.

Table 4.18: S3 sizing results.

	P^{CPE} (kVA)	P^{GN} (kW)	P^{ELEC} (kW)	C^{Tank} (kg)	P^{FC} (kW)
Member 1	276.94	0.00	0	0	0
Member 2	550.37	753.93	0	0	0
Member 3	45.88	0.00	0	0	0
Member 4	303.90	406.06	0	0	0
Member 5	512.76	702.91	0	0	0
Member 6	39.19	0.00	0	0	0
Member 7	276.51	383.75	0	0	0
Member 8	972.40	2131.42	842.67	17.11	2.71
Member 9	37.14	0.00	0	0	0
Total	3043.58	4378.06	842.67	17.11	2.71

The sizing results show an increase in contracted power of 16.09%, even compared to the base scenario. This sharp rise is mainly due to the installation of the electrolyzer for member 8, which significantly raises peak demand.

The installed H_2 tank has a limited capacity of 17.11 kg, which matches the maximum H_2 demand from the CHP client. Given the H_2 price, the sizing model focuses on producing just enough H_2 to meet this specific need. The FC system is only minimally installed, partly due to the small tank capacity. As a result, H_2 is not used for energy storage but instead serves as a revenue source through supply to the CHP client. Each year, approximately 68.31 tons of H_2 are sold to the CHP client, generating 409.855 k€ in revenue.

In Table 4.19, a summary of the discussed economic indicators can be found. The total CAPEX stands at 6.132 M€, with contracted power representing 23.26% of the investment, PV systems 64.25%, the electrolyzer 12.37%, and the combined cost of the H_2 tank and FC system just 0.18%.

The annual OPEX is 1.366 M€, resulting in yearly savings of 474 k€. This scenario achieves the shortest payback period, recovering the investment in 12.93 years.

Table 4.19: Summary of economic indicators (M€) and payback for S3.

Indicator	**Value**
OPEX (total)	27.322
OPEX (annual)	1.366
CAPEX	6.132
TOTEX	33.454
Savings (annual)	0.474
Payback [years]	12.93

The economic viability of the DER configuration is assessed with the NPV in Table 4.20 by using multiple discount rates. From the results, the project shows a positive NPV across all discount rates, including the proposed discount rate of 3.84%, which leads to a NPV of 407.71 k€.

Table 4.20: NPV at multiple discount rates for S3.

Discount Rate [%]	0	0.875	1.75	2.625	3.5	3.84
NPV [M€]	3.356	2.538	1.816	1.177	0.611	0.408

Compared to S2, this scenario showed a decrease in ESR from 19.92% to 15.61%, albeit greater than S1.

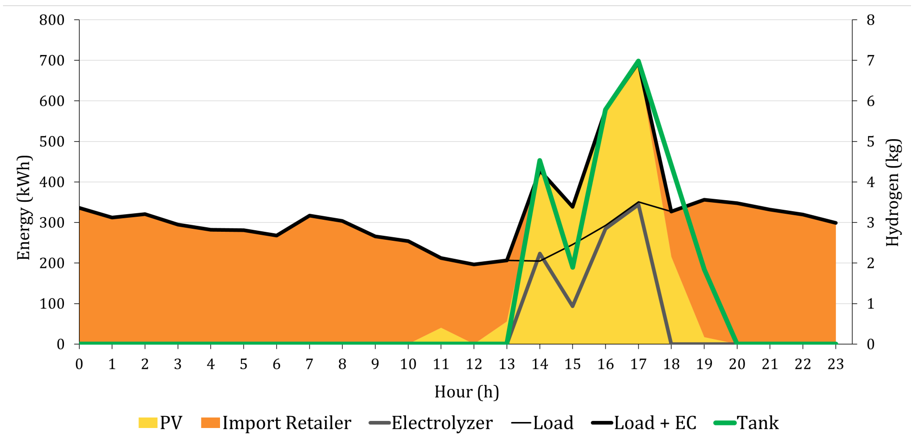

Figure 4.3: S3 operation over 24 hours.

In Figure 4.3, the first 24 hours are displayed for member 8. From hours 0 AM to 1 PM, member 8 only imports energy from the retailer until there's enough PV system generation to power the electrolyzer. The electrolyzer operates from 1 PM to 6 PM, producing 25.44 kg of H_2 during this period and the decline in stored H_2 can be explained by its export to the CHP client.

4.3.5 S4 - Full integration

This REC configuration examines how the REC functions when equipped with PV, BESS, and P2H systems. S4 is designed to determine how members manage all DERs.

Table 4.21: S4 sizing results.

	P^{CPE} (kVA)	P^{GN} (kW)	E^{BN} (kWh)	P^{ELEC} (kW)	C^{Tank} (kg)	P^{FC} (kW)
Member 1	276.94	0.00	0.00	0.00	0.00	0.00
Member 2	444.56	1079.02	424.71	0.00	0.00	0.00
Member 3	45.88	0.00	0.00	0.00	0.00	0.00
Member 4	300.20	801.87	697.29	0.00	0.00	0.00
Member 5	449.02	1050.27	405.90	0.00	0.00	0.00
Member 6	39.19	0.00	0.00	0.00	0.00	0.00
Member 7	236.30	483.62	193.09	0.00	0.00	0.00
Member 8	498.33	2384.31	1085.19	842.67	17.11	8.56
Member 9	37.14	0.00	0.00	0.00	0.00	0.00
Total	2356.07	5799.09	2806.18	842.67	17.11	8.56

From Table 4.21, the reintegration of BESS caused a decrease in contracted power compared to S3 (22.59%), indicating that both PV and BESS contribute to reducing peak demand. Comparing S2 to S4, shows a reduction in BESS installation (37.5%), as the members of the REC pool their surplus energy to the P2H for H_2 production. With this, S4 shadows what was observed in S3, where the price of H_2 is valued above energy storage.

The total investment in DERs amounts to 8.202M€, with contracted power and PV systems reaching 13.46% and 63.63% of the total, respectively. The BESS represents 13.69%, the electrolyzer 9.25%, H_2 storage and the FC collectively accounted for 0.25% of the overall investment. The cost of operation of the REC drops to 1.238 M€, which translates to yearly savings of 603k€. In this context, the payback period is 13.6 years.

Table 4.22: Summary of economic indicators (M€) and payback for S4.

Indicator	**Value**
OPEX (total)	24.751
OPEX (annual)	1.238
CAPEX	8.202
TOTEX	32.953
Savings (annual)	0.603
Payback [years]	13.60

Table 4.23 shows the results of the NPV sensitivity analysis for S4 under different discount rates. As expected, the NPV declines as the discount rate increases, reflecting the lower present value of future cash flows. However, even at the highest discount rate considered (3.84%), the investment remains economically sound, with a positive NPV of 110 k€. This suggests that S4 remains financially robust under varying financing conditions.

Table 4.23: NPV sensitivity analysis for different discount rates.

Discount Rate [%]	0	0.875	1.75	2.625	3.5	3.84
NPV [M€]	3.858	2.817	1.900	1.088	0.368	0.110

Like in other scenarios, the addition of PV and BESS systems results in a boost in ESR. S4 reaches an ESR of 18.46%, which is nearly identical to that of S2 (19.92%).

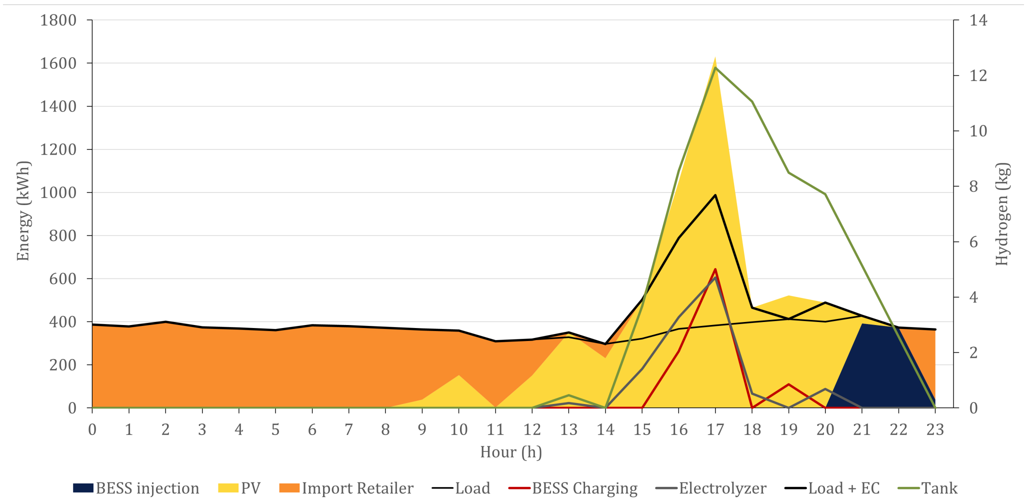

Figure 4.4: S4 operation over 24 hours.

In Figure 4.4, it becomes clear that there are many similarities with S3, however generation is higher due to the greater amount of PV systems installed. This energy can also be managed more efficiently, for it can be stored in BESS for later use or directed to the electrolyzer for hydrogen production. The graph shows a clear peak in PV generation between 3 PM and 5 PM, during which both the BESS and the electrolyzer are actively charged/powered.

The H_2 tank level increases significantly during this period, followed by a gradual decline to satisfy the CHP client's demand. Later in the day, the system draws on stored electricity from the BESS and the retailer to meet the evening demand.

4.3.6 Scenario summary

This subsection summarizes the main findings from the simulation results by comparing the economic and operational performance of each scenario. In Table 4.24, the various economic results across all scenarios are aggregated.

The simulation results across all scenarios show that S4 delivers the best overall performance, particularly when evaluated through NPV, which is a critical indicator of long-term economic viability. With a NPV of 3.858 M€, S4 outperforms all other configurations, surpassing S2 (3.714 M€) and S3 (3.356 M€), despite requiring the highest capital investment (8.202 M€).

Table 4.24: Summary of scenario economic metric results (M€), with 0% discount rate.

Scenario	OPEX	CAPEX	TOTEX	Savings	Payback	NPV
S1	1.686	2.249	35.962	0.155	14.52	0.849
S2	1.253	8.029	33.096	0.587	13.67	3.714
S3	1.366	6.132	33.454	0.474	12.93	3.356
S4	1.238	8.202	32.953	0.603	13.60	3.858

This indicates that, while S4 demands a greater CAPEX, due to the combination of all DERs, the long-term returns justify the investment.

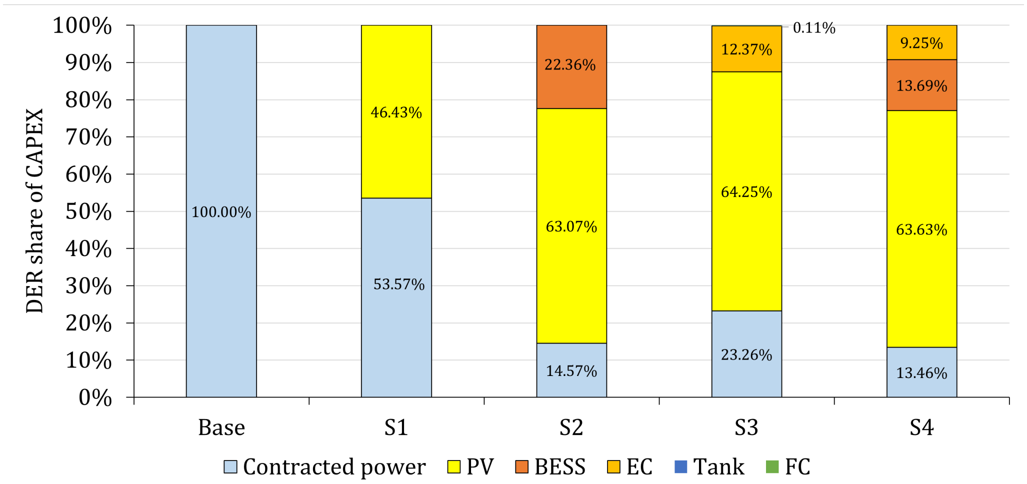

Figure 4.5: DER shares of the CAPEX for each scenario.

Figure 4.5 presents each DER's share of the CAPEX observed for each scenario. As mentioned, the contracted power declines when a new DER is introduced into the REC, except for S3, which accomodates the installation of the electrolyzer to H_2 production.

Among all technologies, the PV system consistently dominates the investment profile. It accounts for approximately 60% of total CAPEX on average, as it enables the generation of surplus electricity required to operate other DERs. The BESS follows with an average share of 18.02% in the scenarios where it is deployed, reflecting its role in enhancing short-term flexibility and self-consumption.

The electrolyzer represents the third most significant share, averaging 10.01% across the relevant scenarios. Minor shares are allocated to the H_2 tank and FC, which appear only in specific scenarios and contribute marginally to the overall investment.

From Table 4.25 displays how each DER affected the behaviour of the REC. In terms of the ESR, it becomes clear that the configuration where only PV and BESS are installed, leads to the highest energy sharing and self-sufficiency. This result emphasizes how energy sharing is closely related to the amount of surplus energy that can be utilized, or stored for later use, to meet any energy demands during periods of no generation.

Table 4.25: Summary of scenario REC metric results.

Scenario	ESR (%)	SSR (%)
S1	5.79	8.84
S2	19.92	41.87
S3	15.61	30.29
S4	18.46	40.45

S3 and S4 maintain relatively high ESR, however the decrease to 15.61% and 18.46%, respectively, can be attributed to the investment in the P2H system and the sizing of PV capacity primarily to cover member 8's both its consumption and the electrolyzer's energy demand.

Table 4.26: NPV by scenario and discount rate (M€)

Scenario	0%	0.875%	1.75%	2.625%	3.5%	3.84%
S1	0.849	0.582	0.346	0.138	-0.047	-0.114
S2	3.714	2.701	1.808	1.017	0.316	0.065
S3	3.356	2.538	1.816	1.177	0.611	0.408
S4	3.858	2.817	1.900	1.088	0.368	0.110

Table 4.26 presents the NPV of each scenario under varying discount rates, ranging from 0% to 3.84%. As expected, higher discount rates result in lower NPV values across all scenarios. S2 consistently shows strong economic performance, maintaining a positive NPV even at the highest discount rate of 3.5% (0.316 M€). Similarly, S3 and S4 also remain economically viable across all rates, with S4 achieving the highest NPV at the lowest discount rate (2.817 M€ at 0.875%). In contrast, S1 becomes economically unfavorable at a 3.5% discount rate, yielding a slightly negative NPV of -0.047 M€ . These results highlight the sensitivity of project viability and suggest that S2 and S4 are more robust under varying economic assumptions.

4.3.7 Sensitivity analysis

A sensitivity analysis is conducted to determine how relevant parameters affect both the equipment selection and the operation of the REC, as well as their impact on the economic metrics.

The parameters considered include the number of clusters, cost of PV systems, the market price of H_2 and the electrolyzer cost. These were selected due to their high uncertainty and significant influence on DER deployment decisions. Table 4.27 summarizes the range of values used for each parameter.

For each evaluated price, the total sizing of the REC is performed (including all DER, within the maximum limits defined in Table 4.7), and with this, the extraction of the total investment. Subsequently, these results are used as inputs for the operation stage, with OSTEC, where the reduction of the cost of operation for the REC is calculated. Relevant economic indicators such as NPV are also used to assess long-term profitability.

Table 4.27: Sensitivity analysis parameters.

Parameter	Minimum	Maximum	Units	Step
PV price	0.4	0.9	€/W	0.1
Electrolyzer cost	400	900	€/kW	100
H_2 price	2	6	€/kg	0.5
Clustering	10	120	days	10

4.3.7.1 PV

This sensitivity analysis highlights the impact of PV prices on community energy systems. In Figure 4.6, the effects of the PV price on both the amount of installed PV and BESS can analyzed, in addition to REC metrics.

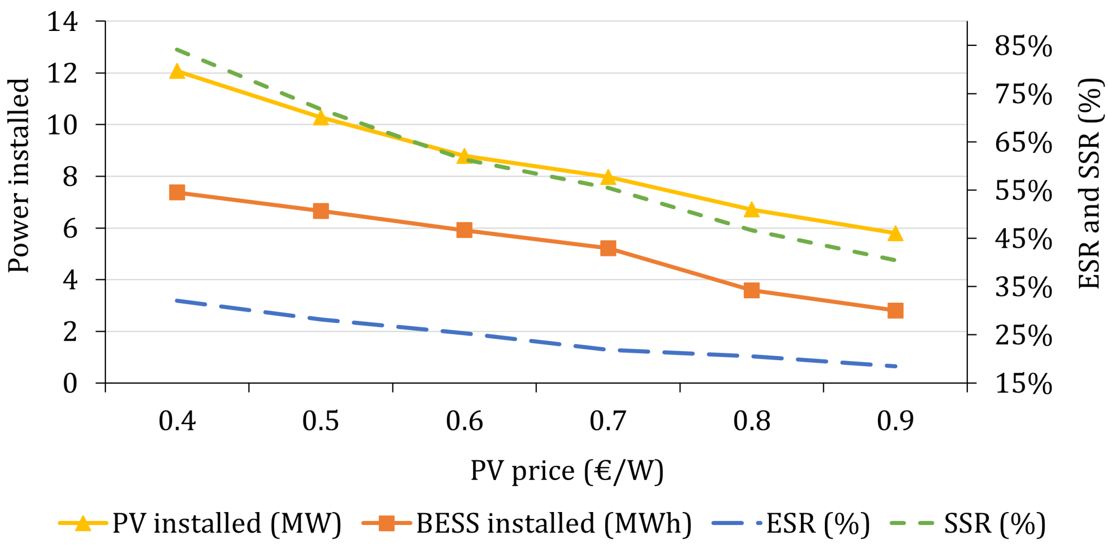

Figure 4.6: PV, BESS and REC metrics with varying PV prices.

From Figure 4.6, the general trend with the PV price increase is an overall reduction for both installation and the REC metrics.

When PV prices are low, the REC tends to install significantly more PV power, reaching 12 MW at 0.4 €/W. As the price rises to 0.9 €/W, the installed capacity drops to approximately 6 MW. A similar pattern is observed for the BESS, with installed capacity decreasing from about 7.5 MWh to just under 3 MWh. This suggests that battery deployment is closely tied to the scale of PV generation, likely to enable the storage of surplus electricity for later use.

The ESR declines steadily from roughly 30% to 15%, indicating a reduced ability or incentive to share energy within the community. Meanwhile, the SSR falls from nearly 80% to around 45%, showing that the community becomes increasingly reliant on external sources as PV prices rise.

Lower PV prices enable larger system installations and lead to higher levels of both ESR and SSR. As prices increase, these benefits diminish, limiting the community's ability to meet its energy needs locally and collaborate through energy sharing.

4.3.7.2 Electrolyzer cost

The electrolyzer cost sensitivity analysis consists of evaluating the impact of varying electrolyzer investment costs on the REC's performance under different H_2 selling prices. For each fixed H_2 price, the electrolyzer cost will be systematically adjusted to assess how it influences the economic viability and optimal configuration of the REC.

The minimum cost of 400 €/kW for the electrolyzer shown in Table 4.27 is based on [117], which includes cost projections for electrolyzer costs up to 2050. This study is also relevant for determining the viability of the EU's goals for 2035, as was researched by [96].

The results from the sensitivity analysis can be seen in Figure 4.7.

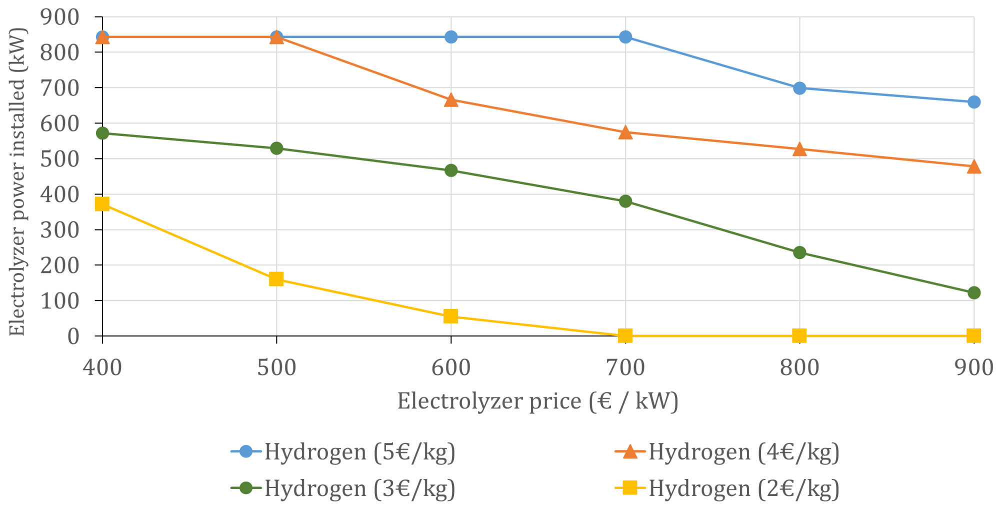

Figure 4.7: Electrolyzer cost sensitivity analysis for multiple H_2 prices.

The sensitivity analysis highlights promising conditions under which H_2 production becomes increasingly viable for the REC. As expected, the economics improve significantly with higher H_2 selling prices and decreasing electrolyzer capital costs. At a H_2 price of 5 €/kg, the investment proves highly attractive across all considered scenarios. Even at the upper bound electrolyzer cost of 900 €/kW, the REC proceeds with a substantial installation of approximately 660 kW, demonstrating strong profitability. As the capital cost drops below 700 €/kW, the system consistently opts for the maximum capacity of 842.67 kW, indicating a very favorable H_2 price.

At a H_2 price of 4 €/kg the REC continues to find the investment worthwhile. While more sensitive to capital cost variations, the system still reaches full capacity installation at or below 500 €/kW. This indicates that modest cost reductions in electrolyzer technology, reinforcing the feasibility of decentralized H_2 production.

At 3 €/kg, often cited as a transitional cost point for green H_2, the investment signal remains positive. Though no capacity is installed at the highest cost, the electrolyzer deployment begins at 800 €/kW and grows steadily, reaching about 572 kW at 400 €/kW. This suggests that ongoing cost declines will play a key role in scaling production, particularly in less favorable pricing scenarios.

Even at the ambitious price target of 2 €/kg, which is aligned with the EU's long-term vision of price parity with fossil-based H_2, REC shows the adoption of H_2 production [118]. While no installations occur above 700 €/kW, deployment initiates as costs fall below this threshold and reaches 372 kW at 400 €/kW. These results affirm that community-based H_2 production can contribute to the EU's clean energy transition, especially as technology matures and economies of scale continue to drive costs downward.

These results highlight H_2 deployment's strong dependence on market conditions and capital cost reductions.

4.3.7.3 Hydrogen price

This analysis considers a range of H_2 prices between 2.5 and 6 €/kg, using increments of 0.5 €/kg. Current green H_2 market prices typically fall between 3.5 and 6 €/kg [119].

Table 4.28: Economic indicators (M€) for different H_2 prices for a discount rate of 0%.

H_2 price (€/kg)	OPEX (year)	CAPEX	Savings	Payback	NPV
2.5	1.39	5.80	0.45	12.88	3.21
3	1.37	6.13	0.47	13.13	3.21
3.5	1.35	6.53	0.49	13.36	3.25
4	1.33	6.96	0.51	13.54	3.32
4.5	1.30	7.37	0.54	13.69	3.40
5	1.28	7.65	0.56	13.69	3.52
5.5	1.25	8.10	0.59	13.75	3.68
6	1.24	8.20	0.60	13.60	3.86

The sensitivity analysis shown in Table 4.28 illustrates how the CAPEX increases steadily with the H_2 price, demonstrating how the REC is continuously integrating more power for the electrolyzer. Notably, the payback period increases with the higher H_2, which may arise due to the sizable CAPEX of the P2H system components. This relation between the payback period and the H_2 can also be explained by SITEC's flaw as it does not account for discount rates.

The data shown in Table 4.28 also emphasizes the growth in NPV with each H_2 price, effectively showing how the REC is steadily profitting more from the CHP client.

To understand the reason behind the selection of the electrolyzer power, we analyze the maximum energy required to meet the H_2 demand of the CHP client. Using Equation 4.2, assuming an electrolyzer efficiency of 80% and a HHV of 39.4 kWh/kg for STP conditions we get the following result:

$$E_t^{ELEC} = \frac{\hat{m}_t^{CHP} \cdot \hat{\text{HHV}}}{\hat{\eta}^{ELEC}} \tag{4.2}$$

$$\tag{4.3}$$

$$\max(E_t^{ELEC}) = \frac{17.11 \cdot 39.4}{0.8} \approx 842.67 \text{ kWh} \tag{4.4}$$

The resulting energy required to satisfy the maximum daily H_2 demand of 17.11 kg is equal to 842.67 kWh, which corresponds to the electrolyzer power selected by SITEC. This outcome indicates that SITEC's solution aims to precisely match the CHP demand, minimizing oversizing while ensuring energy needs are met.

4.3.7.4 Clustering

Figure 4.8 illustrates the trade-off between computational cost and accuracy as the number of clusters increases. In this analysis, the solution obtained with 120 clusters is treated as the reference (with 0% error), and the error for fewer cluster sets is calculated relative to it. In reality,

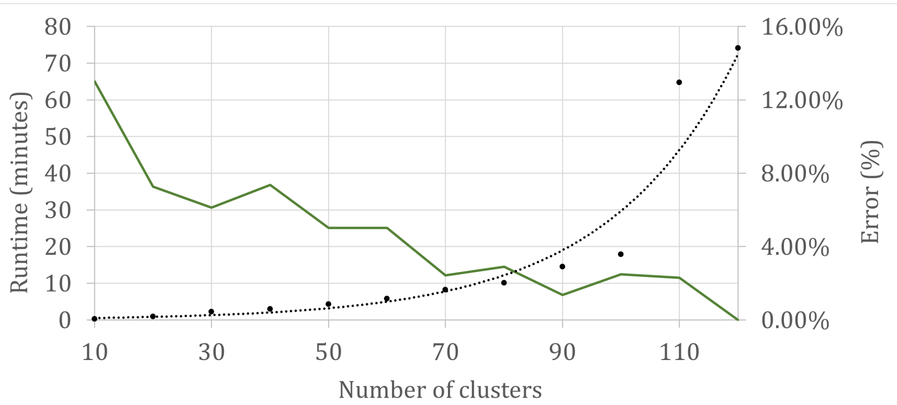

Figure 4.8: Change in runtime and error (%) with varying number of clusters.

the solution that would result in a 0% error would imply using 365 clusters, which implies no clustering occurs as every point represents itself.

As shown in Figure 4.8, the runtime (depicted in black) follows an exponential trend, becoming particularly pronounced beyond 100 clusters. In contrast, the error (shown in green) steadily decreases as the number of clusters increases, with most of the improvement occurring below 70 clusters. Beyond this point, additional clusters yield diminishing returns in accuracy.

Chapter 5

Conclusion

This chapter summarizes the main findings of the work, including a critical analysis of the developed models, the proposed scenarios, and their outcomes. It also outlines the key contributions of the study and identifies areas for future research to expand on the work.

5.1 Conclusions

Meeting global decarbonization goals requires substantial investment in RES. RECs contribute to this transition by enabling P2P energy trading and promoting self-sufficiency. However, the variability of RES introduces operational challenges, driving interest in complementary solutions like H_2, which offers cross-sector integration, and increases flexibility.

The work developed in this dissertation presented a comprehensive methodology for the integration of P2H systems within RECs, structured around two key stages: the SITEC model for optimal sizing of DERs and the OSTEC model for operational scheduling. The models of the components of a P2H system were implemented in these tools, which allowed for a detailed techno-economic analysis of various combinations of DER configurations.

S1, which includes only PV systems, showed limited economic benefits, with annual savings of 155 k€ and a payback period of 14.52 years. However, it becomes unfeasible under higher discount rates, as the NPV drops to -114 k€ at 3.84%.

S2, S3, and S4 introduced additional technologies, namely BESS and P2H. S2, combining PV and BESS, offered the most balanced configuration, with a payback period of 13.67 years and a consistently positive NPV from 3.714 M€ at 0% to 65 k€ at 3.84%. S3, which replaces BESS with a P2H system, achieved the shortest payback period (12.93 years), despite a higher investment of 6.132 M€ and increased contracted power. Finally, S4, which integrates all available DERs, achieved the lowest OPEX (1.238 M€) and the highest NPV for discount rates below 1.75% though it required the highest CAPEX (8.202 M€).

With this, the combination of all DERs lead to the most economically atractive scenario, for it managed to deliver the highest NPV out of all scenarios and closely matches the payback period of S3.

From an energy performance standpoint, S2 delivered the highest ESR and SSR, at 19.92% and 41.87%, respectively. These values highlight the effectiveness of PV and BESS in maximizing surplus energy utilization and supporting local energy autonomy. Scenarios S3 and S4 also maintain a relatively high ESR values (15.61% and 18.46%), with a sizable portion of surplus REC energy being allocated for the production of H_2. The results also show that, under this case study, H_2 was primarily used as feedstock, rather than a long-term energy storage vector.

The sensitivity analysis provided additional insights into how key parameters influence the performance and viability of the REC when a P2H system is integrated. Regarding technology costs, lower PV prices significantly boosted system adoption, with installed PV capacity doubling from approximately 6 MW to 12 MW as the price dropped from 0.9 to 0.4 €/W. This increase also drove higher BESS deployment and improved ESR and SSR, with the rise from 15% to 30%, and from 45% to nearly 80%, respectively.

The electrolyzer costs under varying H_2 price scenarios showed that even at a target price of 2 €/kg, the REC opted to adopt P2H systems when electrolyzer costs fell below 700 €/kW. This finding is significant, as it supports the EU's objective of making green H_2 cost-competitive with fossil-based alternatives.

The analysis of H_2 confirms that higher H_2 selling prices significantly improve the economic viability of P2H integration in the REC. The steady increase in NPV reflects growing profitability, while the selection of electrolyzer power closely aligns with the maximum energy required to meet client demand.

Clustering results showed that beyond 100 clusters, improvements in accuracy diminish while computational costs increase exponentially.

In summary, this work demonstrates that integrating P2H systems into RECs can improve both economic performance and energy autonomy, especially when combined with other DERs like PV and BESS. The proposed methodology effectively guides sizing and operation, and the results highlight key trade-offs across different scenarios. While technology costs and market conditions play a critical role, the findings suggest that P2H can be a viable and valuable addition to future RECs.

5.2 Future work

This dissertation opens up various opportunities for further research to enhance and extend the proposed framework.

- Expanding the optimization framework to account for multiple objectives, including environmental impact, social equity, and energy resilience, which could provide a more comprehensive evaluation of REC performance;
- Integrating degradation effects for H_2 storage technologies and lifecycle considerations;
- Evaluating the scalability of the proposed approach to larger, more diverse RECs;

- Collaborations with real-world pilot projects would be essential for validating and refining the model's assumptions;

References

[1] UNFCCC. The paris agreement | UNFCCC. URL: https://unfccc.int/process-and-meetings/the-paris-agreement.

[2] SDG. Goal 7 | department of economic and social affairs. https://sdgs.un.org/goals/goal7#progress_and_info.

[3] Unni Pillai. Drivers of cost reduction in solar photovoltaics. *Energy Economics*, 50:286–293, 2015. URL: https://www.sciencedirect.com/science/article/pii/S014098831500167X, doi:10.1016/j.eneco.2015.05.015.

[4] Muhammad Umar, Yasir Riaz, and Imran Yousaf. Impact of russian-ukraine war on clean energy, conventional energy, and metal markets: Evidence from event study approach. *Resources Policy*, 79:102966, 2022. URL: https://www.sciencedirect.com/science/article/pii/S0301420722004093, doi:10.1016/j.resourpol.2022.102966.

[5] REPowerEU. URL: https://commission.europa.eu/strategy-and-policy/priorities-2019-2024/european-green-deal/repowereu-affordable-secure-and-sustainable-energy-europe_en.

[6] Where does the EU's gas come from? URL: https://www.consilium.europa.eu/en/infographics/eu-gas-supply/.

[7] Adolfsen, Jakob Feveile and Kuik, Friderike and Schuler, Tobias and Lis, Eliza. The impact of the war in ukraine on euro area energy markets. *ECB Economic Bulletin*, 2022. URL: https://www.ecb.europa.eu/press/economic-bulletin/focus/2022/html/ecb.ebbox202204_01~68ef3c3dc6.en.html.

[8] Francesco Vetrò and Nicola Brignoli. Renewable energy communities: Paradigmatic example of a new decentralised governance of the energy market. *Athens Journal of Law*, 11:25–44, 01 2025. doi:10.30958/ajl.11-1-2.

[9] Mikołaj Jasiak. *Energy Communities in the EU: Challenges for the Implementation of the EU Legal Framework*, pages 197–218. 12 2021. doi:10.1017/9781839702211.012.

[10] Michiel A. Heldeweg and Séverine Saintier. Renewable energy communities as 'socio-legal institutions': A normative frame for energy decentralization? *Renewable and Sustainable Energy Reviews*, 119:109518, March 2020. URL: https://www.sciencedirect.com/science/article/pii/S1364032119307269, doi:10.1016/j.rser.2019.109518.

[11] EU. URL: https://eur-lex.europa.eu/legal-content/EN/TXT/PDF/?uri=OJ:L_202302413.

[12] Cleanwatts. 100 aldeias a++ - cleanwatts. URL: https://cleanwatts.energy/pt-pt/100-aldeias/, https://cleanwatts.energy/pt-pt/100-aldeias/.

[13] Cleanwatts. Como a santa casa da misericordia de miranda do douro poupou €18.000 com uma comunidade de energia renovável - cleanwatts. URL: https://cleanwatts.energy/pt-pt/case-study/miranda-do-douro/, https://cleanwatts.energy/pt-pt/case-study/miranda-do-douro/.

[14] Longxi Li, Kequn Peng, Xiaohui Yang, and Ke Liu. Coordinated design of multi-stakeholder community energy systems and shared energy storage under uncertain supply and demand: A game theoretical approach. *Sustainable Cities and Society*, 100:105028, 2024. URL: https://www.sciencedirect.com/science/article/pii/S221067072300639X, doi:10.1016/j.scs.2023.105028.

[15] Dina A. Elalfy, Eid Gouda, Mohamed Fawzi Kotb, Vladimír Bureš, and Bishoy E. Sedhom. Comprehensive review of energy storage systems technologies, objectives, challenges, and future trends. *Energy Strategy Reviews*, 54:101482, 2024. URL: https://www.sciencedirect.com/science/article/pii/S2211467X24001895, doi:10.1016/j.esr.2024.101482.

[16] Bidattul Syirat Zainal, Pin Jern Ker, Hassan Mohamed, Hwai Chyuan Ong, I. M. R. Fattah, S. M. Ashrafur Rahman, Long D. Nghiem, and T M Indra Mahlia. Recent advancement and assessment of green hydrogen production technologies. *Renewable and Sustainable Energy Reviews*, 189:113941, 2024. URL: https://www.sciencedirect.com/science/article/pii/S1364032123007992, doi:10.1016/j.rser.2023.113941.

[17] International Energy Agency. Net zero by 2050 – analysis. URL: https://www.iea.org/reports/net-zero-by-2050.

[18] Britannica. Hydrogen | properties, uses, & facts | britannica. URL: https://www.britannica.com/science/hydrogen.

[19] Hydrogen - element information, properties and uses | periodic table. URL: https://www.rsc.org/periodic-table/element/1/hydrogen.

[20] Geography of Transport Systems. Energy density of some combustibles | the geography of transport systems. URL: https://transportgeography.org/contents/chapter4/transportation-and-energy/combustibles-energy-content/.

[21] High heating value - an overview | ScienceDirect topics. URL: https://www.sciencedirect.com/topics/engineering/high-heating-value.

[22] The difference between green hydrogen and blue hydrogen. URL: https://www.petrofac.com/media/stories-and-opinion/the-difference-between-green-hydrogen-and-blue-hydrogen/.

[23] Jose M. Marín Arcos and Diogo M. F. Santos. The hydrogen color spectrum: Techno-economic analysis of the available technologies for hydrogen production. *Gases*, 3(1):25–46, 2023. Number: 1 Publisher: Multidisciplinary Digital Publishing Institute. URL: https://www.mdpi.com/2673-5628/3/1/2, doi:10.3390/gases3010002.

[24] Gayatri Udaysinh Ingale, Hyun-Min Kwon, Soohwa Jeong, Dongho Park, Whidong Kim, Byeingryeol Bang, Young-Il Lim, Sung Won Kim, Youn-Bae Kang, Jungsoo Mun, Sunwoo Jun, and Uendo Lee. Assessment of Greenhouse Gas Emissions from Hydrogen Production Processes: Turquoise Hydrogen vs. Steam Methane Reforming. *Energies*, 15(22):8679, January 2022. Number: 22 Publisher: Multidisciplinary Digital Publishing Institute. URL: https://www.mdpi.com/1996-1073/15/22/8679, doi:10.3390/en15228679.

[25] SFC Energy. Blue hydrogen | overview | definition, advantages & more » SFC energy AG. URL: https://www.sfc.com/glossary/blue-hydrogen/.

[26] Hydrogen Europe. In a nutshell. URL: https://hydrogeneurope.eu/in-a-nutshell/.

[27] Mohamad K. Khawaja, Razan Al-Mohamad, Tareq Salameh, and Ammar Alkhalidi. Strategies to promote nuclear energy utilization in hydrogen production. *International Journal of Hydrogen Energy*, 82:36–46, 2024. URL: https://www.sciencedirect.com/science/article/pii/S0360319924030830, doi:10.1016/j.ijhydene.2024.07.395.

[28] International Energy Agency. Global hydrogen review 2024. https://www.iea.org/reports/global-hydrogen-review-2024, 2024. IEA, Paris. Licence: CC BY 4.0.

[29] International Energy Agency. Global hydrogen review 2024 – analysis - IEA. URL: https://www.iea.org/reports/global-hydrogen-review-2024.

[30] European Hydrogen Observatory. Observatory reports | european hydrogen observatory. URL: https://observatory.clean-hydrogen.europa.eu/tools-reports/observatory-reports.

[31] M. Khan and J. Smith. Recent developments in water electrolysis for hydrogen production. *Renewable Energy Review*, 12:45–62, 2018.

[32] Mustafa Ergin Şahin. An Overview of Different Water Electrolyzer Types for Hydrogen Production. *Energies*, 17(19):4944, January 2024. Number: 19 Publisher: Multidisciplinary Digital Publishing Institute. URL: https://www.mdpi.com/1996-1073/17/19/4944, doi:10.3390/en17194944.

[33] DOE Hydrogen Program. Water electrolysis, 2023. Accessed: 2024-12-01. URL: https://www.energy.gov/eere/fuelcells/hydrogen-production-electrolysis.

[34] Meng Ni, Michael K.H. Leung, and Dennis Y.C. Leung. Energy and exergy analysis of hydrogen production by a proton exchange membrane (pem) electrolyzer plant. *Energy Conversion and Management*, 49(10):2748–2756, 2008. URL: https://www.sciencedirect.com/science/article/pii/S0196890408001210, doi:https://doi.org/10.1016/j.enconman.2008.03.018.

[35] Abdullah A. AlZahrani and Ibrahim Dincer. Modeling and performance optimization of a solid oxide electrolysis system for hydrogen production. *Applied Energy*, 225(C):471–485, 2018. URL: https://ideas.repec.org/a/eee/appene/v225y2018icp471-485.html, doi:10.1016/j.apenergy.2018.04.124.

[36] The Four Main Types of Water Electrolysis Technology - thyssenkrupp nucera, January 2024. URL: https://www.new-era-insights.com/article/the-four-main-types-of-water-electrolysis-technology/.

[37] Solid Oxide Electrolysis: A Technology Status Assessment. URL: https://www.catf.us/resource/solid-oxide-electrolysis-technology-status-assessment/.

[38] IEA. Electrolysers - Energy System. URL: https://www.iea.org/energy-system/low-emission-fuels/electrolysers.

[39] Zhipeng Yu and Lifeng Liu. Recent advances in hybrid seawater electrolysis for hydrogen production. *Advanced Materials*, 36, 12 2023. doi:10.1002/adma.202308647.

[40] Avigail Landman, Hen Dotan, G. Shter, Michael Wullenkord, Anis Houaijia, Artjom Maljusch, Gideon Grader, and Avner Rothschild. Photoelectrochemical water splitting in separate oxygen and hydrogen cells. *Nature materials*, 16, 03 2017. doi:10.1038/nmat4876.

[41] Aparna Sharma, Syed Ejaz Hussain Mehdi, Soumya Pandit, Sang Eun-Oh, and Varagunapandiyan Natarajan. Factors affecting hydrogen production in microbial electrolysis cell (MEC): A review. *International Journal of Hydrogen Energy*, 61:1473–1484, April 2024. URL: https://www.sciencedirect.com/science/article/pii/S0360319924006153, doi:10.1016/j.ijhydene.2024.02.193.

[42] Bent Sørensen and Giuseppe Spazzafumo. 3 - Fuel cells. In Bent Sørensen and Giuseppe Spazzafumo, editors, *Hydrogen and Fuel Cells (Third Edition)*, pages 107–220. Academic Press, January 2018. URL: https://www.sciencedirect.com/science/article/pii/B9780081007082000035, doi:10.1016/B978-0-08-100708-2.00003-5.

[43] (PDF) Thermodynamic performance judgment of organic Rankine cycle based on Gibbs free energy change. URL: https://www.researchgate.net/publication/363329994_Thermodynamic_performance_judgment_of_organic_Rankine_cycle_based_on_Gibbs_free_energy_change, doi:10.21203/rs.3.rs-2008226/v1.

[44] Colin Tong. Hydrogen and Fuel Cells. In *Introduction to Materials for Advanced Energy Systems*, pages 587–653. Springer International Publishing, Cham, 2019. URL: https://doi.org/10.1007/978-3-319-98002-7_9, doi:10.1007/978-3-319-98002-7_9.

[45] Angelika Heinzel. *Fuel cells and hydrogen technology*, pages 368–373. Springer Nature, 01 2009. doi:10.1007/978-3-540-88546-7_69.

[46] Jeffrey W. Fergus. Electrolytes for solid oxide fuel cells. *Journal of Power Sources*, 162(1):30–40, November 2006. URL: https://www.sciencedirect.com/science/article/pii/S0378775306012110, doi:10.1016/j.jpowsour.2006.06.062.

[47] Liwei Ding, Hongkun Lv, Kang Zhang, Chenglong Hou, Xiaodong Peng, Jibiao Hou, and Wei Kang. Simulation and efficiency analysis of hydrogen production in

proton exchange membrane electrolyzer system. In *2024 6th International Conference on Energy Systems and Electrical Power (ICESEP)*, pages 142–149, June 2024. URL: https://ieeexplore.ieee.org/document/10651767, doi:10.1109/ICESEP62218.2024.10651767.

[48] Renewable energy directive. URL: https://energy.ec.europa.eu/topics/renewable-energy/renewable-energy-directive-targets-and-rules/renewable-energy-directive_en.

[49] A. R. Di Fazio, F. Conte, and G. Natrella. Enhancing Management and Control of Renewable Energy Communities: A Practical Implementation. In *2024 3rd International Conference on Energy Transition in the Mediterranean Area (SyNERGY MED)*, pages 1–5, October 2024. URL: https://ieeexplore.ieee.org/document/10799371, doi:10.1109/SyNERGYMED62435.2024.10799371.

[50] Huan Zhou and Jie Wei. Research on pricing strategy of shared electro-thermal-hydrogen energy storage in integrated energy multi-microgrid based on hybrid game. *Frontiers in Energy Research*, 13, May 2025. Publisher: Frontiers. URL: https://www.frontiersin.org/journals/energy-research/articles/10.3389/fenrg.2025.1602891/full, doi:10.3389/fenrg.2025.1602891.

[51] Energy communities. URL: https://energy.ec.europa.eu/topics/markets-and-consumers/energy-consumers-and-prosumers/energy-communities_en.

[52] João Mello, José Villar, Ricardo Jorge Bessa, Ana Rita Antunes, and Miguel Macias Sequeira. Decarbonized and inclusive energy: A two-fold strategy for renewable energy communities. *IEEE Power and Energy Magazine*, 22(4):49–63, 2024. Conference Name: IEEE Power and Energy Magazine. URL: https://ieeexplore.ieee.org/document/10659273, doi:10.1109/MPE.2024.3396442.

[53] Hanan Wehbi. Powering the future: An integrated framework for clean renewable energy transition. *Sustainability*, 16(13):5594, 2024. Number: 13 Publisher: Multidisciplinary Digital Publishing Institute. URL: https://www.mdpi.com/2071-1050/16/13/5594, doi:10.3390/su16135594.

[54] Tiago Tavares, João Mello, Ricardo Silva, Armando Moreno, André Garcia, João Pacheco, Carlos Pereira, Mário Amorim, Clara Gouveia, and José Villar. Operation and simulation of a renewable energy community based on a local post-delivery pool market. In *2023 19th International Conference on the European Energy Market (EEM)*, pages 1–6, 2023. ISSN: 2165-4093. URL: https://ieeexplore.ieee.org/document/10161761, doi:10.1109/EEM58374.2023.10161761.

[55] What is collective self-consumption? | e-REDES. URL: https://www.e-redes.pt/en/what-collective-self-consumption.

[56] C. Pons-Seres de Brauwer and J. J. Cohen. Analysing the potential of citizen-financed community renewable energy to drive europe's low-carbon energy transition. *Renewable and Sustainable Energy Reviews*, 133:110300, 2020. URL: https://www.sciencedirect.com/science/article/pii/S1364032120305888, doi:10.1016/j.rser.2020.110300.

[57] Shoaib Ahmed, Amjad Ali, and Antonio D'Angola. A review of renewable energy communities: Concepts, scope, progress, challenges, and recommendations. *Sustainability*, 16(5):1749, 2024. Number: 5 Publisher: Multidisciplinary Digital Publishing Institute. URL: https://www.mdpi.com/2071-1050/16/5/1749, doi:10.3390/su16051749.

[58] Laura Campagna, Giuliano Rancilio, Lucio Radaelli, and Marco Merlo. Renewable energy communities and mitigation of energy poverty: Instruments for policymakers and community managers. *Sustainable Energy, Grids and Networks*, 39:101471, September 2024. URL: https://www.sciencedirect.com/science/article/pii/S2352467724002005, doi:10.1016/j.segan.2024.101471.

[59] Francesca Ceglia, Elisa Marrasso, Samiran Samanta, and Maurizio Sasso. Addressing Energy Poverty in the Energy Community: Assessment of Energy, Environmental, Economic, and Social Benefits for an Italian Residential Case Study. *Sustainability*, 14(22):15077, January 2022. Number: 22 Publisher: Multidisciplinary Digital Publishing Institute. URL: https://www.mdpi.com/2071-1050/14/22/15077, doi:10.3390/su142215077.

[60] MARMARA-IT. OurPower - die Energiecooperative. Mach Deinen Strombezug zur Strombeziehung. URL: https://www.ourpower.coop.

[61] StartSun Projectmanager. Case Study #8: OurPower (Austria), October 2024. URL: https://interreg-baltic.eu/project-posts/startsun/case-study-8-ourpower-austria/.

[62] European Commission. Energy community in Crete wins European Sustainable Energy Award for paving the way for free electricity for all - European Commission. URL: https://sustainable-energy-week.ec.europa.eu/energy-community-crete-wins-european-sustainable-energy-award-paving-way-free-electricity-all_en.

[63] yawdevs. , February 2022. URL: https://minoanenergy.com/en/ÏĎÎ¿-ÏĂÏĄÏŐÏĎÎ¿-Î■ÏĄÎşÎ¿-ÎµÎ¡ÎµÏĄÎşÎµÎźÎśÎžÎ¿Ï■-ÏČÏĚÎijÏĹÎůÏĘÎźÏČÎijÎ¿/.

[64] ERSE. Self-Consumption - ERSE. URL: https://www.erse.pt/en/activities/regulations-electricity/self-consumption/.

[65] ERSE. Tariffs and prices - electricity - ERSE. URL: https://www.erse.pt/en/activities/market-regulation/tariffs-and-prices-electricity/.

[66] E-REDES. Self-consumption energy sharing models | E-REDES. URL: https://www.e-redes.pt/en/self-consumption-energy-sharing-models.

[67] Humberto Queiroz, Rui Amaral Lopes, João Martins, Filipe Silva, Luis Fialho, and Nuno Bilo. Assessment of energy sharing coefficients under the new portuguese renewable energy communities regulation. *Heliyon*, 9:e20599, 10 2023. doi:10.1016/j.heliyon.2023.e20599.

[68] Royal Decree 244/2019 (consolidated text) regulating the administrative, technical and economic conditions of the self-consumption of electric energy - Climate Change Laws of the

World. URL: https://climate-laws.org/documents/royal-decree-244-2019-consolidated-text-regulating-the-administrative-technical-and-economic-conditions-of-the-self-consumption-of-electric-energy_79fe.

[69] Daniela Contreras, Luis Aguiar, and Eduardo Fuentes. Technical economic study of a collective photovoltaic installation. pages 1755–1766, 01 2023. doi:10.52202/069564-0159.

[70] Guía de autoconsumo colectivo | Idae. URL: https://www.idae.es/publicaciones/guia-de-autoconsumo-colectivo.

[71] Tiago Sousa, Tiago Soares, Pierre Pinson, Fabio Moret, Thomas Baroche, and Etienne Sorin. Peer-to-peer and community-based markets: A comprehensive review. *Renewable and Sustainable Energy Reviews*, 104:367–378, 2019. URL: https://www.sciencedirect.com/science/article/pii/S1364032119300462, doi:10.1016/j.rser.2019.01.036.

[72] Amir Zare, Mehdi Mehdinejad, and Mehrdad Abedi. Designing a decentralized peer-to-peer energy market for an active distribution network considering loss and transaction fee allocation, and fairness. *Applied Energy*, 358:122527, 2024. URL: https://www.sciencedirect.com/science/article/pii/S0306261923018913, doi:10.1016/j.apenergy.2023.122527.

[73] Timothy Capper, Anna Gorbatcheva, Mustafa A. Mustafa, Mohamed Bahloul, Jan Marc Schwidtal, Ruzanna Chitchyan, Merlinda Andoni, Valentin Robu, Mehdi Montakhabi, Ian J. Scott, Christina Francis, Tanaka Mbavarira, Juan Manuel Espana, and Lynne Kiesling. Peer-to-peer, community self-consumption, and transactive energy: A systematic literature review of local energy market models. *Renewable and Sustainable Energy Reviews*, 162:112403, 2022. URL: https://www.sciencedirect.com/science/article/pii/S1364032122003112, doi:10.1016/j.rser.2022.112403.

[74] Aziz Saif, Shafi K. Khadem, Michael F. Conlon, and Brian Norton. Impact of distributed energy resources in smart homes and community-based electricity market. *IEEE Transactions on Industry Applications*, 59(1):59–69, 2023. Conference Name: IEEE Transactions on Industry Applications. URL: https://ieeexplore.ieee.org/document/9870539/?arnumber=9870539, doi:10.1109/TIA.2022.3202756.

[75] María-Victoria Gasca, Remy Rigo-Mariani, Vincent Debusschere, and Yousra Sidqi. Fairness in energy communities: Centralized and decentralized frameworks. *Renewable and Sustainable Energy Reviews*, 208:115054, 2025. URL: https://www.sciencedirect.com/science/article/pii/S1364032124007809, doi:10.1016/j.rser.2024.115054.

[76] Sharon J. W. Klein and Stephanie Coffey. Building a sustainable energy future, one community at a time. *Renewable and Sustainale Energy Reviews*, 60:867–880, 2016. URL: https://www.sciencedirect.com/science/article/pii/S1364032116001854, doi:10.1016/j.rser.2016.01.129.

[77] Hydroglen. HydroGlen. URL: https://www.hutton.ac.uk/scientific-services/research-collaborations/green-hydrogen-and-renewables/hydroglen/.

[78] Publications. URL: https://www.seafuel.eu/downloads/.

[79] HyP SA. Hydrogen Park South Australia. URL: https://www.agig.com.au/hydrogen-park-south-australia.

[80] HydroGlen. Hydroglen renewable hydrogen powered farm. URL: https://www.google.com/url?sa=t&rct=j&q=&esrc=s&source=web&cd=&cad=rja&uact=8&ved=2ahUKEwjmmM3D16-KAxV6xAIHHV0jH7EQFnoECBIQAQ&url=https%3A%2F%2Fwww.hutton.ac.uk%2Fsites%2Fdefault%2Ffiles%2Ffiles%2Fpublications%2FGlensaugh_HydroGlen_NonTech_Feasibility_March2021.pdf&usg=AOvVaw2JnAcL_1ElLVA9QwAa3o6J&opi=89978449.

[81] Scottish Government. Climate change. URL: https://www.gov.scot/policies/climate-change/.

[82] Scottish Government. Scottish agriculture greenhouse gas emissions and nitrogen use: 2022-23. URL: https://data.gov.scot/scottish-agriculture-greenhouse-gas-emissions-nitrogen-use-2022-23/.

[83] Haneen Al-Ali, Dallia Ali, and Ayatte I. Atteya. Investigating the potential of renewable-hydrogen energy storage systems (RHES) in enabling scotland's farming communities net-zero transition and sizing the proposed RHES system. *Green energy and environment technology*, 2, 2023. Publisher: InTechOpen. URL: https://rgu-repository.worktribe.com/output/1977067, doi:10.5772/geet.16.

[84] SEAFUEL. Seafuel Report into Hydrogen Applications on Árainn, Madeira and Tenerife | Energy Co-operatives Ireland. URL: https://www.energyco-ops.ie/seafuel-report-into-hydrogen-applications-on-inis-mor-madeira-and-tenerife/.

[85] Yazan Qiblawey, Abdulrahman Alassi, Mohammed Zain ul Abideen, and Santiago Bañales. Techno-economic assessment of increasing the renewable energy supply in the canary islands: The case of tenerife and gran canaria. *Energy Policy*, 162:112791, 2022. URL: https://www.sciencedirect.com/science/article/pii/S0301421522000167, doi:10.1016/j.enpol.2022.112791.

[86] Case studies & RoadMaps. URL: http://communityh2.eu/case-studies/.

[87] Redeia. In 2021, spain was the european country that generated the second highest amount of electricity with wind and solar power. URL: https://www.ree.es/en/press-office/news/press-release/2022/07/2021-spain-was-european-country-generated-second-highest-amount-electricity-with-wind-solar-power.

[88] Melina Gillespie. Hydrogen Park South Australia, March 2024. URL: https://research.csiro.au/hyresource/hydrogen-park-south-australia/.

[89] AGIG. HyP SA_explainer video. URL: https://vimeo.com/554545092.

[90] Hydrogen park south australia. URL: https://www.agig.com.au/hydrogen-park-south-australia.

[91] Australian electricity generation - fuel mix | energy.gov.au. URL: https://www.energy.gov.au/energy-data/australian-energy-statistics/data-charts/australian-electricity-generation-fuel-mix.

[92] Giulio Raimondi and Giuseppe Spazzafumo. Exploring renewable energy communities integration through a hydrogen power-to-power system in italy. *Renewable Energy*, 206:710–721, 2023. URL: https://www.sciencedirect.com/science/article/pii/S0960148123002252, doi:10.1016/j.renene.2023.02.074.

[93] Deboleena Das, Ishan Chakraborty, Aashish Kumar Bohre, Prince Kumar, and Raja Agarwala. Sustainable integration of green hydrogen in renewable energy systems for residential and EV applications. *International Journal of Energy Research*, 2024(1):8258624, 2024. _eprint: https://onlinelibrary.wiley.com/doi/pdf/10.1155/2024/8258624. URL: https://onlinelibrary.wiley.com/doi/abs/10.1155/2024/8258624, doi:10.1155/2024/8258624.

[94] Lingkang Jin, Mosè Rossi, Andrea Monforti Ferrario, Jacopo Carlo Alberizzi, Massimiliano Renzi, and Gabriele Comodi. Integration of battery and hydrogen energy storage systems with small-scale hydropower plants in off-grid local energy communities. *Energy Conversion and Management*, 286:117019, 2023. URL: https://www.sciencedirect.com/science/article/pii/S0196890423003655, doi:10.1016/j.enconman.2023.117019.

[95] Giulio Raimondi and Giuseppe Spazzafumo. Integrating renewable energy communities and italian UVAM project through renewable hydrogen chain. *e-Prime - Advances in Electrical Engineering, Electronics and Energy*, 10:100819, 2024. URL: https://www.sciencedirect.com/science/article/pii/S2772671124003991, doi:10.1016/j.prime.2024.100819.

[96] Md Morshed Alam, M. J. Hossain, Muhammad Ahsan Zamee, and Ahmed Al-Durra. Design and operation of future low-voltage community microgrids: An AI-based approach with real case study. *Applied Energy*, 377:124523, 2025. URL: https://www.sciencedirect.com/science/article/pii/S0306261924019068, doi:10.1016/j.apenergy.2024.124523.

[97] Luka Budin and Marko Delimar. Renewable Energy Community Sizing Based on Stochastic Optimization and Unsupervised Clustering. *Sustainability*, 17(2):600, January 2025. Number: 2 Publisher: Multidisciplinary Digital Publishing Institute. URL: https://www.mdpi.com/2071-1050/17/2/600, doi:10.3390/su17020600.

[98] Paolo Marocco, Domenico Ferrero, Emanuele Martelli, Massimo Santarelli, and Andrea Lanzini. An MILP approach for the optimal design of renewable battery-hydrogen energy systems for off-grid insular communities. *Energy Conversion and Management*, 245:114564, 2021. URL: https://www.sciencedirect.com/science/article/pii/S0196890421007408, doi:10.1016/j.enconman.2021.114564.

[99] Massimiliano Ferrara, Fabio Mottola, Daniela Proto, Antonio Ricca, and Maria Valenti. Local energy community to support hydrogen production and network flexibility. *Energies*, 17(15):3663, 2024. Number: 15 Publisher: Multidisciplinary Digital Publishing Institute. URL: https://www.mdpi.com/1996-1073/17/15/3663, doi:10.3390/en17153663.

[100] Ayesha Kaleem, Atiq Zaman, and Sumedha Rajakaruna. Hydrogen at home: The current and future landscape of green hydrogen in residential settings. *Sustainable Energy Technologies and Assessments*, 72:104058, 2024. URL: https://www.sciencedirect.com/science/article/pii/S2213138824004545, doi:10.1016/j.seta.2024.104058.

[101] Milkhatun Milkhatun. (PDF) Performance Assessment of University Lecturers: A Data Mining Approach. *ResearchGate*, 2020. URL: https://www.researchgate.net/publication/346005407_Performance_Assessment_of_University_Lecturers_A_Data_Mining_Approach, doi:10.23917/khif.v6i2.9069.

[102] Scikit Documentation. KMedoids Demo — scikit-learn-extra 0.3.0 documentation. URL: https://scikit-learn-extra.readthedocs.io/en/stable/auto_examples/plot_kmedoids.html#sphx-glr-auto-examples-plot-kmedoids-py.

[103] Potências EDP: Preços, Simulador, Qual Contratar e Como Alterar? URL: https://lojaluz.com/fornecedores/edp/gestoes/potencia.

[104] Electricity prices in Portugal below EU average. URL: https://www.theportugalnews.com/news/2024-10-29/electricity-prices-in-portugal-below-eu-average/93157?src=newsletter-30/10/2024.

[105] Voltaicos. Can You Sell Electricity Back to the Grid in Portugal? Earn Up to €0.08 per kWh in the Algarve - Voltaicos, December 2024. Section: Solar Panels. URL: https://voltaicos.pt/blog-solar-panels/sell-electricity-back-to-the-grid/.

[106] LuzeGas. Quanto pago pela tarifa de acesso às redes? URL: https://luzegas.pt/faq/tarifa-acesso-redes.

[107] MIBGAS - green energy. URL: https://greenenergy.mibgas.es/en.

[108] Clearcurrency. What's the mid-market rate? - Clear Currency. URL: https://clearcurrency.co.uk/stories/whats-the-mid-market-rate.

[109] Capstone. C200S :: Capstone Green Energy Holdings, Inc. (CGEH). URL: https://www.capstonegreenenergy.com/products/capstone-microturbines/c200s.

[110] EV Database. URL: https://ev-database.org/.

[111] Marek Toman, Radoslav Cipin, Dalibor Cervinka, Pavel Vorel, and Petr Prochazka. Li-Ion Battery Charging Efficiency. *ECS Transactions*, 74(1):37, December 2016. Publisher: IOP Publishing. URL: https://iopscience.iop.org/article/10.1149/07401.0037ecst/meta, doi:10.1149/07401.0037ecst.

[112] Study: Levelized Cost of Electricity - Renewable Energy Technologies - Fraunhofer ISE. URL: https://www.ise.fraunhofer.de/en/publications/studies/cost-of-electricity.html.

[113] Jinming Gao, Yixin Sun, and Xianlong Su. A Risk Preference-Based Optimization Model for User-Side Energy Storage System Configuration from the Investor's Perspective. *Electricity*, 6(1):3, March 2025. Number: 1 Publisher: Multidisciplinary Digital Publishing Institute. URL: https://www.mdpi.com/2673-4826/6/1/3, doi:10.3390/electricity6010003.

[114] Hyun Kyu Shin and Sung Kyu Ha. A Review on the Cost Analysis of Hydrogen Gas Storage Tanks for Fuel Cell Vehicles. *Energies*, 16(13):5233, January 2023. Number: 13 Publisher: Multidisciplinary Digital Publishing Institute. URL: https://www.mdpi.com/1996-1073/16/13/5233, doi:10.3390/en16135233.

[115] Via Aurea s.r.o. 8 Types of Fuel Cell by Price Point. URL: https://www.horizoneducational.com/8-types-of-fuel-cell-by-price-point/t1418.

[116] Taxas de juro e montantes de novos empréstimos e depósitos: nota de informação estatística de janeiro de 2025, March 2025. URL: https://bpstat.bportugal.pt/conteudos/noticias/2397/?utm_source=bportugal.pt.

[117] Hadi Vatankhah Ghadim, Rafaella Canessa, Jannik Haas, and Rebecca Peer. Electrolyzer cost projections compared to actual market costs: A Critical Analysis. In *2023 IEEE PES Innovative Smart Grid Technologies - Asia (ISGT Asia)*, pages 1–5, November 2023. ISSN: 2378-8542. URL: https://ieeexplore.ieee.org/document/10372757, doi:10.1109/ISGTAsia54891.2023.10372757.

[118] Koen van Greevenbroek, Johannes Schmidt, Marianne Zeyringer, and Alexander Horsch. Little to lose: The case for a robust European green hydrogen strategy. *Joule*, 9(7):101974, July 2025. URL: https://www.sciencedirect.com/science/article/pii/S2542435125001552, doi:10.1016/j.joule.2025.101974.

[119] Anders Andreasen and Jasper van Baten. Techno-Economic Analysis and Optimization of Gray and Green Methanol Synthesis Using Flowsheet Automation and Surrogate Modeling. *Energy & Fuels*, 39(6):3359–3374, February 2025. Publisher: American Chemical Society. URL: https://doi.org/10.1021/acs.energyfuels.4c05806, doi:10.1021/acs.energyfuels.4c05806.